

**SYNTHESIS AND CHARACTERISATIONS OF TITANIUM DIOXIDE  
(TiO<sub>2</sub>)/ CELLULOSE BIOCHAR COMPOSITES FOR  
PHOTOCATALYTIC DEGRADATION OF CONGO RED**

**WONG WAI TECK**

**A project report submitted in partial fulfilment of the  
requirements for the award of Bachelor of Engineering  
(Honours) Chemical Engineering**

**Lee Kong Chian Faculty of Engineering and Science  
Universiti Tunku Abdul Rahman**

**April 2020**

## DECLARATION

I hereby declare that this project report is based on my original work except for citations and quotations which have been duly acknowledged. I also declare that it has not been previously and concurrently submitted for any other degree or award at UTAR or other institutions.

Signature :



Name : Wong Wai Teck

ID No. : 15UEB01948

Date : 15/5/2020

**APPROVAL FOR SUBMISSION**

I certify that this project report entitled **“SYNTHESIS AND CHARACTERISATIONS OF TITANIUM DIOXIDE (TiO<sub>2</sub>)/CELLULOSE BIOCHAR COMPOSITES FOR PHOTOCATALYTIC DEGRADATION OF CONGO RED”** was prepared by **WONG WAI TECK** has met the required standard for submission in partial fulfilment of the requirements for the award of Bachelor of Engineering (Honours) Chemical Engineering at Universiti Tunku Abdul Rahman.

Approved by,

Signature

:



Supervisor

:

Dr. Pang Yean Ling

Date

:

15/5/2020

The copyright of this report belongs to the author under the terms of the copyright Act 1987 as qualified by Intellectual Property Policy of Universiti Tunku Abdul Rahman. Due acknowledgement shall always be made of the use of any material contained in, or derived from, this report.

© 2020, Wong Wai Teck. All right reserved.

## **ACKNOWLEDGEMENTS**

I would like to thank everyone who had contributed to the successful completion of this project. I would like to express my gratitude to my research supervisor, Dr. Pang Yean Ling for her invaluable advice, guidance and his enormous patience throughout the development of the research.

In addition, I would also like to express my gratitude to my loving parents and friends who had helped and given me encouragement to complete this project. I would not resolve the problems which I faced when my research without their cooperation.

## ABSTRACT

In this research, cellulose biochar/ titanium dioxide ( $\text{TiO}_2$ ) composites were synthesised using sol-gel method and being calcined at different temperature for photocatalytic degradation of Congo Red. The characteristics of cellulose biochar/  $\text{TiO}_2$  composites were studied using the X-ray diffraction (XRD), scanning electron microscopy- energy dispersive X-ray analysis (SEM-EDX), Fourier transformed infrared (FTIR) spectroscopy, Thermogravimetric analysis (TGA) analyses and zeta potential analyses. Anatase and rutile phases of  $\text{TiO}_2$  had been detached and distributed on the cellulose biochar surface of the composite materials. EDX results showed mainly of carbon, oxygen and titanium elements. The zero charge point of cellulose biochar/  $\text{TiO}_2$ -700 was pH 5.1. A few operating parameters studies such as type of catalysts, catalyst dosage, solution pH, potassium peroxymonosulfate (PMS) dosage, dye concentration, solution temperature and type of organic dyes to determine the optimum conditions for photocatalytic degradation of organic dye. It was found that increasing the calcination temperature of cellulose biochar/  $\text{TiO}_2$  composites increased the photocatalytic degradation efficiency of Congo Red before it reached the optimum point and decreased beyond the calcination temperature. The optimum conditions for the photocatalytic degradation of Congo Red were 0.5 g/L of cellulose biochar/  $\text{TiO}_2$ -700 with 0.3 mM of PMS used to treat an initial dye concentration of 10 mg/L under 30 °C and solution pH 5. Under these conditions, the degradation efficiency of Congo Red was 100 % in 30 minutes whereas the COD removal efficiency was 84.5 % in 120 minutes. The reusability was also studied and photocatalytic degradation of Congo Red was followed pseudo second-order kinetics with activation energy ( $E_a$ ) and pre-exponential factor ( $A_0$ ) values of  $38.16 \frac{\text{kJ}}{\text{mol}}$  and  $7.90 \times 10^5 \frac{\text{L}}{\text{mg min}}$  respectively. In a nutshell, Congo Red could be decomposed easily by photocatalytic degradation in the presence of cellulose biochar/  $\text{TiO}_2$ -700.

## TABLE OF CONTENTS

<b>DECLARATION</b>		<b>i</b>
<b>APPROVAL FOR SUBMISSION</b>		<b>ii</b>
<b>ACKNOWLEDGEMENTS</b>		<b>iv</b>
<b>ABSTRACT</b>		<b>v</b>
<b>TABLE OF CONTENTS</b>		<b>vi</b>
<b>LIST OF TABLES</b>		<b>ix</b>
<b>LIST OF FIGURES</b>		<b>x</b>
<b>LIST OF SYMBOLS / ABBREVIATIONS</b>		<b>xiii</b>
<b>LIST OF APPENDICES</b>		<b>xvi</b>
<b>CHAPTER</b>		
<b>1</b>	<b>INTRODUCTION</b>	<b>1</b>
1.1	Textile Pollution	1
1.2	Dye Production and Classifications	3
1.3	Dye Removal Methods	4
1.4	Problem Statement	8
1.5	Aim and Objective	9
1.6	Scope and Limitation of the Study	10
1.7	Outline of the Report	10
<b>2</b>	<b>LITERATURE REVIEW</b>	<b>12</b>
2.1	Biomass	12
2.1.1	Cellulose	12
2.1.2	Biochar	14
2.1.3	Activated Carbon	15
2.2	Metal Oxide Photocatalysts	15
2.2.1	Titanium Dioxide	16
2.2.2	Other Type of Metal Oxides	20
2.2.3	Effect of Calcination Temperature	21

2.3	Synthesis Methods of Cellulose Biochar/ TiO <sub>2</sub>	21
2.4	Characterisation Study	23
2.5	Photocatalysis	25
2.6	Effect of Parameters on the Photocatalytic Degradation	28
2.6.1	Effect of Catalyst Dosage	28
2.6.2	Effect of Solution pH	29
2.6.3	Effect of Initial Dye Concentration	30
2.6.4	Effect of Solution Temperature	30
2.6.5	Effect of Types of Organic Dyes	31
2.7	Summary	31
<b>3</b>	<b>METHODOLOGY AND WORK PLAN</b>	<b>33</b>
3.1	Materials and Chemicals	33
3.2	Equipment	36
3.3	Overall Research Flowchart	36
3.4	Experimental Setup	38
3.5	Preparation of Cellulose, Cellulose Biochar, TiO <sub>2</sub> and Cellulose Biochar / TiO <sub>2</sub> composites	38
3.5.1	Preparation of Cellulose from EFB	39
3.5.2	Preparation of Cellulose Biochar	39
3.5.3	Preparation of TiO <sub>2</sub>	39
3.5.4	Preparation of Cellulose Biochar/ TiO <sub>2</sub> Composites	40
3.6	Characterisations of Catalysts	40
3.6.1	XRD	40
3.6.2	SEM-EDX	41
3.6.3	FTIR Spectroscopy	41
3.6.4	TGA	41
3.6.5	Zeta Potential	41
3.7	Parameter Studies	42
3.7.1	Effect of Types of Catalysts	42
3.7.2	Effect of Catalyst Dosage	42
3.7.3	Effect of Solution pH	43
3.7.4	Effect of PMS Dosage	43



3.7.5	Effect of Initial Dye Concentration	44
3.7.6	Effect of Solution Temperature	44
3.7.7	Effect of Types of Organic Dyes	45
3.8	Reusability Study	45
3.9	Kinetic Study	46
3.10	COD Analysis	47
3.11	Summary	47
<b>4</b>	<b>RESULTS AND DISCUSSIONS</b>	<b>49</b>
4.1	Characterisation of Photocatalysts	49
4.1.1	XRD	49
4.1.2	SEM-EDX	50
4.1.3	FTIR Spectroscopy	52
4.1.4	TGA	54
4.1.5	Zeta Potential	55
4.2	Parameter Studies	56
4.2.1	Photocatalytic Degradation of Congo Red	56
4.2.2	Effect of Catalyst Dosage	57
4.2.3	Effect of solution pH	59
4.2.4	Effect of PMS Dosage	60
4.2.5	Effect of Initial Dye Concentration	62
4.2.6	Effect of Solution Temperature	63
4.2.7	Effect of Types of Organic Dyes	64
4.3	Reusability Study	65
4.4	Kinetic Study	66
4.5	COD Analysis	69
4.6	Summary	70
<b>5</b>	<b>CONCLUSION AND RECOMMENDATIONS</b>	<b>72</b>
5.1	Conclusion	72
5.2	Recommendations for future work	73
	<b>REFERENCES</b>	<b>74</b>
	<b>APPENDICES</b>	<b>91</b>

**LIST OF TABLES**

Table 1.1:	Degree of Fixation of Different Dye Classes on Fibres (Carmen and Daniela, 2012).	2
Table 1.2:	Table 1.2: Typical Water Usage in Textile Wet Processing for 1 kg of Woven Fabrics (Judd and Jefferson, 2003).	3
Table 1.3:	Properties and Applications for Different Classes of Dye (Pavithra, et al., 2019).	4
Table 2.1:	Composition of Cellulose, Hemicellulose and Lignin in Different Types of Raw Materials.	13
Table 3.1:	Chemical Reagents Used in This Research with Their Respective Specifications.	33
Table 3.2:	Chemical Properties of Organic Dyes Used in This Study.	34
Table 3.3:	List of Equipment with its Respective Model.	36
Table 4.1:	Distribution of Elements in Various Samples.	52
Table 4.2:	Rate Coefficients for Degradation of Congo Red by Cellulose Biochar/ TiO <sub>2</sub> -700 under Different Temperature.	68

## LIST OF FIGURES

Figure 1.1:	Figure 1.1: World Consumption of Synthetic Dyes in year 2017 (IHS, 2018).	3
Figure 2.1:	Molecular Structure of Cellulose (Trache, et al., 2016).	14
Figure 2.2:	Band Gap Energy of Some Metal Oxide Semiconductors on Potential Scale (V) against Normal Hydrogen Electrode (NHE) (Lee, Jung and Kang, 2017).	16
Figure 2.3:	Crystalline Structure of TiO <sub>2</sub> (a) Anatase, (b) Brookite, (c) Rutile (Khatee and Kasiri, 2010).	17
Figure 2.4:	General Mechanism of Photocatalyst Degradation Reactions in The Presence of TiO <sub>2</sub> (Zangeneh, et al., 2014).	27
Figure 3.1:	Overall Flowchart for Research Activities.	37
Figure 3.2:	Experimental Setup Diagram (1) Retort Stand with Clamp, (2) Power Socket Adaptor, (3) Fluorescent Bulb, (4) Aluminium Foil, (5) Beaker, (6) Magnetic Stir Bar, (7) Hot Plate Magnetic Stirrer.	38
Figure 4.1:	XRD Patterns for (a) Pure TiO <sub>2</sub> , Cellulose Biochar/ TiO <sub>2</sub> Composite at Various Calcination Temperature (b) 300 °C, (c) 500 °C, (d) 700 °C, (e) 900 °C and (f) Cellulose Biochar.	49
Figure 4.2:	SEM Images of (a) Pure TiO <sub>2</sub> , Cellulose Biochar/ TiO <sub>2</sub> Composite at Various Calcination Temperature (b) 300 °C, (c) 500 °C, (d) 700 °C, (e) 900 °C and (f) Cellulose Biochar.	51
Figure 4.3:	FTIR Patterns for (a) Pure TiO <sub>2</sub> , Cellulose Biochar/ TiO <sub>2</sub> Composite at Various Calcination Temperature (b) 300 °C, (c) 500 °C, (d) 700 °C, (e) 900 °C and (f) Cellulose Biochar.	53
Figure 4.4:	TGA Curves for all Samples.	54

Figure 4.5:	Zeta Potential Patterns for Pure TiO <sub>2</sub> , Cellulose Biochar/ TiO <sub>2</sub> -700 and Cellulose Biochar.	55
Figure 4.6:	Photocatalytic Degradation of Congo Red by TiO <sub>2</sub> , Cellulose Biochar/ TiO <sub>2</sub> Composite at Various Calcination Temperature and Cellulose Biochar (Catalyst Dosage = 0.5 g/L, Initial Dye Concentration = 10 mg/L, Solution Temperature = 30 °C, Reaction Time = 60 minutes, Initial pH = 7).	56
Figure 4.7:	Effect of Catalyst Dosage on the Photocatalytic Degradation of Congo Red in the Presence of Cellulose Biochar/ TiO <sub>2</sub> -700 (Initial Dye Concentration = 10 mg/L, Solution Temperature = 30 °C, Reaction Time = 60 minutes, Initial pH = 7).	58
Figure 4.8:	Effect of pH on the Photocatalytic Degradation of Congo Red in the Presence of Cellulose Biochar/ TiO <sub>2</sub> -700 (Catalyst Dosage = 0.5 g/L, Initial Dye Concentration = 10 mg/L, Solution Temperature = 30 °C, Reaction Time = 60 minutes).	59
Figure 4.9:	Effect of PMS Dosage on the Photocatalytic Degradation of Congo Red in the Presence of Cellulose Biochar/ TiO <sub>2</sub> -700 (Catalyst Dosage = 0.5 g/L, Dye Concentration = 10 mg/L, Solution Temperature = 30 °C, Reaction Time = 30 minutes, Initial pH = 5).	61
Figure 4.10:	Effect of Initial Dye Concentration on the Photocatalytic Degradation of Congo Red in the Presence of Cellulose Biochar/ TiO <sub>2</sub> -700 (Catalyst Dosage = 0.5 g/L, PMS Dosage = 0.3 mM, Solution Temperature = 30 °C, Reaction Time = 30 minutes, Initial pH = 5).	62
Figure 4.11:	Effect of Solution Temperature on the Photocatalytic Degradation of Congo Red in the Presence of Cellulose Biochar/ TiO <sub>2</sub> -700 (Catalyst Dosage = 0.5 g/L, PMS Dosage = 0.3 mM, Dye Concentration = 10 mg/L, Reaction Time = 5 minutes, Initial pH = 5).	63

Figure 4.12:	Photocatalytic Degradation of Type of Organic Dyes by Cellulose Biochar/ TiO <sub>2</sub> -700 (Catalyst Dosage = 0.5 g/L, PMS Dosage = 0.3 mM, Dye Concentration = 10 mg/L, Solution Temperature = 30 °C, Reaction Time = 30 minutes, Initial pH = 5).	64
Figure 4.13:	Photocatalytic Degradation of Congo Red by Fresh and Reuse Cellulose Biochar/ TiO <sub>2</sub> -700 (Catalyst Dosage = 0.5 g/L, PMS Dosage = 0.3 mM, Dye Concentration = 10 mg/L, Solution Temperature = 30 °C, Reaction Time = 30 minutes, Initial pH = 5).	66
Figure 4.14:	Pseudo Second-Order Reaction Kinetics Plot for Photocatalytic Degradation of Congo Red.	67
Figure 4.15:	Arrhenius Plot of $k_{app}$ against 1/T.	69
Figure 4.16	The COD Removal Efficiency of Congo Red by the Cellulose Biochar/ TiO <sub>2</sub> -700 and PMS, Cellulose Biochar/ TiO <sub>2</sub> -700 and Photolysis (only visible light).	70

## LIST OF SYMBOLS / ABBREVIATIONS

$A_0$	pre-exponential factor, $\frac{L}{mg \text{ min}}$
$C$	concentration of the dye, $\frac{mg}{L}$
$C_1$	stock solution's concentration, $\frac{g}{L}$
$C_2$	diluted solution's final concentration, $\frac{g}{L}$
$C_0$	initial dye concentration, $\frac{mg}{L}$
$C_t$	dye concentration at time $t$ , $\frac{mg}{L}$
$E_a$	activation energy, $\frac{kJ}{mol}$
$k$	reaction rate constant, $\frac{mg}{L \text{ min}}$
$k_0$	apparent pseudo zero-order rate constant, $\frac{mg}{L \text{ min}}$
$k_1$	apparent pseudo first-order rate constant, $\frac{1}{min}$
$k_2$	apparent pseudo second-order rate constant, $\frac{L}{mg \text{ min}}$
$k_{app}$	second-order rate constant, $\frac{L}{mg \text{ min}}$
$K$	shape factor, 0.89
$K_a$	adsorption coefficient of the dye, $\frac{L}{mg}$
$L$	average crystalline size, nm
$r$	oxidation rate of the dye, $\frac{mg}{L \text{ min}}$
$R$	ideal gas constant, $8.314 \frac{kJ}{mol \text{ K}}$
$t$	reaction time, $min$
$T$	absolute temperature, $K$
$V_1$	stock solution's volume, L
$V_2$	diluted solution's final volume, L
$\beta$	full width at half maximum (FWHM), $^\circ$
$\theta$	Bragg diffraction angle, $^\circ$
$\lambda$	wavelength of X-ray, nm
AOP	advanced oxidation processes
APCVD	atmospheric pressure chemical vapour deposition

BET	brunauer-emmett-teller
CB	conduction band
COD	chemical oxygen demand
CVD	chemical vapour deposition
-CH <sub>2</sub> OH	methylol group
EFB	empty fruit bunch
$e^-$	electron
Fe <sup>2+</sup>	ferrous iron
Fe <sub>2</sub> O <sub>3</sub>	iron (III) oxide
FTIR	fourier transformed infrared
HCl	hydrogen chloride
HO <sub>2</sub> <sup>·</sup>	hydroperoxyl radical
H <sub>2</sub> O <sub>2</sub>	hydrogen peroxide
HPCVD	hybrid physical chemical vapour deposition
HSC	hemp stem biochar carbon
$h^+$	positive hole
$h\nu$	photons energy
ICP-OES	inductively coupled plasma-optical emission spectroscopy
MOCVD	metal organic chemical vapour deposition
NaClO <sub>2</sub>	sodium chlorite
NaOH	sodium hydroxide
NHE	normal hydrogen electrode
O <sub>2</sub> <sup>·-</sup>	superoxide radical anions
O <sub>3</sub>	ozonation
•OH	hydroxyl radical
PMS	potassium peroxymonosulfate
SEM-EDX	scanning electron microscopy-energy dispersive X-ray analysis
SnO <sub>2</sub>	tin dioxide
TGA	thermogravimetric analysis
TiO <sub>2</sub>	titanium dioxide
TOC	total organic carbon
TTIP	titanium (IV) isopropoxide
UV	ultraviolet

V	potential scale
VB	valence band
WO <sub>3</sub>	tungsten trioxide
XRD	X-ray diffraction
ZnO	zinc oxide



**LIST OF APPENDICES**

APPENDIX A: EDX Analysis	91
APPENDIX B: Preparation of Various Concentrations of Organic Dyes	92
APPENDIX C: Calibration Curve of Congo Red	94
APPENDIX D: Reaction Kinetics Plot	95

## CHAPTER 1

### INTRODUCTION

#### 1.1 Textile Pollution

About 70 % of the earth's surface consists of water, which indicates that water is one of the most precious natural resource to human beings and environment (Chanwala, et al., 2018). However, demographic changes and urbanization, climatic conditions, economic growth and social, industrialization and cultural values contribute to the reduction of the availability of water sources as well as to pollute the water (Proskuryakova, Saritas and Sivaev, 2017). There are two sources of pollutant, which are point source, and non-point source. Point source are industrial discharges or sewage from treatment plants which can be identified from a specific location. On the other hand, non-point source is usually more intermittent and characterised by many sources such as runoff from agricultural lands (Masters, 2013).

In 21<sup>st</sup> century, industrialisation is the primarily factor that causes pollution to increase in various water sources. Industrial processes usually used different type of chemicals in their production pathways and causing water pollution. The textile and dyeing industries discharge about 280 000 tons of textile dyes annually worldwide (Chanwala, et al., 2018). The processes in textile industries such as desizing, bleaching, mercerizing, dyeing, printing and finishing the products produce variety of organic and inorganic pollutants which will be discharge into the nearby rivers (Tara, et al., 2019). The amount of textile dyeing wastewater is related to the degree of fixation of dye in the fibres type because the binding of dye in fibres relay on how well the textile fibres form bonding with the dye (Carmen and Daniela, 2012). According to Saini (2017), the strongest bond formation is covalent bond that occurs when both fibres and dye have opposite charges. Table 1.1 depicts the degree of fixation for different dye classes on fibres. The reactive dye shows the highest percentage loss in effluent due to reactive dye undergoes hydrolysis when react with water indicated that they do not have any affinity between the products and fibres (Saini, 2017).

Table 1.1: Degree of Fixation of Different Dye Classes on Fibres (Carmen and Daniela, 2012).

<b>Dye class</b>	<b>Fibre type</b>	<b>Degree of fixation (%)</b>	<b>Loss in effluent (%)</b>
<b>Acid</b>	Polyamide	80-95	5-20
<b>Basic</b>	Acrylic	95-100	0-5
<b>Direct</b>	Cellulose	70-95	5-30
<b>Disperse</b>	Polyester	90-100	0-10
<b>Metal complex</b>	Wool	90-98	2-10
<b>Reactive</b>	Cellulose	50-90	10-50
<b>Sulphur</b>	Cellulose	60-90	10-40
<b>Vat</b>	Cellulose	80-95	5-20

Most of the textile industries are based on chemical wet processing operation which required high demand of fresh water for operation. Table 1.2 illustrates the typical water usage in textile wet processing for 1 kg of woven fabrics (Judd and Jefferson, 2003). As a result, textile industries generate huge amount of wastewater compared to other industries because pollution load is added to the water from degree of fixation as well as removal of impurities from the fibres (Judd and Jefferson, 2003). Wastewater from textile industries involve variable pH, dark colour, high chemical oxygen demand (COD) and total organic carbon (TOC) (Hossain, Sarker and Khan, 2018). Textile dyeing wastewater was found to be carcinogenic, tremendously harmful pollutants as well as deteriorate the water quality that affecting human beings, wildlife, and other biodiversity (Liang, et al., 2018). Hussain, et al. (2015) stated that congenital malformations, lungs problem, skin irritations, nausea and headaches are problems when human interacted with textile dye. About 50 % of world textile industry wastewater is contributed by Asian countries, where China and India produced about 10 % and 35 % of organic pollutants respectively. Textile pollution has been raising awareness in China, Bangladesh, India, and also, Malaysia as many reports have been published in Asian countries regarding water pollution caused by textile dye (Ito, et al., 2016).

Table 1.2: Typical Water Usage in Textile Wet Processing for 1 kg of Woven Fabrics (Judd and Jefferson, 2003).

Subcategory	Minimum (L/kg)	Maximum (L/kg)
Simple processing	12.5	275.2
Complex processing	10.8	276.9
Complex processing plus desizing	5.0	507.9

## 1.2 Dye Production and Classifications

Dyes are manufacture over 700 000 tons each year globally and there are more than 100 000 different type of commercially available dye (Zhou, et al., 2019). The rapid growth of dye production industry is due to the demand of synthetic dyes for textile, paper and printing, paints, cosmetics and pharmaceuticals (Chanwala, et al., 2018). Figure 1.1 shows that China is the largest consumer for synthetic dye where their consumption about 40 – 50 % of the world production capacity (IHS, 2018).

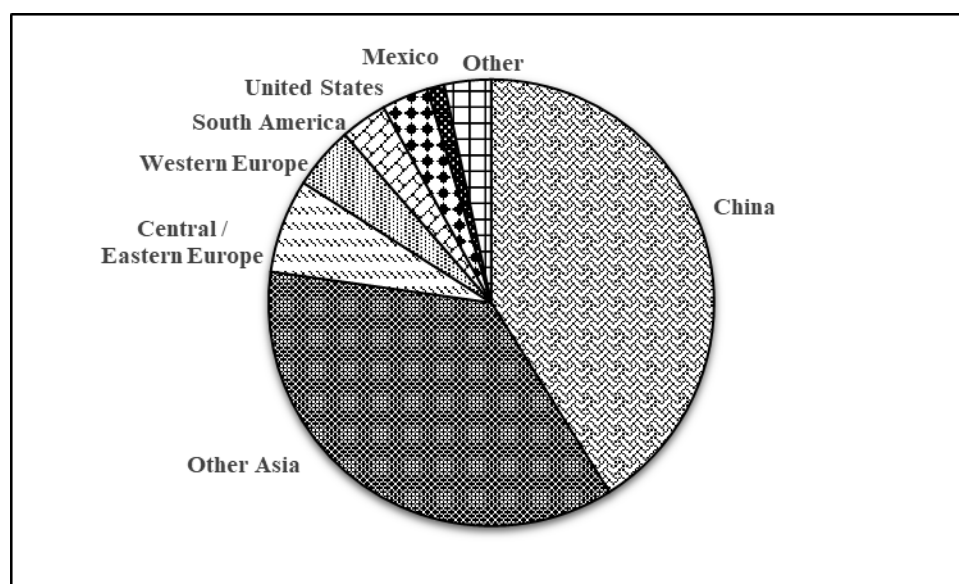


Figure 1.1: World Consumption of Synthetic Dyes in year 2017 (IHS, 2018).

The two main component that differentiate dye from other chemical components are chromophore and auxochrome. Chromophore is a chemical component that give colour for dye while auxochrome assists chromophore to

enhance colour appearance (Christie, 2015). Thus, dyes have affinity toward substrates as well as water soluble (Guerra, et al., 2019). Dye can be categorised based on their application of dye and molecular structure. Table 1.3 portrays the properties and applications for different classes of dye. There are many classes of dye such as direct dye, vat dye, sulphur dye, reactive dye, disperse dye, acid dye, azo dye and basic dye (Pavithra, et al., 2019). Among all these classes of dyes, Azo dyes are the brightest and highest colour intensity that account for 60 – 70 % of the dye groups (Ghaly, et al., 2014).

Table 1.3: Properties and Applications for Different Classes of Dye (Pavithra, et al., 2019).

<b>Dye class</b>	<b>Properties</b>	<b>Applications</b>
<b>Direct dye</b>	Water soluble	Cellulose, cotton and blended fibers
<b>Vat dye</b>	Water insoluble	Cellulose, cotton and blended fibers
<b>Sulphur dye</b>	Water insoluble	Cellulose fiber and cotton
<b>Reactive dye</b>	Water soluble	Fabric and cellulosic fiber
<b>Disperse dye</b>	Water insoluble	Synthetic fibers, nylon, Vylene and velvet
<b>Acid dye</b>	Water soluble	Synthetic fibers, silk, wool and paper
<b>Azo dye</b>	Water insoluble	Pigments and printing inks
<b>Basic dye</b>	Water soluble	Wool, cotton and silk.

### 1.3 Dye Removal Methods

Textile industries used various type of dyes and chemical additives during the processes of dyeing and finishing (Hussain, 2015). The utilisation of dye molecules raise concern among human beings because of their visible colour and some raw materials of synthetic dyes are toxic (Pekakis, Xekoukoulotakis and Mantzavinos, 2006). There are various types of wastewater treatment methods such as physical, chemical, biological processes and advanced oxidation processes (AOP) to remove organic dyes (Chen, et al., 2018).

Physical treatment methods to remove organics dyes include adsorption, filtration and ion exchange. For the preliminary, adsorption is used in wastewater treatment due to the capability to decolourise variety of organic dyes.

Adsorption is a phase transfer process which able to remove organic dye molecule from gases phase or liquid phase on the surface of a solid (Worch, 2012). Adsorbent is referred to the solid that performed adsorption process while adsorbate is the compounds that will be adsorbed. Chiban, et al. (2011) claimed that several low-cost materials acted as adsorbents such as wood charcoal, red mud, tree bark, coca shells and others had been used to remove organic dyes. The main factor of adsorption method is the adsorption capacity of the adsorbent as it determined how well the performance of the adsorbent at equilibrium condition (Jadhav and Srivastava, 2013). The adsorption efficiency can also be affected by contact time between the adsorbent and dye, solution temperature, pH of solution and dye concentration (Katheresan, Kansedo and Lau, 2018). Worch (2012) stated that the most efficient adsorbent was activated carbon due to its characteristic of adsorption mainly related to the van der Waals forces as well as high adsorption capacity.

Researchers have been adopted different types of filtration processes to treat wastewater in textile industries such as micro-filtration, ultra-filtration, nano-filtration and reverse osmosis (Laqbaqbi, et al, 2019). Filtration methods mentioned above can be used for recycling and filtering of pigment rich, bleaching and mercerising wastewater (Verma, Dash and Bhunia, 2012). Laqbaqbi, et al. (2019) claimed that the drawback of ultra-filtration is low rejection factors while nano-filtration and reverse osmosis are restricted by high osmotic pressure when high concentration condition occur. Cinperi, et al. (2019) stated that nano-filtration is the most appropriate in colour removal as nano-filtration has been achieved 97 % of colour removal performance. Moreover, membrane separation process is also an alternative to treat wastewater due to its capability to remove low molecular weight organic pollutants (Isik, et al., 2019). However, fouling of membrane occur when the foulants accumulative on the surface or in the membrane which will greatly decrease the permeability and selectivity of the membrane (Pavithra, et al., 2019).

Ion exchange is also one of wastewater treatment methods which enables the removing of opposite dye ions based on the strong affinity of resins to the ions (Zhang, et al, 2019). Hassan and Carr (2018) stated that ion exchange adsorbents are used in ion exchange process to bind with the opposite charge

ions. Ion exchange is very selective as only anion exchange resin can bind with anionic reactive dyes and resins have no effect on treating the textile effluent (Hassan and Carr, 2018). The merits of ion exchange process are affordable, eco-friendly and resistant to high temperature (Kaur and Jindal, 2018). On the other hands, inorganic ion exchanger has low chemical and mechanical strength while organic ion exchanger sensitive to thermal property (Kaur and Jindal, 2018).

Chemical coagulation and flocculation are chemical processes which requires addition of coagulant to change the physical condition so that suspended or dissolved substances can be settled in the sedimentation tank (Verma, Dash and Bhunia, 2011). The textile effluent consists of colour colloid particle which is too small that cannot be separated out by using simple gravitational methods. Thus, the addition of coagulants such as aluminium sulphate, aluminium chloride, ferric sulphate, ferric chloride, lime, ferrous sulphate and etcetera are utilised during chemical coagulation process (Saini, 2017). Coagulants act as a neutraliser to neutralise charge of the dye molecules so that the organic dye compounds can agglomerate to form large floc before settling down by gravitational force (Saini, 2017). Pavithra, et al. (2019) stated that coagulation method is less expensive and can deal with large initial concentration of organic dyes. However, the disadvantages of coagulants which may affect human health like cancer and Alzheimer (Pavithra, et al., 2019).

Another method of treating textile wastewater is biological process which can be classified into anaerobic and aerobic condition (Holkar, et al., 2016). Anaerobic condition is the absence of oxygen during textile wastewater treatment, whereas aerobic process involve the presence of oxygen (Holkar, et al., 2016). Both anaerobic and aerobic methods can use microbes for treating effluent such as bacteria, fungi and algae (Isik, et al., 2019). Metabolic or adsorption pathways together with microbes is the key to degrade dye which it will be converted into carbon dioxide, water and inorganic salts (Pavithra, et al., 2019). Activated sludge or flocculated are used to treat low concentrated wastewater which consists of vat, direct, disperse and basic dyes (Pazdzior, et al., 2017). Anaerobic process is comparative better than aerobic process in term of degradation of azo dye as the sulfonic and nitro groups of azo dyes are

recalcitrant (Carmen and Daniela, 2012). The merits of biological process are eco-friendly, less sludge production, less consumption of water compared to physical and oxidation process and cost competitive (Holkar, et al., 2016). Isik, et al. (2019) claimed that the discharge textile effluent treated by biological process usually does not meet the standard required by department of environment. Moreover, large reactor volume and longer retention is needed in fungal treatment of textile wastewater which will greatly affects the treatment process (Isik, et al., 2019).

Furthermore, chemical oxidations process such as ozonation ( $O_3$ ) is an efficient process to treat textile effluent due to ozone is a strong oxidising agent which can be used to decolourise dye molecule (Bilinska, et al., 2019). Pazdzior, et al. (2017) stated that ozonation process is strongly depend on the pH value which it can be separated into two pathways. At acidic pH, ozone is target to attack electrophilic compounds that consist of aromatic structure and amine groups (Liang, et al., 2018). Hence, double bond chromophores of azo dye that corresponded to dye colour is easily being attacked by ozone. This indicated that auxiliary agents do not affect ozonation of textile wastewater (Bilinska, et al., 2019). Under basic conditions, complex chain mechanism take place instead of direct ozonation as ozone decomposes rapidly to form hydroxyl radical that responsible for degradation of organic compounds (Pazdzior, et al., 2017). However, ozone is usually used along with chemicals like hydrogen peroxide ( $H_2O_2$ ) or sodium hypochlorite, or with UV radiation because low mineralisation rate of COD and generation of toxic by-products during the treatment of ozonation (Asgari, et al., 2019).

Finally, yet importantly, advanced oxidation processes (AOP) is also one of most appropriate methods to treat wastewater that contain of recalcitrant organic compounds. AOP is a technique that generated hydroxyl radical ( $\bullet OH$ ) that responsible for the decomposition of the recalcitrant organic compounds into carbon dioxide and water (Cetinkaya, et al., 2018). Fenton and photocatalysis process are the most common methods in AOP. Fenton process can be express as a process that produced hydroxyl radical when ferrous iron ( $Fe^{2+}$ ) reacts with  $H_2O_2$  and undergoes decomposition in acidic condition (Sreeja and Sosamony, 2015). The iron (II) ions are being oxidised to iron (III)



ions during the oxidising reaction (Sreeja and Sosamony, 2015). Photo-Fenton processes had been discovered as an alternative technique for Fenton process with the used of visible radiation or ultraviolet, which can increase the generation of hydroxyl radical (Brito, et al., 2019). The major merits of this method are effective decomposition of organic pollutants and easy to be operated (Bello, Raman and Asghar, 2019). The drawbacks of Fenton process include the generation of large amount sludge, requirement of acidic environment during decomposition of hydrogen peroxide and catalyst is no recyclable (Mahamallik and Pal, 2017).

#### **1.4 Problem Statement**

Shanmugarjah, et al. (2019) claimed that Malaysia is the second largest producer of palm oil in the world. To simplify, by 2020, there will be roughly 100 million tonnes of palm oil waste stockpiled in Malaysia (Shanmugarjah, et al., 2019). As a result, large amounts of biomass would create waste disposal problems as well as environmental issues (Okahisa, et al., 2018). Therefore, empty fruit bunch (EFB) of the palm oil is being converted to cellulose due to its unique properties such as high surface area, high cellulose content, low mechanical strength and moderate thermal properties (Cheng, et al., 2018). Cellulose then undergoes pyrolysis process to produce biochar which is a substitution for activated carbon with the difference that no activation process is done to the cellulose before pyrolysis as compared to the synthesis of AC (Delannoy, et al., 2018). Thus, this study focussed on the extraction of cellulose from EFB for the synthesis of biochar.

Pure metal oxides have several defects which will reduce photocatalytic activity such as high band gap energy, aggregate together to form large particle when high catalyst loading which reduce specific surface area availability, low adsorption capacity and high recombination charge carrier rate (Mishra, Mehta and Basu, 2018). Therefore, support such as biochar is being investigate to stabilise with pure metal oxide to improve photocatalytic degradation. Biochar has a large surface area and macropores which makes it appropriate for wastewater treatment that contains a variety of pollutant with varying size as compared to activated carbon which has micropores that could be easily blocked

by large organic dye (Hao, et al., 2018). Besides that, biochar is comparatively cheaper than activated carbon (Delannoy, et al., 2018). Thus, this study focussed on the cellulose biochar /TiO<sub>2</sub> at different calcination temperature.

Textile industry is the main cause of water pollution due to incomplete degree of fixation during manufacturing processes which leads to the discharge of synthetic dyes and harmful substances to the nearby water resource. The textile wastewater is high in colour in and contains toxic contaminants that can affect health of living organism as well as creating environmental problems (Liang, et al., 2018). Various conventional dye removal methods such as adsorption, filtration, ion exchange, biological methods, coagulation and flocculation have been employed (Chen, et al., 2018). However, all these conventional techniques only convert organic pollutant from water phase to liquid phase which additional treatments are required to treat the secondary pollutants (Ong, Ng and Mohammad, 2018). As a result, AOP such as photocatalysis process is invented to degrade recalcitrant organic dye by generating hydroxyl radicals that are strong oxidising agents for the oxidation of organic compounds into less harmful products such as carbon dioxide and water molecules. Photocatalysis involves the utilisation of visible light or ultraviolet radiation to overcome the band gap energy of the photocatalyst and produce high redox potential, ( $\bullet\text{OH} = 2.80 \text{ V}$ ) as compared to other oxidants like ozone (2.08 V) (Collivignarelli, et al., 2019). Thus, this study focussed on photocatalytic degradation of organic dyes under various operating parameters.

### **1.5 Aim and Objective**

The main goal of this research is to prepare metal oxide/ cellulose biochar composite for photocatalytic degradation of organic dye. Specific objectives of this research includes the following:

- i. To extract and characterise cellulose from oil palm EFB.
- ii. To synthesis and characterise cellulose biochar/ TiO<sub>2</sub> composites at different calcination temperatures.
- iii. To study the process behaviour of the photocatalytic degradation of organic dye in the presence of cellulose biochar/ TiO<sub>2</sub> composites.

## **1.6 Scope and Limitation of the Study**

The research is focussed on the extraction of cellulose oil palm EFB, followed by carbonisation at various temperatures to form biochar. Titanium dioxide ( $\text{TiO}_2$ ) is used as a metal oxide photocatalyst throughout the whole experiment. The process behaviour of the photocatalytic degradation of organic dye using cellulose biochar/  $\text{TiO}_2$  composite at different temperatures will be studied accordingly. Pure biochar,  $\text{TiO}_2$  composite materials will be characterised to determine their crystallinity content, surface morphology, chemical elemental composition, functional group and thermal stability using X-ray diffraction (XRD), scanning electron microscopy- energy dispersive X-ray analysis (SEM-EDX), Fourier transformed infrared (FTIR) spectroscopy, Thermogravimetric analysis (TGA) analyses and zeta potential analyses respectively. Various parameters will be tested in this research such as various types of organic dyes, catalyst dosage, oxidant dosage, initial dye concentration, pH and temperature of solution.

## **1.7 Outline of the Report**

The report is divided into 5 Chapter. Chapter 1 covers the textile pollution, dye production and classification as well as dye removal methods. The problem statement clearly stated all the problems for this research. The aim and objective list out the problems that need to be investigated and tackled throughout this study. The scope and limitations describe the details of the research work in this study.

Chapter 2 consists of literature reviews on the biomass, metal oxide photocatalysts, synthesis methods of cellulose biochar /  $\text{TiO}_2$ , characterisation study, photocatalysis mechanism as well as effect of parameters on the photocatalytic degradation.

Chapter 3 provides information about the research methodology. All the chemical reagents and equipment used are listed in this chapter. The details for preparation of the cellulose biochar/  $\text{TiO}_2$  composites are described. The experimental setup and characterisation of the catalyst are also being described.

Chapter 4 discussed the results of this research. It consists of the characterisation of catalyst, the parameter that affect the photocatalytic degradation, kinetic study as well as reusability study of catalyst.

Chapter 5 conclude the summary of the entire research. It makes conclusion and recommendation for future work related to the results obtained.

## CHAPTER 2

### LITERATURE REVIEW

#### 2.1 Biomass

In 21<sup>th</sup> century, fossil fuels such as coal and oil have been depleted due to the extensive usage which also bring a lot of environmental issues. Therefore, biomass is the alternative resource to replace fossil fuel as it is a renewable energy source to produce biofuels and bioenergy (Hammed, et al., 2019). Biomass can come from different type of sources which, include agriculture residues like rice straw, cotton stalk, palm oil residue and forest residue such as wood chips, bark and sawdust (Mehrpooya, Khalili and Sharifzadeh, 2018). EFB from palm oil has received a great attention as a biomass source due to about 100 million tonnes of palm oil wastes is being produced in Malaysia by 2020 (Shanmugarjah, et al., 2019). Besides that, EFB contains about 37.3 – 46.5 % cellulose and 25.3 – 33.8 % hemicellulose make it a possible source for the extraction of cellulose (Mohamad, 2018). Pyrolysis is one of the commonly thermal decomposition technology to convert biomass to more useful components like bio-oil, biochar, and biogas. Activated carbon is also one of the derivative from biomass that it is utilised in degradation organic dyes.

##### 2.1.1 Cellulose

Cellulose is being considered as renewable biopolymer due to the availability of cellulose components in biomass (Gopi, et al., 2019). Cellulose is biodegradable, cheap, water insoluble and appear white at pure condition. Nowadays, cellulose is being extracted out from various type of biomass wastes due to the availability and also to reduce the disposal treatment needed for wastes (Okahisa, et al., 2018). Table 2.1 shows the different type of raw materials such as coconut shell, corn stalk, mango pit seed, palm oil mesocarp, palm oil EFB and palm oil kernel shell with their respective composition of cellulose, hemicellulose and lignin. Although Table 2.1 shows the amount of cellulose contains in the respective raw material, the extracted amount is usually less than the exact amount due to ineffective extraction methods and also short life time of the resource (Trache, et al., 2016). One of methods to extract out the

cellulose constituents from biomass is chlorite method. Unfortunately, chlorite method is not a green method, so autoclave-based and ultra-sonication are being invented to recently (Abdullah, et al., 2016).

Table 2.1: Composition of Cellulose, Hemicellulose and Lignin in Different Types of Raw Materials.

<b>Raw material</b>	<b>Cellulose (%)</b>	<b>Hemicellulose (%)</b>	<b>Lignin (%)</b>	<b>Reference</b>
<b>Coconut shell</b>	19.8	68.7	30.1	Daud and Ali (2004)
<b>Corn stalk</b>	42.4	29.6	21.7	Lv and Wu (2012)
<b>Mango pit seed</b>	14.5	52.4	3.8	Elizalde-Gonzalez and Hernandez-Montoya (2007)
<b>Palm oil mesocarp</b>	39.7	15.0	31.4	Okahisa, et al. (2018)
<b>Palm oil EFB</b>	38.7	31.0	25.6	Okahisa, et al. (2018)
<b>Palm oil kernel shell</b>	25.4	27.5	38.7	Okahisa, et al. (2018)

Cellulose is a polysaccharide as it made up of glucose monomers to form long chain polymer as shown in Figure 2.1. The size of the cellulose is depends on the number of the anhydroglucose units present in the cellulose structure (Trache, et al., 2016). For each anhydroglucose, it consists of three hydroxyl group attached to different carbon atoms, a C-6 carbon attached to methylol group (-CH<sub>2</sub>OH) with two C-2 and C-3 carbon atoms (Gopi, et al., 2019). The hydroxyl group plays a very important role in the crystallisation of the cellulosic chain as it helps to form hydrogen bonds (Gopi, et al., 2019). Cellulose fibre is the combination of a group micro-fibril that, generated by a bundle of cellulosic chain (Trache, et al., 2016). Each cellulosic chain consists of a reducing end that

has carbonyl functional group and a non-reducing end with hydroxyl attached to its C-4 carbon atom. The crystalline and amorphous structure of cellulose is closely related to the hydrogen bonding and Van der Waals force of attraction (Trache, et al., 2016). Klemm (1988) stated that cellulose shows the following properties such as non-toxic, adsorbent for organic dye, hydrophilic and harmless to environment because it can undergo decomposition process to break down the structure. However, cellulose shows low adsorption capability as compared to biochar and activated carbon (Wu, Cheng and Ma, 2011).

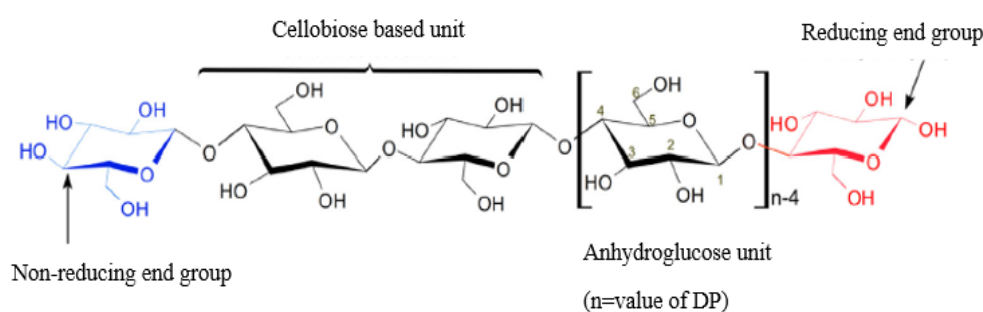


Figure 2.1: Molecular Structure of Cellulose (Trache, et al., 2016).

### 2.1.2 Biochar

Biochar is a carbon rich solid which resulted from a thermal treatment of biomass in the absence or little oxygen environment (Dai, et al., 2019). Biochar has large specific surface area, high porosity structure and functional groups like carbonyl and hydroxyl which made biochar as a good adsorbent to remove various type of contaminants from wastewater (Mayakaduwa, et al., 2015). The contaminants are organic dyes, heavy metals and pharmaceuticals (Mayakaduwa, et al., 2015). Therefore, biochar is being used in textile industry for the removal of organic dyes due to its economically and environmentally friendly characteristics (Mui, et al., 2010). Generally, biochar is produced from biomass through slow pyrolysis at temperature range from 200 – 700 °C with heating rate of 10 °C/min (Li, et al., 2014). Fast pyrolysis method is not suitable in biochar production due to high temperature condition, high heating rate and short residence time to promote the formation of biofuel instead of biochar (Elkhalifa, et al., 2019). Hence, temperature and residence time are the most important factors that affect the biochar yield during pyrolysis as gasification of

biochar might occur to form gaseous fuels which result in the reduction amount of biochar (Kong, et al., 2014). The surface area of the biochar did not show obvious change at calcination temperature before 400 °C, started to increase steeply from 400 – 500 °C and followed an upward trend until 900 °C before destruction (Chen, et al., 2017). Fu, et al. (2009) stated that the decrease of surface area was mainly due to the widening of pore, structural ordering and coalescence of adjacent pore which, result in the destruction of the porous structure of biochar.

### **2.1.3 Activated Carbon**

Activated carbon is being widely studied due to its unique properties. Activated carbon has a large specific surface area and high porosity structure which, made it a good adsorbent for various type of organic substances (Suhas, et al., 2016). Moreover, activated carbon consists of weak Van der Waals force of attraction which aid in the adsorption of organic pollutants (Worch, 2012). Therefore, activated carbon is being widely used in wastewater treatment industry especially during the removal of organic components due to its high adsorption capacity. Activated carbon is obtained from the carbonization of biomass followed by activation process in order to activate the carbon atoms which make it different from biochar as biochar does not undergoes activation process (Delannoy, et al., 2018). There are two type of activation methods which are physical and chemical activations (Suhas, et al., 2016). Activated carbon which has a higher microporous structure than biochar might lead to the blockage of large organic dyes molecules (Hao, et al., 2018). Activated carbon is comparatively expensive than biochar as activated carbon required additional step to activate the carbonized materials (Delannoy, et al., 2018).

## **2.2 Metal Oxide Photocatalysts**

Recently, the application of metal oxide semiconductors in heterogeneous photocatalysis to degrade recalcitrant organic dyes have been investigated by many researchers. Several types of metal oxides that commoly used in heterogeneous photocatalysis are titanium dioxide (TiO<sub>2</sub>), zinc oxide (ZnO), tungsten trioxide (WO<sub>3</sub>), tin dioxide (SnO<sub>2</sub>) iron (III) oxide (Fe<sub>2</sub>O<sub>3</sub>) and others (Carp, Huisman and Reller, 2004). A few important criteria that determine the



capability of catalytic activities during photocatalysis process include band gap energy, surface morphology, surface area and pore volume (King Saud University, 2015). Band gap energy of metal oxides is the most crucial properties in photocatalysis as it indicated the lowest energy needed to excite the electrons (Gomis-Berenguer, et al., 2016). To simplify, electrons can only be promoted from the valence band (VB) to conduction band (CB) if the photons provided by the ultraviolet (UV) irradiation or visible light is higher or equal to the band gap energy required by the particular metal oxide (Carp, Huisman and Reller, 2004). Besides, the recombination rate of electrons and holes also affected by the band gap energy which, greatly reduce photocatalytic reaction between the radical and organic dyes (Gomis-Berenguer, et al., 2016). Figure 2.2 shows the band gap energy of some metal oxide semiconductors on potential scale (V) against normal hydrogen electrode (NHE) (Lee, Jung and Kang, 2017). Based on Figure 2.2, CdSe has the lowest band gap energy among all the metal oxides which means lowest energy is need to excite the electrons. TiO<sub>2</sub> has slightly lower band gap energy than ZnO which is 3.2 eV.

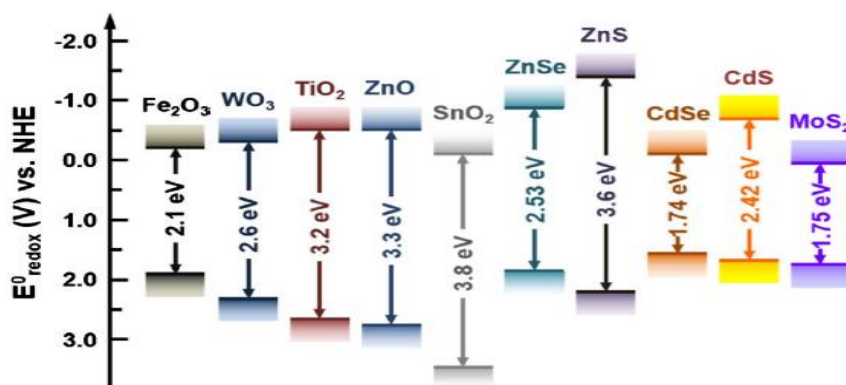


Figure 2.2: Band Gap Energy of Some Metal Oxide Semiconductors on Potential Scale (V) against Normal Hydrogen Electrode (NHE) (Lee, Jung and Kang, 2017).

### 2.2.1 Titanium Dioxide

Titanium dioxide (TiO<sub>2</sub>) is the most commonly used metal oxide photocatalysts due to its large availability, low cost, low toxicity, photocatalytic activity, environmental friendly, chemical inertness and corrosion resistance (Yang, et

al., 2014).  $\text{TiO}_2$  consists of three crystalline polymorphs which are anatase, brookite and rutile as shown in Figure 2.3 (Khatee and Kasiri, 2010). The basic structural unit for all these  $\text{TiO}_2$  crystalline forms is octahedron which composes of one titanium atom attached with six oxygen atoms. In anatase, the 4 edges of the octahedron are linked with other octahedron in a zigzag arrangement to form the crystalline structure. While in rutile, chain is formed by joining edge of octahedron and three dimensional shape is formed when chains linked together with oxygen atom corner. Brookite is having an orthorhombic structure by sharing of edges and corners of octahedral (Khatee and Kasiri, 2010). Both anatase and rutile are constructed with tetragonal shape while brookite is orthorhombic structure (Carp, Huisman and Reller, 2004).

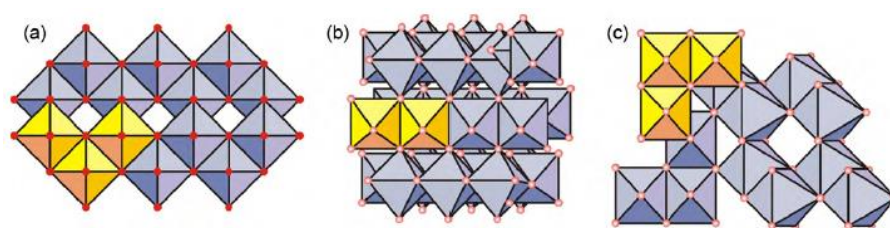


Figure 2.3: Crystalline Structure of  $\text{TiO}_2$  (a) Anatase, (b) Brookite, (c) Rutile (Khatee and Kasiri, 2010).

Among all these three crystalline structures anatase  $\text{TiO}_2$  is the most suitable candidate to be used during photocatalytic process (Allen, et al., 2018). Although anatase has a large energy band gap than rutile, which decrease the amount of light that can be absorbed but it increases electron oxidation power and enhance the transfer of electron to adsorbed molecules from  $\text{TiO}_2$  (Zangeneh, et al., 2014). Besides that, anatase has an indirect band gap instead of direct band gap in rutile. This property is important in photocatalysis as it inhibits the recombination rate of electron-hole pair so that anatase has a longer charge carrier lifetime to degrade the organic dye compounds (Fisher, et al., 2017). Even though brookite is considered as the most active phase it does not being applied in photocatalytic activity due to the difficulty to prepare high purity of brookite (Lee and Yang, 2005).

One of the main problem by using  $\text{TiO}_2$  as a photocatalyst is related to low solar photoconversion efficiency due to large band gap energy. The band

gap energies of anatase and rutile crystalline structure are 3.2 eV and 3.0 eV respectively (Colmenares, Varma and Lisowski, 2016). It indicated that only UV light with a wavelength less than 380 nm could be used to excite the electron from the VB to CB, which could be found less than 5 % of the solar energy (Colmenares, Varma and Lisowski, 2016). Cheng, et al. (2015) stated that visible light consists of 46 % of the solar spectrum. Therefore, various methods had been applied to lower the band gap of TiO<sub>2</sub> energy so that visible light can be used for photocatalytic activity.

The methods to improve visible light adsorption are doping process and dye sensitisation. Doping metals on TiO<sub>2</sub> had been studied all over the years to improve the catalytic activity of TiO<sub>2</sub> using visible light instead of UV light. The example of metals that usually doped on TiO<sub>2</sub> are copper, cobalt, nickel, manganese, iron, gold, silver and others (Dong et al., 2015). The metal-doped TiO<sub>2</sub> had a lower band gap energy as compared to pure TiO<sub>2</sub>, and low band gap energy is played an important role in photocatalytic degradation (Tran, et al., 2006). Besides, the presence of metal ions in the TiO<sub>2</sub> also aid in the decrement of the recombination rate for charge carriers because metal ions are being activated after absorbing enough photons (Tran, et al., 2006). Xu, Gao and Liu. (2002) stated that TiO<sub>2</sub> has a greater catalytic capacity when doping with rare earth metals due to the alternation of the surface properties of TiO<sub>2</sub>. The dopant ion concentration is related to the photocatalytic degradation. Excessive amount of dopant concentration, the photocatalytic activity would decrease because the space charge region became narrow. This promote the recombination of electron-hole pair when the penetration of light is higher than the space charge region (Xu, Gao and Liu, 2002). Thermal instability of the metal-doped TiO<sub>2</sub> is one the drawback (Dong et al., 2015).

Besides, doping with non-metal on TiO<sub>2</sub> is also being investigated. The example of non-metal dopants are carbon, sulphur, nitrogen, phosphorus, boron and ecetera (Marschall and Wang, 2013). Non-metals have impurity states that close to the valence band edge of TiO<sub>2</sub> which charge carrier recombination (Dong et al., 2015). Non-metal doped TiO<sub>2</sub> also shows similar characteristics as metal doping such as swift of UV spectrum to visible light, reduction of band gap energy as well as improvement of catalytic capability. Visible light is still no practical in non-metal doped TiO<sub>2</sub> as the photocatalytic activity is relatively

low as compared to UV irradiation (Dong et al., 2015). Dye sensitisation is an alternative approach for metal and non-metal doping as the doping process required multiple steps and high temperature. Dye sensitisation is the adsorption of sensitisers on the  $\text{TiO}_2$  surface which modified the  $\text{TiO}_2$  affinity towards visible light. Organic dye molecule can reach its excited state when absorb in visible light (O'Regan and Gratzel, 1991). This followed by the transfer of electron from the excited dye to CB for the formation of charge carrier to mineralise recalcitrant organic dye molecule (O'Regan and Gratzel, 1991). To simply, it improved the efficiency of exciting the electron in VB. Zhao, Chen and Ma. (2005) stated that there is no chemical bonding between dye and  $\text{TiO}_2$  which mean dye can undergo desorption process that lead to a decrement in the photocatalytic efficiency. Organic dyes that used as sensitisers are Alizarian Red, Eosin, Ethyl ester of fluorescein, Rhodamine B and etcetera (Zhao, Chen and Ma, 2005).

$\text{TiO}_2$  coupling with other semiconductors such as ZnO,  $\text{SiO}_2$ ,  $\text{WO}_3$ ,  $\text{SnO}_2$ , MgO and others have been widely studied to increase the specific surface area of  $\text{TiO}_2$  and decrease the band gap energy (Silva-Castro, et al., 2017). Moreover, coupling with semiconductors could increase the range of wavelength spectrum that can use to excite the electron in the VB. ZnO is the most suitable semiconductor to couple with  $\text{TiO}_2$  because it has similar band gap energy around 3.3 eV as compared to 3.2 eV of  $\text{TiO}_2$  which result in similar photocatalytic degradation of organic dyes (Khaki, et al., 2017). Khaki, et al. (2017) stated that ZnO/  $\text{TiO}_2$  had a low recombination rate and longer charge carrier lifetime due to the high conductivity of ZnO while chemical stability of  $\text{TiO}_2$ . This system is generally called heterojunction photocatalyst system (Fagan et al., 2016).

Nano size  $\text{TiO}_2$  which could attain high surface area to volume ratio for better performance of photocatalytic degradation also created a lot of problems. Firstly, the difficulty to recover or reuse the  $\text{TiO}_2$  as it is too small to separate from the wastewater (Gomis-Berenguer, et al., 2016). Besides, nano size  $\text{TiO}_2$  tend to agglomerate form large particle size especially during high catalyst loading, which will greatly reduce the specific surface area available for the degradation of organic dyes (Mishra, Mehta and Basu, 2018). The supports such as glass beads, zeolite, silica gel, quartz, clay, activated carbon, biochar and

cellulose have the same characteristics which are high specific surface area, high porosity, strong adhesion force between support and  $\text{TiO}_2$ , strong adsorption capacity toward organic dyes (Shan, Ghazi, Rashid, 2010).

### **2.2.2 Other Type of Metal Oxides**

ZnO is an alternative metal oxide that can be used as photocatalyst. For ZnO has a band gap energy of 3.3 eV and might also show a better degradation efficiency over a broad solar spectrum (Khaki, et al., 2017). Besides, ZnO has the properties of high stability, good mechanical strength as well as high electron availability (Ong, Ng and Mohammad, 2018). ZnO with large specific surface area is beneficial for the adsorption of organic pollutants. Liang, et al. (2011) claimed that the price of nano size ZnO was about one quarter cheaper than  $\text{TiO}_2$ . It means that ZnO has potential to be used in heterogeneous photocatalysis process. However, ZnO has a rapid recombination for electron-hole pair due to its large band gap energy (Ong, Ng and Mohammad, 2018).

$\text{SnO}_2$  has a large band gap energy of 3.6 eV which can be excited by UV irradiation spectrum to produce free radical to degrade organic compounds to less harmful substances such as carbon dioxide or water molecules (Al-Hamdi, Rinner and Sillanpaa, 2017). Moreover, large specific surface area and porous structure of  $\text{SnO}_2$  contributed to for the excellent photocatalytic degradation (Zhao and Wu, 2017).  $\text{SnO}_2$  also has high stability and low toxicity properties. Wu, et al. (2009) claimed that  $\text{SnO}_2$  synthesised from amino acid could achieve a degradation of Rhodamine B close to 100 % after exposure to UV irradiation for 150 minutes. This indicated that  $\text{SnO}_2$  has a high catalytic activity in degradation of organic pollutants.

Szilagyi, et al. (2012) reported that  $\text{WO}_3$  was the second most researched metal oxide semiconductors after  $\text{TiO}_2$  due to its relatively small band gap range from 2.5 eV to 3.0 eV which can absorb visible light for the excitation of electron.  $\text{WO}_3$  played important factors in photocatalysis reaction (Szilagyi, et al., 2012). This means that photocatalytic degradation of organic dyes has a better performance in oxidised monoclinic  $\text{WO}_3$  than oxidised hexagonal  $\text{WO}_3$  (Szilagyi, et al., 2012). Besides,  $\text{WO}_3$  is large availability, non-toxicity, chemical and physical resistance as well as strong oxidation powder (Asim, et

al., 2014). On the other hands, pure  $\text{WO}_3$  has less light energy conversion efficiency than  $\text{TiO}_2$  due to its low reduction potential (Xu, et al., 2011).

### **2.2.3 Effect of Calcination Temperature**

Calcination temperatures of the cellulose biochar/  $\text{TiO}_2$  composite play an important role to determine its catalytic activity. The structure of biochar might undergo degradation when exposing to high temperature as biochar was usually prepared under low pyrolysis temperature (Chen, et al., 2017). Zhang, et al. (2017) stated that the crystalline structure of acid pretreated biochar (pBC) for pBC calcinated at temperature of 500 °C started to degrade compared to the sample calcinated at 300 °C or 400 °C which still maintain the original structure. Besides, high calcination temperature could cause the burning of carbon as well as aggregation of particle which reduce the specific surface area for photocatalytic degradation (Zhang et al., 2017). This low calcination temperature was needed to maintain the structure properties of the biochar.

Moreover, the crystalline structure of  $\text{TiO}_2$  would change from anatase phase to rutile during high calcination temperature which was not preferable for photocatalysis process (Allen, et al., 2018). Peng, et al. (2018) reported that hemp stem biochar carbon (HSC) doped  $\text{TiO}_2$  that calcinated at 700 °C, consisted of anatase and rutile phase due to the formation of burning between oxygen atom and titanium atom. In addition, high calcination temperature would cause the reduction in the absorption capability of visible light which indicated lower range of visible light need to be used for the photocatalysis reaction (Peng, et al., 2018). This could be explained by the formation of rutile phase at high calcination temperature which had less tendency for visible light absorption.

## **2.3 Synthesis Methods of Cellulose Biochar/ $\text{TiO}_2$**

There are various types of methods that have been developed over the years for the preparation of  $\text{TiO}_2$  composites include sol-gel, chemical vapour deposition (CVD) and hydrothermal.

Among all these methods sol-gel is the most commonly used technique to synthesis  $\text{TiO}_2$  composite (Shan, Ghazi, Rashid, 2010) Sol-gel is comparatively low cost than others preparation methods and can manipulate for various sizes and shapes morphology (Shan, Ghazi, Rashid, 2010). Sol-gel is

the formation of ceramic or inorganic polymers solution that undergoes transformation from liquid precursor to sol and lastly form a network structure named gel (Danks, Hall and Schnepf, 2016). Danks, Hall and Schnepf. (2016) reported that metal alkoxide precursor was underwent hydrolysis and condensation during the sol formation. The examples of precursors are titanium alkoxide, titanium tetrachloride, tetrabutyl titanate, titanium tetra-isopropoxide and etcetera. The gel was then being calcined at high temperature to obtain oxygen bridge between hydroxyl group of both biochar and  $\text{TiO}_2$  (Shan, Ghazi, Rashid, 2010). This improved the adhesions property between the biochar and  $\text{TiO}_2$ . The sol-gel method had been successful being applied to fabricate cellulose biochar/  $\text{TiO}_2$  using tetrabutyl titanate as precursor as reported by both Zhang and Lu. (2018) and Zhang, et al. (2017).

CVD is also another technique used to synthesis supported  $\text{TiO}_2$  composite. CVD process is usually carried out by injecting single or multicomponent volatile gaseous precursor to the support at high temperature and pressure under a vacuum chamber (Alhaji, et al., 2017). Thin film material will be deposit on the surface of the  $\text{TiO}_2$  when the volatile gaseous precursor undergoes decomposition (Alhaji, et al., 2017). The merits of utilised CVD are  $\text{TiO}_2$  can be deposited on the biochar regardless of shape or size of the substrate within a short period of time (Shan, Ghazi, Rashid, 2010). Moreover, CVD have high thermal stability and strong adhesion between biochar and  $\text{TiO}_2$  (El-Sheikh, et al., 2004). There are several types of CVD include metal organic chemical vapour deposition (MOCVD), atmospheric pressure chemical vapour deposition (APCVD) and hybrid physical chemical vapour deposition (HPCVD).

At last but not least, hydrothermal can also be used for the preparation of cellulose biochar photocatalyst. Hydrothermal method is utilised water as the reaction buffer to synthesis of  $\text{TiO}_2$  composite under low temperature-controlled system (Wong, Tan and Mohamed, 2011). Autoclave is usually being used in hydrothermal method as its provide a controlled temperature and pressure (Wong, Tan and Mohamed, 2011). Alhaji, et al. (2017) stated that temperature was a crucial factor during hydrothermal as it determined the immobilisation of the  $\text{TiO}_2$  on the biochar surface. When comparing hydrothermal method to sol-gel and CVD, hydrothermal do not required precursor as  $\text{TiO}_2$  can be

immobilised directly (Alhaji, et al., 2017). Chen, et al. (2019) reported that biochar/ ZnFe<sub>2</sub>O<sub>4</sub> had been successful synthesis using hydrothermal method.

## 2.4 Characterisation Study

Characterisation study plays an important role to determine the chemical properties and physical properties of the new fabricated catalyst. The chemical and physical properties can help researcher to understand better about the synthesised and to determine the catalytic activity. Therefore, XRD, SEM-EDX, FTIR and TGA were used to study the crystallinity content, surface morphology, chemical elemental composition, functional group and thermal stability of the synthesised catalysts.

XRD is commonly used to characterise the crystallographic structure, preferred orientation, and also crystallite size of the material. Diffraction occurred when the wavelength of the X-rays was identical with the interatomic distances of the crystalline solids (Trache, et al., 2016). The diffraction peaks are based on the crystalline structure of the particular material (Trache, et al., 2016). Diffraction peaks for anatase TiO<sub>2</sub> are at  $2\theta$  values of 25.36°, 37.91°, 48.16°, 54.05°, 55.20°, 62.86°, 68.97°, 70.48°, and 75.28° corresponding to (101), (004), (200), (105), (211), (204), (116), (220), and (215) (Yu, et al., 2018). Cai, et al. (2017) stated that there was no rutile phase with peak of  $2\theta = 27.48^\circ$  being detected for biochar/ TiO<sub>2</sub> calcined at 500 °C which proved. Rutile phase is not preferable in photocatalytic degradation as it has high recombination rate of electron-hole pairs and low adsorption capability towards organic dyes (Lisowski, et al., 2017). Besides, anatase TiO<sub>2</sub> has high electron mobility, low dielectric constant as well as low mass density (Lu, et al., 2019). The average crystallite size can be calculated using Scherrer equation as shown in Equation (2.1) (Cai, et al., 2017). Crystallite size plays an important role in the adhesion of TiO<sub>2</sub> on the cellulose biochar because the smaller crystalline size, the larger the surface area.

$$L = \frac{\kappa\lambda}{\beta\cos\theta} \quad (2.1)$$



where

$L$  = average crystalline size, nm

$K$  = shape factor, 0.89

$\lambda$  = wavelength of X-ray, nm

$\beta$  = full width at half maximum (FWHM), °

$\theta$  = Bragg diffraction angle, °

SEM is utilised to study the topography and morphology of the sample. A clear and great view of three-dimensional image can be formed from SEM due to shadow relief effect for backscattered electron and secondary electron (Trache, et al., 2016). Khataee, et al. (2017) reported that biochar showed a smooth and bulky morphology whereas biochar/ TiO<sub>2</sub> has a rough surface area of the side wall and adhesion of TiO<sub>2</sub> on the biochar pore. EDX is complementary to SEM to identify the elemental composition of the catalyst (Khataee, et al., 2017).

FITR can be used to determine the functional group and chemical structure for the synthesised catalyst. The principle of FTIR is to measure the wavelength and intensity of infrared radiation being absorbed by the specimen (Trache, et al., 2016). The FTIR spectrum shows various peaks which corresponding to the identical functional group. Khataee, et al. (2017) stated that there was a new absorbance peak at 1468 cm<sup>-1</sup> when comparing both bare TiO<sub>2</sub> and biochar/ TiO<sub>2</sub> because of the formation of new Ti-O-Ti group between TiO<sub>2</sub> and biochar. Besides, a strong peak at 3430 cm<sup>-1</sup> in both bare TiO<sub>2</sub> and biochar/ TiO<sub>2</sub> was observed which indicate the O-H stretching (Cai, et al., 2017). O-H stretching is to confirm the present of hydroxyl group in the catalyst as it is responsible for the generation of electron hole pair during photocatalysis.

TGA is usually used to determine the thermal stability of the particular sample by measuring the changes in sample mass. TGA is technique that combined both electronic microbalance and temperature-controlled furnace to analyse the sample weight loss (Polini and Yang, 2017). A graph of weight versus temperature is usually being plotted to examine the weight loss of the sample due to oxidation, decomposition or loss of volatile such as water molecule (Polini and Yang, 2017). Therefore, TGA can assist in determine the carbon content in the cellulose biochar/ TiO<sub>2</sub> compare with pure TiO<sub>2</sub>.

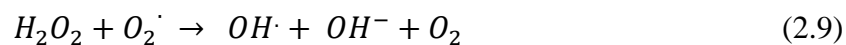
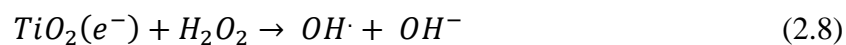
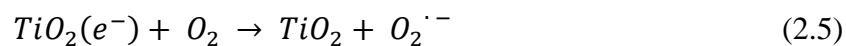
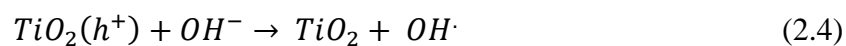
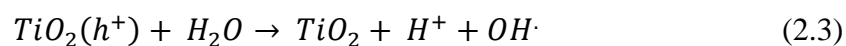
## 2.5 Photocatalysis

Photocatalysis is a photochemical reaction to activate surface of photocatalyst by absorbing sufficient light energy for the subsequent chemical reaction (Natarajan, Bajaj, Tayade, 2017). During activation, electron and holes will be generated and undergoes two simultaneous reactions which are oxidation reaction by the generated hole and reduction reaction by the generated electron (Fujishima, Zhang and Tryk, 2008). The advantages of photocatalysis process include decomposition of organic contaminants into carbon dioxide and water without usage of auxiliary chemicals, conducted at ambient operating conditions, and low operating cost (Mahmoodi, et al., 2018). Photocatalysis can be categorised into homogeneous and heterogeneous reaction. Homogeneous photocatalysis involves both reactant and catalyst at the same phase whereas heterogeneous photocatalysis involves both reactant and catalyst in different phase during photocatalytic reaction.

Reactions that involve heterogeneous photocatalysis are water splitting, wastewater treatment, gaseous pollutant removal, photoreduction and others. Majority of photocatalysis reaction involve titanium assisted heterogeneous photocatalysis (Gaya and Addullah, 2008). Generally, heterogeneous photocatalysis can be divided into five steps in order to mineralise the organic pollutants: 1) mass transfer of the organic pollutants in the liquid phase to the photocatalysts surface, 2) adsorption of organic pollutants on the photocatalysts active sites, 3) photocatalysis reaction take place on the photocatalysts surface, 4) desorption of products from the photocatalysts surface, 5) mass transfer of the products into the bulk fluid (Ani, et al., 2018). The overall rate of reaction is usually based on the slowest steps in the reaction which is reaction step or mass transfer step in this case (Dong, et al., 2015).

The general photocatalytic mechanism with the used of  $\text{TiO}_2$  as photocatalyst is being illustrated in Figure 2.4 (Zangeneh, et al., 2014). When the photons energy ( $h\nu$ ) from the UV irradiation of visible light is greater or equal to the band gap energy required by the  $\text{TiO}_2$ , an electron ( $e^-$ ) will be promoted from the VB to the CB, which result in leaving a positive hole ( $h^+$ ) behind in the VB (Chong, et al., 2010; Zangeneh, et al., 2014). Heat energy will be released if the incoming photon particle has lower energy than the band gap energy required. The hole in the VB can oxidise the organic compound directly

or react with water molecule or hydroxide ion to form hydroxyl radicals. On the other hand, the electron in the CB can also reduce the organic compound directly or recombine with oxygen molecule or  $H_2O_2$  to form superoxide radical anions ( $O_2^{\cdot-}$ ). The  $O_2^{\cdot-}$  radical can react with a proton to form hydroperoxyl radical ( $HO_2^{\cdot}$ ) and eventually forming  $H_2O_2$ .  $HO_2^{\cdot}$  radical can reduce the recombination rate of the electron hole pairs due to the present of scavenging property. Hydroxyl radical plays a very important part in photocatalytic activity as it can actively mineralise organic pollutants to smaller substances like carbon dioxide and water molecule. The reactions of photocatalytic process are shown as Equations (2.2) to (2.9).



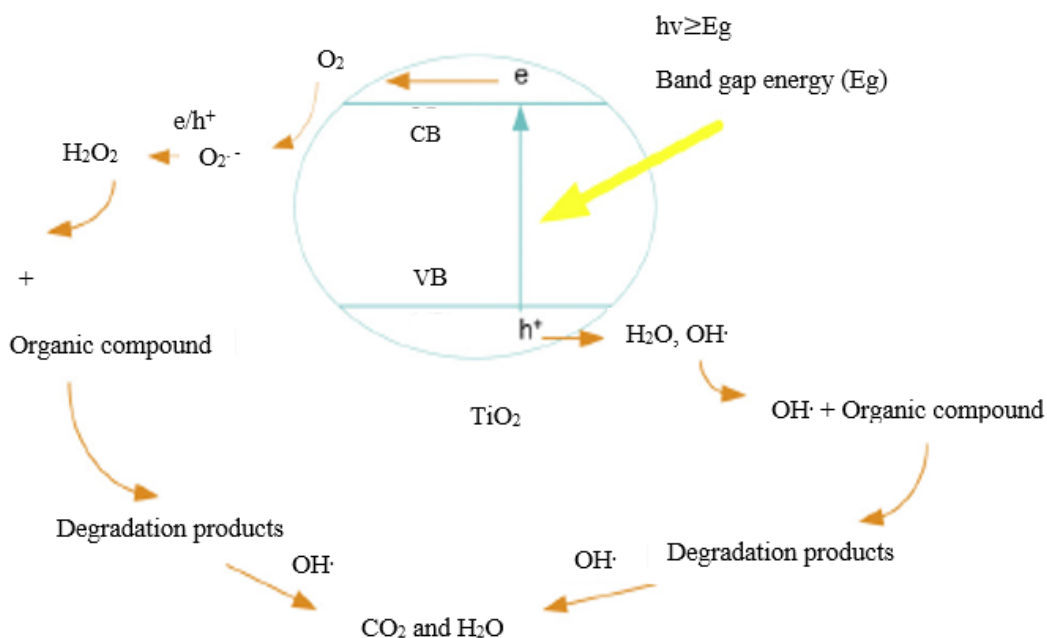


Figure 2.4: General Mechanism of Photocatalyst Degradation Reactions in The Presence of  $\text{TiO}_2$  (Zangeneh, et al., 2014).

Reaction kinetic model is usually used to describe the photocatalytic activity of a particular catalyst. Reaction kinetic order needs to be determined before an appropriate kinetic model can be formulated. Previously, several research showed that photocatalytic degradation of organic dyes over  $\text{TiO}_2$  catalyst were fitted to the Langmuir Hinshelwood kinetic model as shown in Equation (2.10) (Natarajan, Bajaj and Tayade, 2017). Gaya and Abdullah (2008) stated that Langmuir Hinshelwood kinetic model was used as a basis model for photocatalytic degradation of organic substances as shown Equation (2.10).

$$r = \frac{dC}{dt} = \frac{kK_a C}{1 + K_a C} \quad (2.10)$$

where

$r$  = oxidation rate of the dye,  $\frac{mg}{L \text{ min}}$

$C$  = concentration of the dye,  $\frac{mg}{L}$

$t$  = reaction time,  $min$

$k$  = reaction rate constant,  $\frac{mg}{L \text{ min}}$

$K_a$  = adsorption coefficient of the dye,  $\frac{L}{mg}$

If the initial dye concentration,  $C_o$  is a millimolar solution, Equation (2.10) can be simplified to an apparent first order equation as depicted in Equation (2.11) (Natarajan, Bajaj and Tayade, 2017).

$$\ln\left(\frac{C_o}{C}\right) = kKt = k_{app}t \quad (2.11)$$

A graph of  $\ln\left(\frac{C_o}{C}\right)$  against time was plotted and a straight line of gradient indicated the apparent first order rate constant,  $k_{app}$ . The rate of reaction increase as increasing the irradiation time, this indicated less organic dyes remained during reaction because Langmuir Hinshelwood kinetic model depends on catalyst surface area availability (Chong et al., 2010). There are four situations which are applicable for Langmuir Hinshelwood kinetic model. These include reaction take place between two adsorbed substances, reaction take place between adsorbed organics and radical in solution, reaction occur between organic in solution and radical on the surface, and reaction take place when both organic and radical in solution (Konstantinou and Albanis, 2003). Besides first order kinetic equation, pseudo zero order and pseudo second order kinetic equations will also be studied in this research to determine the appropriate kinetic order. Nguyen, Fu and Juang (2018) claimed that the degradation of Methylene Blue and Methyl Orange were fitted with pseudo first order kinetic equation with the used of palladium doped  $TiO_2$ .

## 2.6 Effect of Parameters on the Photocatalytic Degradation

Over the years, there have been many articles and journals reported using different types of semiconductors as photocatalysts to decompose organic dyes into less harmful substances. Based on all those reports, a few parameters would affect the photocatalytic degradation such as catalyst dosage, solution pH, initial dye concentration, solution temperature and types of organic dyes.

### 2.6.1 Effect of Catalyst Dosage

The catalyst amount plays a very important role in the degradation of organic dyes. The photocatalytic degradation of organic dyes was directly proportional to the amount of catalyst present until it reached the optimum point. Beyond the

optimum point, any further increment of catalyst would result in a decrement of degradation rate. Shende, et al. (2017) reported that the degradation rate for Crystal Violet dye at 2 mg and 4 mg catalyst loading were 53.1 % and 58.7 %, respectively after 35 minutes. As increasing the amount of catalyst, the number of active site available for degradation increase and also more hydroxyl radicals could be formed through the protonated of catalyst which result in higher rate of degradation. Guettai and Amar (2005) claimed that beyond the optimum dosage of 0.8 g/L, the decolourisation of Methyl Orange started to decrease. This could be explained by an excessive amount of catalyst could create a light scattering and light screening effect which would reduce the light exposure on the catalyst surface for photo excitation to affect the photocatalytic efficiency. Therefore, optimum catalyst dosage should be chosen to obtain high photocatalytic degradation, at minimum cost of catalyst usage and catalyst separation (Zhang and Lu, 2018).

### **2.6.2 Effect of Solution pH**

pH of the solution also plays a significant parameter during photocatalytic degradation because the surface charge of  $\text{TiO}_2$  alter in different pH condition. The surface charge of the catalyst determined the electrostatic force of attraction between the dye molecule and the catalyst surface which enhance the degradation. The zero charge point is a condition which neutral or zero surface charge was found on the  $\text{TiO}_2$ , zero charge point various with type of  $\text{TiO}_2$  based catalyst used normally in the range of 4.5 pH – 7.0 pH (Chong, et al., 2010). A low degradation rate at zero charge point because of low electrostatic attraction between the catalyst surface and dye molecule. The surface of the catalyst become positively charge when operating pH less than zero charge point whereas negatively charge catalyst surface when operating pH more than zero charge point. Nguyen, Fu and Juang (2018) reported that palladium doped  $\text{TiO}_2$  with a zero charge point of pH 5.4, showed a favour adsorption of cationic Methylene Blue as compared to anionic Methyl Orange when operated at higher pH. Therefore, strong electrostatic force of attraction between both opposite charge catalyst surface and dye molecule at the optimum pH solution. However, at low pH, positive hole is present as a major oxidation species, whereas at

neutral or high pH, hydroxyl group is the primary species which both species take part in photocatalytic degradation (Guettai and Amar, 2005).

### **2.6.3 Effect of Initial Dye Concentration**

Initial dye concentration is also another parameter that affect the degradation rate. In generally, as increasing the dye concentration, the degradation rate would increase until certain extend. The degradation rate started to decrease with further increment in dye concentration. Based on the study of Jantawasu, Sreethawong and Chavadej (2009), the rate of degradation increased until the Methyl Orange concentration reached 5 mg/L and showed a downward degradation trend from 5 mg/L to 15 mg/L. When there were insufficient dye molecules, increment of dye molecule could improve the collision between the substrates which led to increment rate of reaction between dye molecules and hydroxyl group (Jantawasu, Sreethawong and Chavadej, 2009). Hence, enhance the rate of photocatalytic activity. On the other hand, the decrement in the rate of colour removal as further increasing dye concentration because at high dye concentration, most of the photon energy is absorbed by the dye molecule instead of the TiO<sub>2</sub> catalyst (Gupta, et al., 2011). Therefore, there would be a lower amount of hydroxyl groups corresponded for degradation as the electron cannot be protonated from the VB. Moreover, high dye concentration causes the dye molecule to occupy all the catalyst active site which led to a decrement in hydroxyl groups generation on the catalyst surface as all the active sites were filled with dye molecules (Gupta, et al., 2011). Hence, optimum dye concentration need to be determined for effective photocatalytic degradation.

### **2.6.4 Effect of Solution Temperature**

Temperature of the solution also showed adverse effect on dye degradation as increasing in temperature, the rate of degradation was increase before decreasing in photocatalytic activity. As the temperature increase, the collision between adsorbent and adsorbate would increase to enhance decolourisation activity (Gupta, et al., 2011). Besides, the degradation activity also depends whether the adsorption process is endothermic or exothermic. If the adsorption process is endothermic, it will increase with the increase of temperature vice versa (Jain, et al., 2007). Based on the study of Mozia, Tomaszewska and

Morawski (2005), there were an increment of rate constant from 0.0066 - 0.0080  $\text{min}^{-1}$  when the solution temperature was increased from 293 to 323 K and decreased beyond 343 K. The decrement in degradation rate was due to the increment recombination rate of electron-hole pairs and also desorption process of the adsorbed dye molecules (Gaya and Adbullah, 2008). Arrhenius equation clearly showed that the rate constant increased linearly with the exponential of inverse solution temperature (Gaya and Adbullah, 2008).

### **2.6.5 Effect of Types of Organic Dyes**

The photocatalytic degradation rate was different when different types of organic dyes were being used to undergo photocatalysis because each organic dyes have difference molecular structure as well as molecular weight (Guerra, Santos and Araujo, 2012). Based on the study conducted by Khataee, Pons and Zahraa (2009), the photocatalytic degradation rate for Acid Orange 8, Acid Orange 10 and Acid Orange 12 were 16 %, 17 % and 8% respectively after 60 minutes irradiation. Acid orange 10 had the best degradation rate than Acid Orange 8 and Acid Orange 12 due to the presence of two sulphonate group ( $-\text{SO}_3^-$ ) as the  $-\text{SO}_3^-$  favour the attachment on the surface of titanium centre with the two sulphonilic oxygens. Lee, et al. (2018) also reported that Reactive Green with six sulphonate groups have a higher decolourisation efficiency than Acid Orange 7 and Methylene Blue. Both Acid Orange 8 and Acid Orange 12 have almost similar molecular structure. However, Acid Orange 8 consists of alkyl group which decrease the degradation rate as hydroxyl group could not break the bond easily.

### **2.7 Summary**

Biomass which can be categorised more specific such as cellulose, biochar and activated had been discussed in literature review. This was due to the properties and structure of these biomass can be used as a support for photocatalyst. Besides, various type of metal oxide photocatalysts had been discussed to understand the characteristic and properties of each metal oxide. Among all these metal oxide,  $\text{TiO}_2$  was the most suitable used metal oxide photocatalysts. This was due to its large availability, low cost, low toxicity, photocatalytic activity, environmental friendly, chemical inertness and corrosion resistance.



Anatase  $\text{TiO}_2$  was the most suitable candidate to be used during photocatalytic process than rutile and brookite as it inhibits the recombination rate of electron-hole pair so that hydroxyl radical can degrade the organic dye compounds.

Moreover, the effect of calcination temperature had also been discussed. High calcination temperature of cellulose biochar/ $\text{TiO}_2$  composite could cause the burning of carbon as well as aggregation of  $\text{TiO}_2$  particle which lower photocatalytic degradation efficiency. In addition, high calcination temperature would form rutile phase  $\text{TiO}_2$  instead of anatase which had less tendency for visible light absorption. Synthesis method of cellulose biochar/ $\text{TiO}_2$  composite as well as characterisation study also been discussed in this chapter. Photocatalysis had also been studied to understand the photocatalytic mechanism with the used of  $\text{TiO}_2$ . During photocatalytic activity, hydroxyl radical played a very important role as it mineralised organic pollutants to smaller substances like carbon dioxide and water molecule. Last but not least, the effect of various parameters such as catalyst dosage, solution pH, initial dye concentration, solution temperature and types of organic dyes were studied on the photocatalytic degradation of organic dyes.

## CHAPTER 3

### METHODOLOGY AND WORK PLAN

#### 3.1 Materials and Chemicals

The chemical reagents used for this research and their respective specifications are listed in Table 3.1. Based on Table 3.1, n-hexane, sodium chlorite ( $\text{NaClO}_2$ ) and sodium hydroxide ( $\text{NaOH}$ ), acetic acid were used for the extraction of cellulose from EFB whereas titanium (IV) isopropoxide (TTIP) and isopropanol were used to the synthesis the  $\text{TiO}_2$  and also cellulose biochar/  $\text{TiO}_2$ . Various types of organic dyes also listed as organic pollutants in this research study. The pH of the solution during parameter studies were adjusted by hydrogen chloride ( $\text{HCl}$ ) and  $\text{NaOH}$ .

Table 3.1: Chemical Reagents Used in This Research with Their Respective Specifications.

Chemical Reagent	Grade	Brand	Usage
<b>n-hexane</b>	Analysis	Merck	Solvent for extraction of oil residue in EFB
<b><math>\text{NaClO}_2</math></b>	80 % Purity	Sigma-Aldrich	Solvent for cellulose extraction
<b><math>\text{NaOH}</math></b>	97 % Purity	Sigma-Aldrich	Solvent for cellulose extraction and pH adjustment
<b>Acetic acid</b>	Analysis	Sigma-Aldrich	Acidified $\text{NaClO}_2$
<b>TTIP</b>	Analysis	Sigma-Aldrich	Titanium precursor
<b>Isopropanol</b>	Analysis	Merck	Solvent $\text{TiO}_2$
<b>Malachite Green</b>	99 % Purity	Fisher Scientific	Model pollutant
<b>Methylene Blue</b>	82 % Purity	R & M Chemical	Model pollutant
<b>Methyl Orange</b>	85 % Purity	R & M Chemical	Model pollutant
<b>Rhodamine B</b>	95 % Purity	Sigma-Aldrich	Model pollutant
<b>Congo Red</b>	40 % Purity	R & M Chemical	Model pollutant
<b><math>\text{HCl}</math></b>	37 % Purity	Sigma-Aldrich	pH adjustment

Table 3.2 depicts the chemical properties of organic dyes such as Malachite Green, Methylene Blue, Methyl Orange, Rhodamine B and Congo Red which acted as model pollutants. The chemical properties include molecular structure, molecular formula, molecular weight, classification and maximum absorption wavelength.

Table 3.2: Chemical Properties of Organic Dyes Used in This Study.

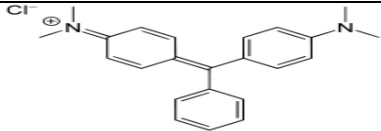
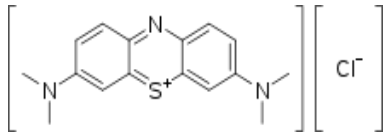
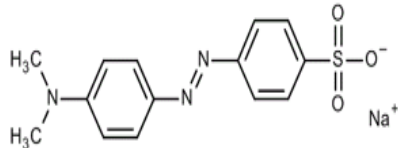
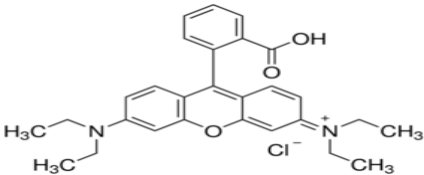
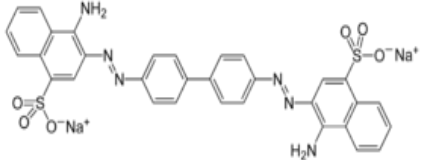
Dye	Molecular structure	Molecular formula	Molecular weight (g/mol)	Classification	Maximum absorption wavelength, $\lambda$ (nm)
Malachite Green		$C_{23}H_{25}ClN_2$	364.91	Cationic basic triarylmethane	619
Methylene Blue		$C_{16}H_{18}N_3SCl$	319.85	Cationic basic thiazine	664
Methyl Orange		$C_{14}H_{14}N_3NaO_3S$	327.33	Anionic acid azo	464

Table 3.2: Continued.

Dye	Molecular structure	Molecular formula	Molecular weight (g/mol)	Classification	Maximum absorption wavelength, $\lambda$ (nm)
Rhodamine B		$C_{28}H_{31}ClN_2O_3$	479.02	Cationic basic xanthene	555
Congo Red		$C_{32}H_{22}N_6Na_2O_6S_2$	696.66	Anionic direct diazo	498

### 3.2 Equipment

The list of equipment that being used in this research along with their model are listed in Table 3.3. Hot plate magnetic stirrer was used to maintain the desired temperature during cellulose extraction as well as photocatalytic degradation of organic dyes. The programmable furnace was utilised to calcine biochar and cellulose biochar/ TiO<sub>2</sub> composites. X-ray Diffractometer, Scanning Electron Microscope, Energy Dispersive X-ray Spectroscopy, Fourier-Transform Infrared spectroscopy, thermal analyser and zeta potential analyser were utilised to analyse the characteristic of the powder samples. The organic dye liquid sample was analysed with UV-Vis Spectrophotometer and COD reactor. pH meter was utilised to measure the pH of the solution.

Table 3.3: List of Equipment with its Respective Model.

<b>Equipment</b>	<b>Model</b>
<b>Hot Plate Magnetic Stirrer</b>	IKA 362001 RET Basic
<b>Programmable Furnace</b>	Wise Therm FP-03
<b>X-ray Diffractometer</b>	Shimadzu XRD-6000
<b>Scanning Electron Microscope-Energy Dispersive X-ray Spectroscopy</b>	Hitachi S-3400 N
<b>Fourier-Transform Infrared Spectroscopy</b>	Nicolet IS10
<b>Thermal Analyser</b>	Perkin Elmer STA8000
<b>UV-Vis Spectrophotometer</b>	Jenway 6320D
<b>COD Reactor</b>	Hach DRB200
<b>pH Meter</b>	Eutech PC300
<b>Zeta Potential Analyser</b>	Horiba Scientific SZ-100

### 3.3 Overall Research Flowchart

Figure 3.1 illustrates the overall flowchart for this research. During preliminary research, cellulose was extracted from EFB followed by calcination of cellulose to form cellulose biochar. Cellulose biochar was impregnated with TiO<sub>2</sub> for the formation of cellulose biochar/ TiO<sub>2</sub> at different calcination temperatures. All powder samples were then characterised through XRD, SEM-EDX, FTIR and TGA and zeta potential analyses. Next, several parameter studies of photocatalytic degradation were carried out by changing the types of catalyst, catalyst dosage, solution pH, potassium peroxydisulfate (PMS) dosage, initial dye concentration, solution temperature and types of organic dyes. Then,

the liquid sample was analysed using UV-Vis spectrophotometer to determine the dye concentration and COD analysis. Last but not least, the reusability and kinetic studies of the photocatalytic degradation were also being studied.

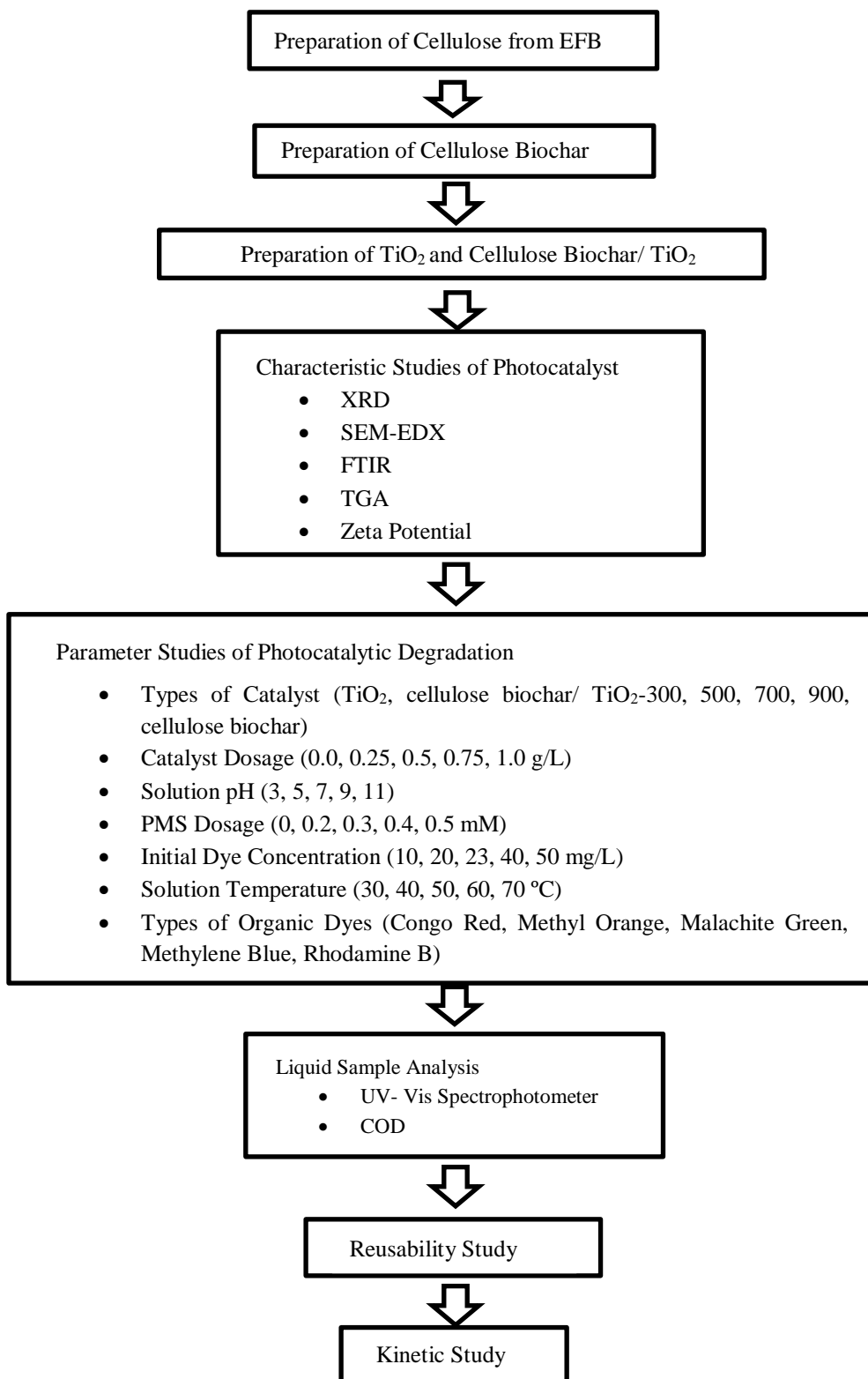


Figure 3.1: Overall Flowchart for Research Activities.

### 3.4 Experimental Setup

Figure 3.2 shows the experimental setup for the photocatalytic degradation. Fluorescent light bulb was utilised to provide visible light for the photocatalytic degradation of organic dyes. The fluorescent light bulb was plugged to a power socket adaptor which clamped by a retort stand clamp so as to fix the light bulb in proper manner. A hot plate magnetic stirrer was used along with a magnetic stirrer bar to ensure a uniform mixing throughout the experiment as well as maintaining the desired solution temperature. Lastly, aluminium foil was used to cover up side of the beaker in order to prohibit light source coming other than from the fluorescent light bulb. Based on the literature review and preliminary study, the experimental conditions were fixed at 100 mL of 10 mg/L organic dyes containing 0.5 g/L of catalyst, solution pH 7 and 30 °C solution temperature otherwise being specified.

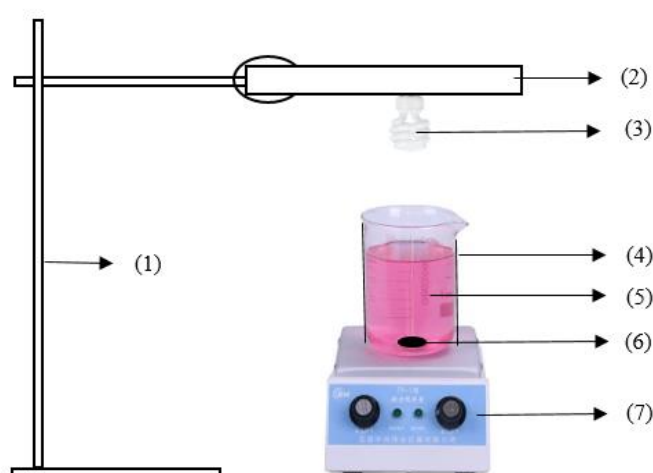


Figure 3.2: Experimental Setup Diagram (1) Retort Stand with Clamp, (2) Power Socket Adaptor, (3) Fluorescent Bulb, (4) Aluminium Foil, (5) Beaker, (6) Magnetic Stir Bar, (7) Hot Plate Magnetic Stirrer.

### 3.5 Preparation of Cellulose, Cellulose Biochar, TiO<sub>2</sub> and Cellulose Biochar / TiO<sub>2</sub> composites

Pure cellulose, cellulose biochar, pure TiO<sub>2</sub> and cellulose biochar/ TiO<sub>2</sub> composites calcined at different temperatures were prepared the details for the preparation steps were described as the following.

### **3.5.1 Preparation of Cellulose from EFB**

The cellulose was prepared by using a modified method performed by Xiang, Mohammed and Baharuddin (2016). Firstly, EFB fibres were cut into smaller pieces. Then, the EFB fibres were soaked in n-hexane for 2 hours to remove the residue oil. The EFB fibres were washed with distilled water for three times. After that, the EFB fibres were dried in an oven at 80 °C. Then, the fibres were mixed with 0.7 % (w/v) NaClO<sub>2</sub> solution in ratio of 1:50 (g/ml) followed by adding of acetic acid until the NaClO<sub>2</sub> solution reached pH 4. The mixture was then heated for two hours at 80 °C. The process was repeated two times before the residues were washed with distilled water for several times to remove yellowish colour and odour from chlorine oxide. Then, the fibres were dried in an oven at 90 °C for overnight. The fibres then soaked with 17.5 % (w/v) NaOH solution in ratio of 1:25 (g/ml) for another two hours. Then, the fibres were washed with distilled water for three times and dried in an oven at 90 °C for overnight.

### **3.5.2 Preparation of Cellulose Biochar**

The cellulose biochar was prepared using a modified method outlined by Li, et al. (2014). The prepared celluloses were calcined at 700 °C for 2 hours at heating rate of 10 °C/ min.

### **3.5.3 Preparation of TiO<sub>2</sub>**

The synthesis of TiO<sub>2</sub> was prepared using sol-gel method (Martins, et al., 2017). 5 mL of TTIP was dissolved in 90 mL of isopropanol and stirred for 5 minutes. After that, 9 mL of distilled water was added dropwise into the mixture and stirred for 2 hours to form a homogeneous gel. Then, the gel was dried in an oven at 100 °C for 5 hours and grounded using a mortar and pestle. Next, the solid materials were calcined at 500 °C for 2 hours. The resulting materials were washed with distilled water several times until the supernatants look clear followed by dried in an oven at 100 °C overnight. The materials obtained was labelled as TiO<sub>2</sub>.



### 3.5.4 Preparation of Cellulose Biochar/ TiO<sub>2</sub> Composites

The synthesis of cellulose biochar/ TiO<sub>2</sub> composites calcined at different temperatures and cellulose/ TiO<sub>2</sub> without calcination were prepared using sol-gel method (Martins, et al., 2017). 5 mL of TTIP was dissolved in 90 mL of isopropanol and stirred for 5 minutes. 1 g of cellulose biochar was added and continued stirred. After that, 9 mL of distilled water was added dropwise into the mixture and stirred for 2 hours to form a homogeneous gel. Then, the gel was dried in an oven at 100 °C for 5 hours and grounded using a mortar and pestle. Next, the solid materials were calcined at 500 °C for 2 hours. The resulting materials were washed with distilled water several times until the supernatants look clear followed by dried in an oven at 100 °C overnight. The materials obtained was labelled as cellulose biochar/ TiO<sub>2</sub>-500. The procedures above were repeated by cellulose biochar calcined at different temperatures which were 300, 700 and 900 °C. The obtained solid materials were labelled as cellulose biochar/ TiO<sub>2</sub>-300, cellulose biochar/ TiO<sub>2</sub>-700 and cellulose biochar/ TiO<sub>2</sub>-900 respectively.

## 3.6 Characterisations of Catalysts

The crystallinity content, surface morphology, chemical elemental composition, functional group and thermal stability of all six samples which consisted of pure TiO<sub>2</sub>, cellulose biochar/ TiO<sub>2</sub>-300, cellulose biochar/ TiO<sub>2</sub>-500, cellulose biochar/ TiO<sub>2</sub>-700, cellulose biochar/ TiO<sub>2</sub>-900 and pure cellulose biochar. All these samples were characterised using XRD, SEM-EDX, FTIR, TGA analyses and zeta potential analyses.

### 3.6.1 XRD

The crystallisation phase of all samples was analysed using the X-ray Diffractometer. The Cu-K $\alpha$  ( $\lambda = 1.54056 \text{ \AA}$ ) radiation source was manipulate at 40 kV and 30 mA. The scanning of the samples was performed at diffraction angle ( $2\theta$ ) ranging from 10 to 80 ° at a rate of 2 °/min and scan step of 0.02 °. The intensity of diffracted X-rays was recorded along with the diffracted angle. The obtained X-rays diffraction pattern was used to analyse the crystal phase as

well as crystallite size based on the peak diffraction angle, peak intensity or peak area.

### **3.6.2 SEM-EDX**

The surface morphology structures of the samples were analysed with a scanning electron microscope. Appropriate sized pin tub was used to hold the sample and then inserted into the brass carrier. Gloves were worn all the time during sample preparation and transfer to avoid contamination to the SEM system. The image was viewed and analysed from point to point and also overall specimen. The chemical element composition of the samples was determined by using Energy Dispersive X-ray Spectroscopy (EDX) coupled to SEM.

### **3.6.3 FTIR Spectroscopy**

The functional groups of all the samples were determined by using the Fourier-Transform Infrared spectroscope. Attenuated total reflectance (ATR) was the sampling technique used in this research. Spectral ranging from 4000 - 400  $\text{cm}^{-1}$  at a resolution of 4  $\text{cm}^{-1}$  and 254 scans were used for the FTIR spectrum. The obtained spectrum was compared with the spectrum in the computer database.

### **3.6.4 TGA**

The thermal stability of all the samples were identified using the thermal stability analyser. The sample was heated ranging from 30 to 830  $^{\circ}\text{C}$  under atmospheric pressure with a heating rate of 10  $^{\circ}\text{C}/\text{min}$  with continuously air input. Then, the amount of weight loss was plotted versus temperature in order to identify the volatile compound percentage present in the sample.

### **3.6.5 Zeta Potential**

The zero charge point of all the samples were identified using the zeta potential analyser. The sample was tested for pH range from 2 to 10 to determine the respective zeta potential (mV) at the specific pH.

### **3.7 Parameter Studies**

Various operating parameters such as types of catalysts (pure TiO<sub>2</sub>, cellulose biochar/ TiO<sub>2</sub>-300, cellulose biochar/ TiO<sub>2</sub>-500, cellulose biochar/ TiO<sub>2</sub>-700, cellulose biochar/ TiO<sub>2</sub>-900, pure cellulose biochar), catalyst dosage (0.0-1.0 g/L), solution pH (3-11), PMS dosage (0-0.5 mM), initial dye concentration (10-50 mg/L), solution temperature (30-70 °C) and types of organic dyes (Congo Red, Methyl Orange, Malachite Green, Methylene Blue, Rhodamine B) were studied to investigate the photocatalytic degradation efficiency of organic dyes.

#### **3.7.1 Effect of Types of Catalysts**

The effect of six types of organic dyes such as pure TiO<sub>2</sub>, cellulose biochar/ TiO<sub>2</sub>-300, cellulose biochar/ TiO<sub>2</sub>-500, cellulose biochar/ TiO<sub>2</sub>-700, cellulose biochar/ TiO<sub>2</sub>-900 and cellulose biochar on the photocatalytic degradation efficiency was investigated. Firstly, 0.5 g/L of cellulose biochar/ TiO<sub>2</sub>-700 was added to 100 mL of 10 mg/L Congo Red in a beaker. pH of the solution was adjusted to pH 7 by utilizing 0.1 M HCl or 1 M NaOH. The solution temperature was set to 30 °C. After that, the mixture was left in the dark condition for 30 minutes to ensure fully adsorption and reached equilibrium state. Then, the mixture was irradiated with visible light for 60 minutes and 5 mL of the mixture was collected every 10 minutes throughout the experiment. The mixture was then filtered to separate the dye solution and catalyst followed by analysed the dye solution using UV-Vis spectrophotometer. All the steps above were repeated for other 5 types of catalysts. Cellulose biochar/ TiO<sub>2</sub>-700 with the highest photocatalytic degradation efficiency was chosen as catalyst for further investigation on the process behaviour photocatalytic degradation.

#### **3.7.2 Effect of Catalyst Dosage**

The effect of catalyst dosage on photocatalytic degradation efficiency of Congo Red was determined by varying the catalyst dosage at 0.0, 0.25, 0.5, 0.75 and 1.0 g/L. Firstly, 0.5 g/L of cellulose biochar/ TiO<sub>2</sub>-700 was added to 100 mL of 10 mg/L Congo Red in a beaker. pH of the solution was adjusted to pH 7 by utilizing 0.1 M HCl or 1 M NaOH. The solution temperature was set to 30 °C. After that, the mixture was left in the dark condition for 30 minutes to ensure

fully adsorption and reached equilibrium state. Then, the mixture was irradiated with visible light for 60 minutes and 5 mL of the mixture was collected every 10 minutes throughout the experiment. The mixture was then filtered to separate the dye solution and catalyst followed by analysed the dye solution using UV-Vis spectrophotometer. All the steps above were repeated for other 4 catalyst dosage. The optimum catalyst dosage 0.5 g/L was chosen for further investigation on the process behaviour photocatalytic degradation.

### **3.7.3 Effect of Solution pH**

The effect of solution pH on photocatalytic degradation efficiency of Congo Red was determined by varying the pH to pH 3, 5, 7, 9 and 11. Firstly, 0.5 g/L of cellulose biochar/ TiO<sub>2</sub>-700 was added to 100 mL of 10 mg/L Congo Red in a beaker. pH of the solution was adjusted to pH 3 by utilizing 0.1 M HCl or 1 M NaOH. The solution temperature was set to 30 °C. After that, the mixture was left in the dark condition for 30 minutes to ensure fully adsorption and reached equilibrium state. Then, the mixture was irradiated with visible light for 60 minutes and 5 mL of the mixture was collected every 10 minutes throughout the experiment. The mixture was then filtered to separate the dye solution and catalyst followed by analysed the dye solution using UV-Vis spectrophotometer. All the steps above were repeated for other 4 solution pH. The optimum solution pH 5 was chosen for further investigation on the process behaviour photocatalytic degradation.

### **3.7.4 Effect of PMS Dosage**

The effect of PMS dosage on photocatalytic degradation efficiency of Congo Red was determined by varying the PMS dosage at 0.0, 0.2, 0.3, 0.4 and 0.5 mM. Firstly, 0.5 g/L of cellulose biochar/ TiO<sub>2</sub>-700 was added to 100 mL of 10 mg/L Congo Red in a beaker. pH of the solution was adjusted to pH 5 by utilizing 0.1 M HCl. The solution temperature was set to 30 °C. After that, the mixture was left in the dark condition for 30 minutes to ensure fully adsorption and reached equilibrium state followed by adding 0.2 mM of PMS into the solution. Then, the mixture was irradiated with visible light for 30 minutes and 5 mL of the mixture was collected every 5 minutes throughout the experiment.

The mixture was then filtered to separate the dye solution and catalyst followed by analysed the dye solution using UV-Vis spectrophotometer. All the steps above were repeated for other 4 PMS dosage. The optimum PMS dosage 0.3 mM was chosen for further investigation on the process behaviour photocatalytic degradation.

### **3.7.5 Effect of Initial Dye Concentration**

The effect of initial dye concentration on photocatalytic degradation efficiency of Congo Red was determined by varying the initial dye concentration to 10, 20, 30, 40 and 50 mg/L. Firstly, 0.5 g/L of cellulose biochar/ TiO<sub>2</sub>-700 was added to 100 mL of 10 mg/L Congo Red in a beaker. pH of the solution was adjusted to pH 5 by utilizing 0.1 M HCl. The solution temperature was set to 30 °C. After that, the mixture was left in the dark condition for 30 minutes to ensure fully adsorption and reached equilibrium state followed by adding 0.3 mM of PMS into the solution. Then, the mixture was irradiated with visible light for 30 minutes and 5 mL of the mixture was collected every 5 minutes throughout the experiment. The mixture was then filtered to separate the dye solution and catalyst followed by analysed the dye solution using UV-Vis spectrophotometer. All the steps above were repeated for other 4 initial dye concentration. The optimum initial dye concentration 10 mg/L with the highest photocatalytic degradation efficiency was chosen for further investigation on the process behaviour photocatalytic degradation.

### **3.7.6 Effect of Solution Temperature**

The effect of solution temperature on photocatalytic degradation efficiency of Congo Red was determined by varying the solution temperature to 30, 40, 50, 60 and 70 °C. Firstly, 0.5 g/L of cellulose biochar/ TiO<sub>2</sub>-700 was added to 100 mL of 10 mg/L Congo Red in a beaker. pH of the solution was adjusted to pH 5 by utilizing 0.1 M HCl. The solution temperature was set to 30 °C. After that, the mixture was left in the dark condition for 30 minutes to ensure fully adsorption and reached equilibrium state followed by adding 0.3 mM of PMS into the solution. Then, the mixture was irradiated with visible light for 5 minutes and 5 mL of the mixture was collected every 1 minute throughout the

experiment. The mixture was then filtered to separate the dye solution and catalyst followed by analysed the dye solution using UV-Vis spectrophotometer. All the steps above were repeated for other 4 solution temperature. The optimum temperature 30 °C was chosen for further investigation on the process behaviour photocatalytic degradation.

### **3.7.7 Effect of Types of Organic Dyes**

The effect of five types of organic dyes such as Congo Red, Methyl Orange, Malachite Green, Methylene Blue and Rhodamine B on the photocatalytic degradation efficiency was investigated. Firstly, 0.5 g/L of cellulose biochar/ TiO<sub>2</sub>-700 was added to 100 mL of 10 mg/L Congo Red in a beaker. pH of the solution was adjusted to pH 5 by utilizing 0.1 M HCl. The solution temperature was set to 30 °C. After that, the mixture was left in the dark condition for 30 minutes to ensure fully adsorption and reached equilibrium state followed by adding 0.3 mM of PMS into the solution. Then, the mixture was irradiated with visible light for 30 minutes and 5 mL of the mixture was collected every 5 minutes throughout the experiment. The mixture was then filtered to separate the dye solution and catalyst followed by analysed the dye solution using UV-Vis spectrophotometer. All the steps above were repeated for other 4 types of organic dyes. Congo Red was chosen as model pollutant for further investigation on the process behaviour photocatalytic degradation.

### **3.8 Reusability Study**

Reusability study was carried out in this research to determine the reusability of the catalyst. 0.5 g/L of cellulose biochar/ TiO<sub>2</sub>-700 was added to 100 mL of 10 mg/L Congo Red in a beaker. pH of the solution was adjusted to pH 5 by utilizing 0.1 M HCl. The solution temperature was set to 30 °C. After that, the mixture was left in the dark condition for 30 minutes to ensure fully adsorption and reached equilibrium state followed by adding 0.3 mM of PMS into the solution. Then, the mixture was irradiated with visible light for 30 minutes and 5 mL of the mixture was collected every 5 minutes throughout the experiment. The mixture was then filtered to separate the dye solution and catalyst followed by analysed the dye solution using UV-Vis spectrophotometer. Then, the

catalyst was retrieved and rinsed thoroughly with distilled water for three times. It was dried in the oven at 90 °C until dry. The catalyst was then used in the subsequent cycles keeping the same standard conditions.

### 3.9 Kinetic Study

Kinetic study was also conducted in this research to determine the kinetic model of the photocatalytic degradation of Congo Red. There were three reactions kinetic order used to determine degradation reaction order of dye by photocatalyst which are pseudo zero-order, pseudo first-order and pseudo second-order as shown in Equations (3.1) to (3.3). The linear regression was determined from all the reactions kinetic order. The reaction kinetic which produced a linear plot was the most appropriate reaction kinetic order to represent the photocatalytic degradation activity.

Pseudo zero-order:

$$C_t = C_o - k_0 t \quad (3.1)$$

Pseudo first-order:

$$\ln C_t = \ln C_o - k_1 t \quad (3.2)$$

Pseudo second-order:

$$\frac{1}{C_t} = \frac{1}{C_o} + k_2 t \quad (3.3)$$

where

$C_o$  = initial dye concentration,  $\frac{mg}{L}$

$C_t$  = dye concentration at time  $t$ ,  $\frac{mg}{L}$

$t$  = reaction time,  $min$

$k_0$  = apparent pseudo zero-order rate constant,  $\frac{mg}{L min}$

$k_1$  = apparent pseudo first-order rate constant,  $\frac{1}{min}$

$k_2$  = apparent pseudo second-order rate constant,  $\frac{L}{mg \text{ min}}$

### 3.10 COD Analysis

The concentration of organic dyes at each time interval was sampling out to study photocatalytic degradation efficiency. The absorbance of the organic dyes was measured at its maximum absorption wavelength as shown in Table 3.2 by using UV-Vis spectrophotometer. According to Beer-Lambert law, absorbance is directly proportional to concentration of the solution. The efficiency of photocatalytic degradation was calculated by using Equation (3.4).

$$\text{Degradation efficiency (\%)} = \frac{C_o - C_t}{C_o} \times 100 \% \quad (3.4)$$

where

$C_o$  = initial dye concentration,  $\frac{mg}{L}$

$C_t$  = dye concentration at time  $t$ ,  $\frac{mg}{L}$

COD analysis was carried out to determine the degree of mineralization of the dye sample. The COD of the liquid sample was measured using the HACH Reactor Digestion Method 8 000. 2 mL dye sample at each time interval was mixed with digestion reagent. The 2 mL distilled water also mixed with digestion reagent which set as blank sample. Then, the samples were heated at 150 °C for 2 hours and left at room temperature to cool the samples. The cooled samples were tested with UV-Vis spectrophotometer to measure the COD values.

### 3.11 Summary

For the preliminary, the material and chemicals together with equipment that had been used in this research were listed out. Secondly, the overall research flowchart was drawn to indicate the research work plan. The preparation of cellulose, cellulose biochar, TiO<sub>2</sub> and cellulose biochar / TiO<sub>2</sub> composites were described for the experiment. Besides, various type of characterisation of



catalysts were discussed such as XRD, SEM-EDX, FTIR Spectroscopy, TGA and Zeta Potential.

Moreover, various parameter studies such as types of catalysts, catalyst dosage, solution pH, PMS dosage, initial dye concentration, solution temperature and types of organic dyes were listed out on the photocatalytic degradation of Congo Red to determine the optimum conditions. Besides, the reusability and kinetic studies of cellulose biochar/ TiO<sub>2</sub>-700 were also carried out in this research. Last but not least, the COD analysis was carried out to determine the degree of mineralization of the organic dye.

## CHAPTER 4

### RESULTS AND DISCUSSIONS

#### 4.1 Characterisation of Photocatalysts

##### 4.1.1 XRD

The crystal phases of the pure TiO<sub>2</sub>, cellulose biochar/ TiO<sub>2</sub> composite at various calcination temperatures and cellulose biochar were analysed using the XRD as depicted in Figure 4.1. The XRD pattern for cellulose biochar showed two broad diffraction peaks at  $2\theta = 23^\circ$  and  $43^\circ$  which indicated the carbon characteristic peaks as well as disordered structural of cellulose biochar (Yu, et al., 2018). The broad diffraction peaks at  $2\theta = 23^\circ$  resulted from the amorphous carbon structure while the graphitic structure  $2\theta = 43^\circ$  was contributed from high calcination temperature range from 700 to 900 °C (Lobos, et al., 2016).

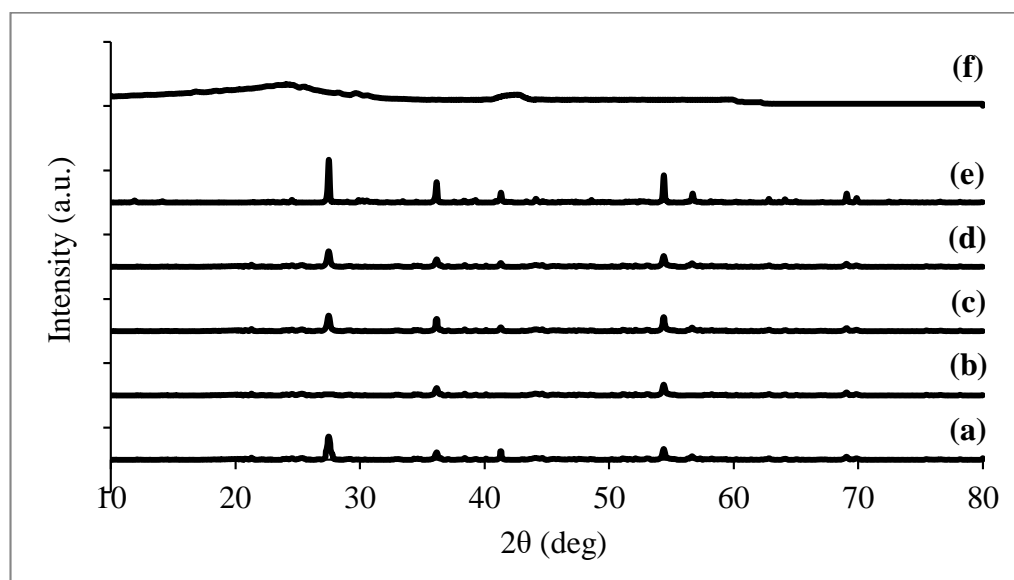


Figure 4.1: XRD Patterns for (a) Pure TiO<sub>2</sub>, Cellulose Biochar/ TiO<sub>2</sub> Composite at Various Calcination Temperature (b) 300 °C, (c) 500 °C, (d) 700 °C, (e) 900 °C and (f) Cellulose Biochar.

For pure TiO<sub>2</sub>, the XRD pattern showed some diffraction peaks. The diffraction peaks at  $2\theta = 37.9^\circ, 54.1^\circ, 55.2^\circ, 62.9^\circ, 68.9^\circ$  and  $70.3^\circ$

corresponded to the (004), (105), (211), (204), (116) and (220) crystal plane of the anatase  $\text{TiO}_2$  (Yu, et al., 2018). Peaks at  $2\theta = 27.7^\circ, 41.3^\circ$  and  $56.4^\circ$  belonged to the (110), (111) and (220) crystal plane of the rutile phase (Peng, et al., 2018). It was observed that there were more diffraction peaks of anatase phase than rutile phase. The presence of rutile phase corresponding to the high calcination temperature which caused the oxygen atom bond well with titanium atom as high stability of rutile structure tend to replace anatase (Peng, et al., 2018).

As for the cellulose biochar/  $\text{TiO}_2$  composite at various calcination temperatures, the diffraction peaks were found similar XRD patterns as pure  $\text{TiO}_2$ . The broad diffraction peaks found in cellulose biochar could not be observed due to the overlapping of high crystalline diffraction peaks of  $2\theta = 27.7^\circ$  and  $41.3^\circ$  (Yu, et al., 2018). It was observed that the cellulose biochar /  $\text{TiO}_2$  composites had reduced the peak intensity of the rutile phase except cellulose biochar/  $\text{TiO}_2$ -900. This indicated cellulose biochar to  $\text{TiO}_2$  had reduced the conversion of anatase to rutile phase. Therefore, photocatalytic degradation efficiency had been increased as anatase has low recombination rate of electron-hole pairs and high adsorption capability towards organic dyes (Lisowski, et al., 2017). The high peak intensity of cellulose biochar/  $\text{TiO}_2$ -900 corresponded to the high calcination temperature of  $900^\circ\text{C}$  which favour the transformation from anatase to rutile phase.

#### **4.1.2 SEM-EDX**

The surface morphology of pure  $\text{TiO}_2$ , cellulose biochar/  $\text{TiO}_2$  composite at various calcination temperatures and cellulose biochar were studied using SEM as showed in Figure 4.2. It can be seen from Figure 4.2(a)  $\text{TiO}_2$  particles show spherical shape structure and agglomerate together to form packed clusters of particles (Martins, et al., 2017). Besides, the morphology of cellulose biochar constructed with smooth inner and outer porosity surface were expected to increase the specific surface area of cellulose biochar as shown in Figure 4.2(f) (Peng, et al., 2018).

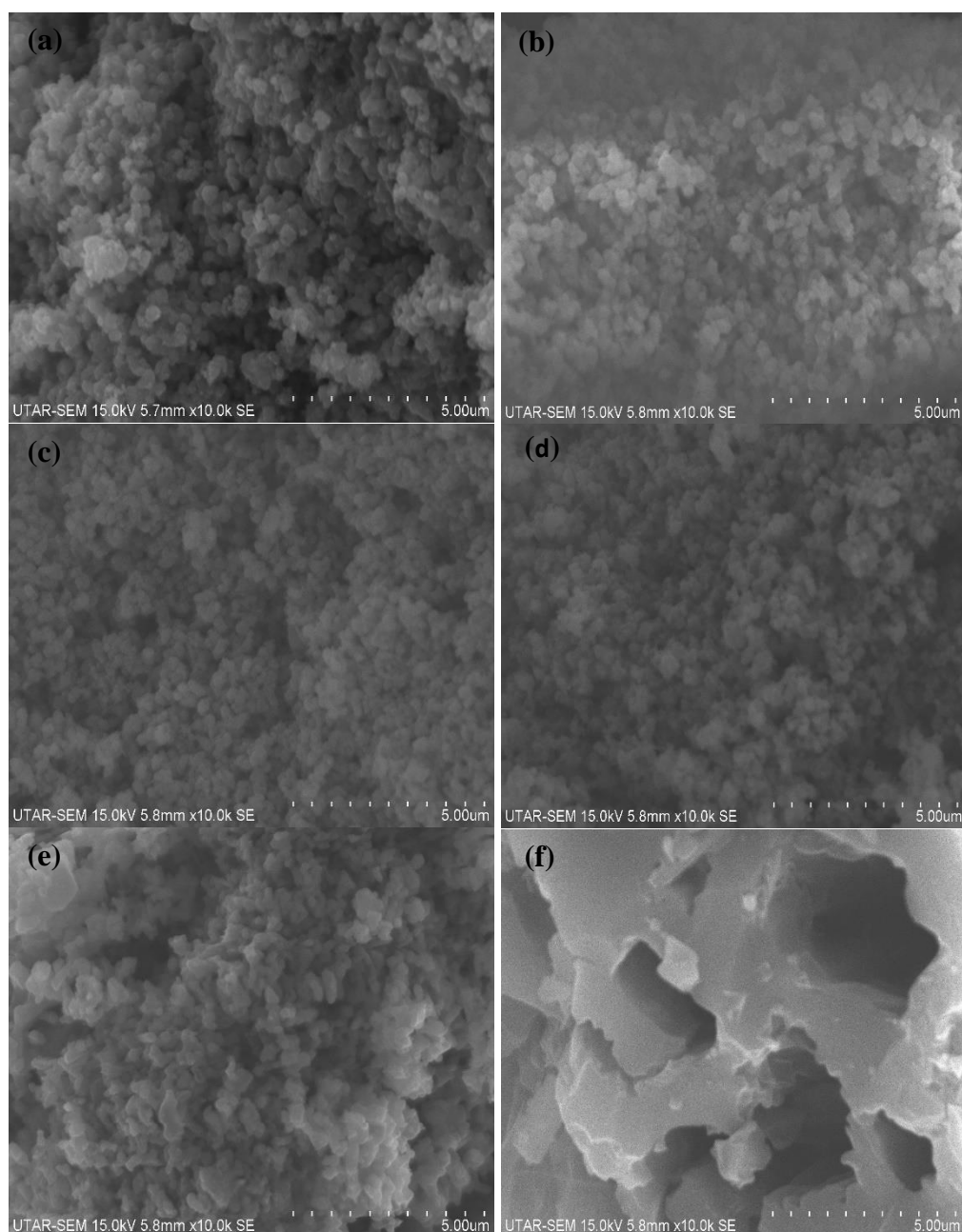


Figure 4.2: SEM Images of (a) Pure TiO<sub>2</sub>, Cellulose Biochar/ TiO<sub>2</sub> Composite at Various Calcination Temperature (b) 300 °C, (c) 500 °C, (d) 700 °C, (e) 900 °C and (f) Cellulose Biochar.

Based on Figure 4.2(b) to 4.2(e), the calcination temperature of the cellulose biochar/ TiO<sub>2</sub> composites increased gradually from 300 °C to 900 °C. In general, TiO<sub>2</sub> particles were immobilised on the cellulose biochar surface which resulted in a lesser agglomeration than pure TiO<sub>2</sub>. The structure of the cellulose biochar might be decomposed at elevated calcination temperature which indicated low temperature aid in maintaining the structure of cellulose

biochar (Peng, et al., 2018). Similar morphology images for biochar / TiO<sub>2</sub> composites were reported by Lu, et al. (2019) as the TiO<sub>2</sub> particles agglomerated and form larger particles in composite due to the size and structural of biochar.

The EDX results of pure TiO<sub>2</sub>, cellulose biochar/ TiO<sub>2</sub> composite at various calcination temperatures and cellulose biochar are tabulated in Table 4.1. TiO<sub>2</sub> based samples consist of carbon, oxygen and titanium elements. The carbon contents for TiO<sub>2</sub>, cellulose biochar/ TiO<sub>2</sub>-300, cellulose biochar/ TiO<sub>2</sub>-500, cellulose biochar/ TiO<sub>2</sub>-700, cellulose biochar/ TiO<sub>2</sub>-900 and cellulose biochar were 7.05 wt. %, 25.37 wt. %, 23.33 wt. %, 18.79 wt. %, 11.48 wt. % and 61.26 wt. % respectively. It can be seen that the carbon content for composites were higher than pure TiO<sub>2</sub> which indicated that cellulose biochar act as a support for TiO<sub>2</sub>. Hence, TiO<sub>2</sub> particles had a better dispersion on the support and might increase the degradation efficiency of organic dye (Mishra, Mehta and Basu, 2018). However, the carbon content of the composite materials reduced when increasing calcination temperature as high calcination temperature could cause the burning of carbon (Zhang et al., 2017).

Table 4.1: Distribution of Elements in Various Samples.

<b>Sample</b>	<b>C (wt. %)</b>	<b>O (wt. %)</b>	<b>Ti (wt. %)</b>
<b>TiO<sub>2</sub></b>	7.05	31.49	61.46
<b>Cellulose Biochar/ TiO<sub>2</sub>-300</b>	25.37	37.26	37.37
<b>Cellulose Biochar/ TiO<sub>2</sub>-500</b>	23.33	34.86	41.81
<b>Cellulose Biochar/ TiO<sub>2</sub>-700</b>	18.79	34.58	46.63
<b>Cellulose Biochar/ TiO<sub>2</sub>-900</b>	11.48	34.89	53.64
<b>Cellulose Biochar</b>	61.26	38.31	0.43

#### 4.1.3 FTIR Spectroscopy

The functional groups of pure TiO<sub>2</sub>, cellulose biochar/ TiO<sub>2</sub> composite at various calcination temperatures and cellulose biochar were studied using FTIR Spectroscopy and the results are depicted in Figure 4.3. All six spectra showed

a broad band at about  $3430\text{ cm}^{-1}$  and  $2380\text{ cm}^{-1}$  which indicated the O-H stretching due to water adsorption on the particles surface (Cai, et al., 2017). Ragupathy, Raghu and Prabu (2014) stated that hydrolysis reaction of sol-gel method would result in  $\text{TiO}_2\text{-OH}$  band formation from the observed broad band. O-H stretching confirmed the presence of hydroxyl group in the particles surface as it was responsible for the generation of electron-hole pair during photocatalysis. Besides, the peak from  $400\text{ cm}^{-1}$  and  $960\text{ cm}^{-1}$  was attributed to the stretching vibration of Ti-O and this confirmed the presence of  $\text{TiO}_2$  (Makrigianni, et al., 2015). The peak width for the Ti-O stretching increased as the composition of  $\text{TiO}_2$  presence in the catalyst increased. The broad peak at  $2960\text{ cm}^{-1}$  was corresponded to the stretching vibration of C-H (Peng, et al., 2018).

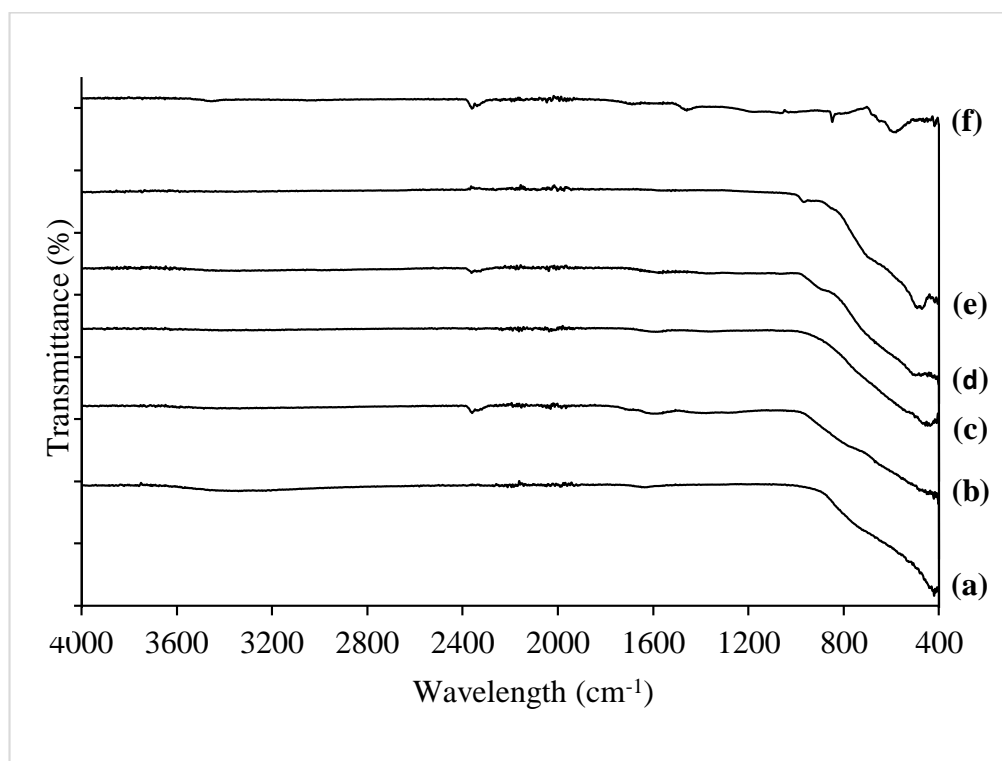


Figure 4.3: FTIR Patterns for (a) Pure  $\text{TiO}_2$ , Cellulose Biochar/ $\text{TiO}_2$  Composite at Various Calcination Temperature (b) 300 °C, (c) 500 °C, (d) 700 °C, (e) 900 °C and (f) Cellulose Biochar.

#### 4.1.4 TGA

The thermal stability of the pure  $\text{TiO}_2$ , cellulose biochar/  $\text{TiO}_2$  composite at various calcination temperatures and cellulose biochar were studied using TGA and the results are shown in Figure 4.4. The TGA curves range from 30 to 95 °C illustrated the weight loss of cellulose biochar/  $\text{TiO}_2$ -300, cellulose biochar/  $\text{TiO}_2$ -500, cellulose biochar/  $\text{TiO}_2$ -700, cellulose biochar/  $\text{TiO}_2$ -900 and cellulose biochar were 2.15 %, 1.90 %, 3.56 %, 4.45 % and 12.66 % respectively. This was corresponded to the evaporation of the water molecule retained in the pore and surface of the particles (Muniandy, et al., 2016). The weight loss happened from 100 to 830 °C and was observed about 25.22 %, 16.68 %, 9.76 %, 4.45 % and 19.87 % for cellulose biochar/  $\text{TiO}_2$ -300, cellulose biochar/  $\text{TiO}_2$ -500, cellulose biochar/  $\text{TiO}_2$ -700, cellulose biochar/  $\text{TiO}_2$ -900 and cellulose biochar respectively. The weight loss ranged from 100 to 830 °C was resulted from the decomposition of carbon content. It could be observed that the weight loss of the composite materials was much lower than cellulose biochar which might due to the increasing thermal stability as  $\text{TiO}_2$  particles embedded on the cellulose biochar. As for the pure  $\text{TiO}_2$ , it showed a negligible weight loss between temperature 30 to 830 °C due to high thermal stability of pure  $\text{TiO}_2$  (Muniandy, et al., 2016).

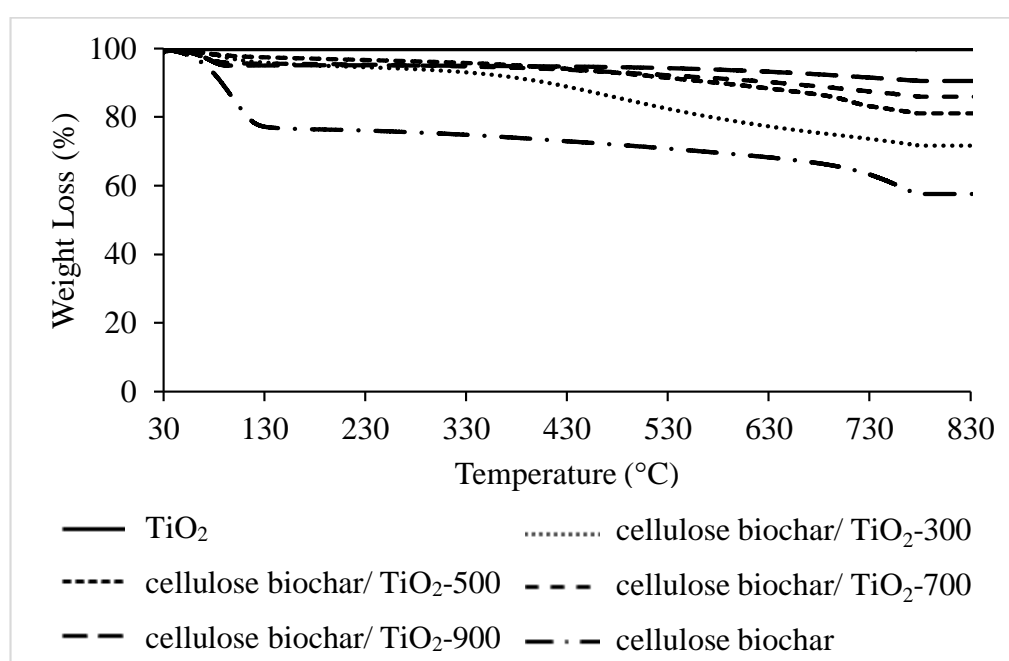


Figure 4.4: TGA Curves for all Samples.

#### 4.1.5 Zeta Potential

The zero charge point of pure  $\text{TiO}_2$ , cellulose biochar/  $\text{TiO}_2$ -700 and cellulose biochar were studied using zeta potential analysis as depicted in Figure 4.5. According to Figure 4.5, it showed that the zero charge point of pure  $\text{TiO}_2$ , cellulose biochar/  $\text{TiO}_2$ -700 and cellulose biochar were about pH 7.5, 5.1 and 2.6 respectively. Similar results were reported by Hu, Wang and Tang (2000) which zero charge point of  $\text{TiO}_2$  particles and titania/ silica were pH 6.2 and 3 respectively. This indicated that presence of acidic group such as silica lower the zero charge point of  $\text{TiO}_2$ . Mohamed, Othaman and Mohamed (2007) reported that zero charge point of manganese (Mn) species which covered 34 % of the support titanium in Mn/  $\text{TiO}_2$  was pH 6.1. The zero charge point is a condition which neutral or zero surface charge was found as surface charge of the particles to determine the electrostatic force of attraction between the particle surface and dye molecules (Chong, et al., 2010). The surface of the particle became positively charge when operating pH less than zero charge point whereas negatively charge when operating pH more than zero charge point.

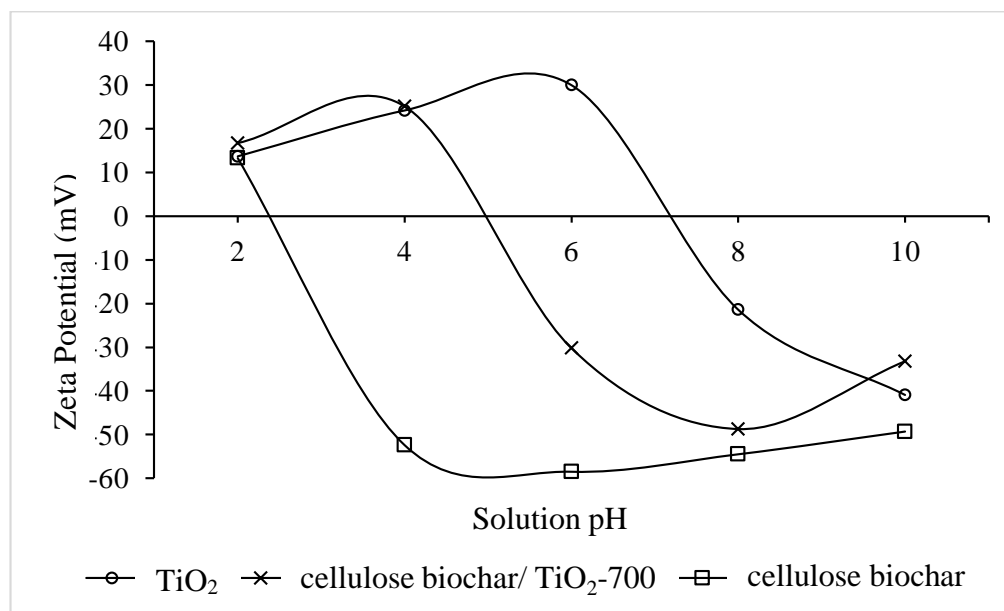


Figure 4.5: Zeta Potential Patterns for Pure  $\text{TiO}_2$ , Cellulose Biochar/  $\text{TiO}_2$ -700 and Cellulose Biochar.



## 4.2 Parameter Studies

### 4.2.1 Photocatalytic Degradation of Congo Red

The photocatalytic degradation of Congo Red using  $\text{TiO}_2$ , cellulose biochar/ $\text{TiO}_2$  composite at various calcination temperatures were investigated. The result is shown in Figure 4.6. Generally, the photocatalytic degradation of Congo Red in the presence of cellulose biochar/ $\text{TiO}_2$  composites which calcined at 700 °C achieved the highest value (29.47 %) and decreased when the sample calcined at 900 °C. The degradation efficiency for pure  $\text{TiO}_2$ , cellulose biochar/ $\text{TiO}_2$ -500 and cellulose biochar/ $\text{TiO}_2$ -900 resulted in degradation efficiencies of 5.54 %, 8.36 % and 20.09 % respectively.

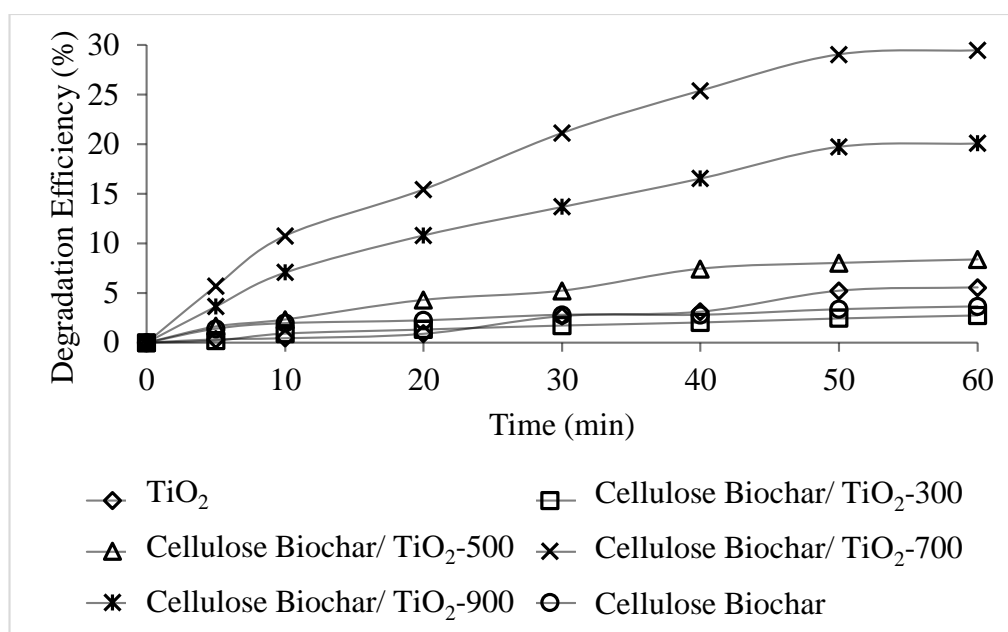


Figure 4.6: Photocatalytic Degradation of Congo Red by  $\text{TiO}_2$ , Cellulose Biochar/ $\text{TiO}_2$  Composite at Various Calcination Temperature and Cellulose Biochar (Catalyst Dosage = 0.5 g/L, Initial Dye Concentration = 10 mg/L, Solution Temperature = 30 °C, Reaction Time = 60 minutes, Initial pH = 7).

There were several reasons to increase the degradation efficiency of Congo Red in the presence of cellulose biochar/ $\text{TiO}_2$  composite materials. First of foremost, cellulose biochar acted as a support for  $\text{TiO}_2$ , lower the recombination of electron-hole pair to increase more free radicals and promoted the decomposition of organic dye (Kim and Kan, 2016). Besides, large surface

area of cellulose biochar enhanced the embedment of  $\text{TiO}_2$  onto the cellulose biochar which prevent the agglomeration of  $\text{TiO}_2$  and led to a low degradation efficiency. Moreover, cellulose biochar also reduced the band gap energy so that visible light can be used for photocatalytic activity (Silvestri, et al., 2019).

The reasons that caused the degradation efficiency to increase from  $500\text{ }^\circ\text{C}$  to  $700\text{ }^\circ\text{C}$ , and decreased when it reached  $900\text{ }^\circ\text{C}$  calcination temperature because biochar did not show obvious change at calcination temperature before  $400\text{ }^\circ\text{C}$  (Chen, et al., 2017). To simplify, high surface area of cellulose biochar provided a better attachment for  $\text{TiO}_2$  which led to a high degradation efficiency. Besides, high calcination temperature increased the transformation of anatase to rutile phase which could be observed from XRD but led to low photocatalytic degradation (Martins, et al., 2017). The optimal catalyst was cellulose biochar/ $\text{TiO}_2$ -700 because it exhibited the highest degradation efficiency.

#### **4.2.2 Effect of Catalyst Dosage**

The effect of catalyst dosage (0, 0.25, 0.5, 0.75 and 1.0 g/L) was studied on the photocatalytic degradation of Congo Red and the results are illustrated in Figure 4.7. It could be observed that photolysis degradation efficiency was the lowest in the absence of catalyst dosage. There was a slight increment in the degradation of Congo Red when the dosage was 0.25 g/L composite. The degradation efficiency increased up to 29.5 % in 60 minutes when the catalyst dosage increased from 0.25g/L to 0.75 g/L, this illustrated that a huge increment in the photocatalytic degradation of Congo Red. As beyond 0.75 g/L, the degradation efficiency started to decrease when the catalyst dosage was 1.0 g/L.

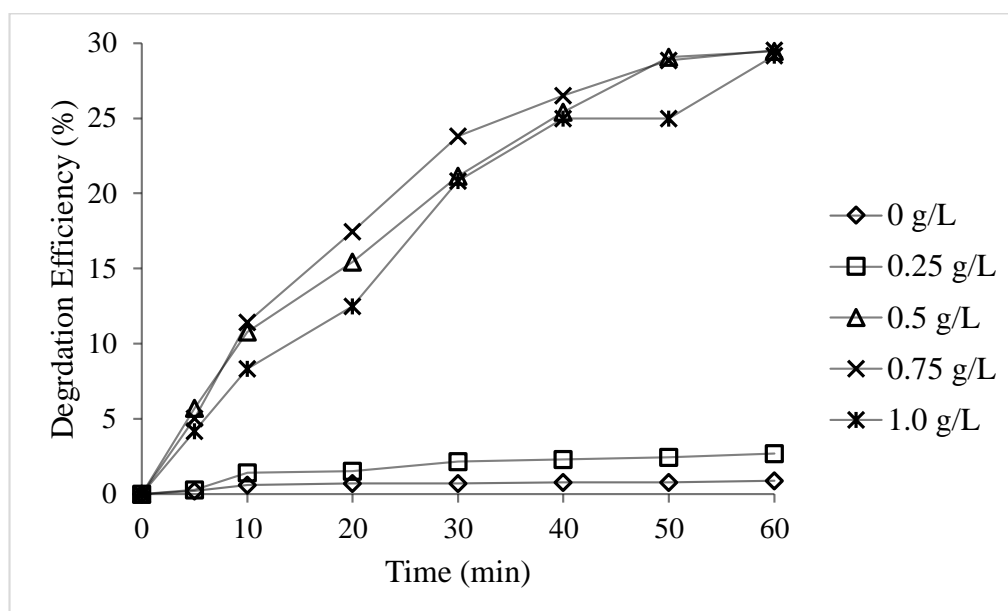


Figure 4.7: Effect of Catalyst Dosage on the Photocatalytic Degradation of Congo Red in the Presence of Cellulose Biochar/ TiO<sub>2</sub>-700 (Initial Dye Concentration = 10 mg/L, Solution Temperature = 30 °C, Reaction Time = 60 minutes, Initial pH = 7).

The huge increment of the degradation of Congo Red could be explained by increasing the amount of catalyst which increased the number of the active site available and also more free radicals through the protonated of catalyst which resulted in a higher rate of degradation (Zangeneh, et al., 2014). On the other hand, the decreased in degradation efficiency was due to the excessive amount of catalyst created a light scattering and light screening effect which reduced the light penetration into the dye solutions for photo-excitation of catalyst (Nguyen, Fu and Juang, 2018).

Similar trends were also reported by Shende, et al. (2017) and Guettai and Amar (2005) on the photocatalytic degradation of Crystal Violet dye and Methyl Orange respectively. Therefore, increasing in catalyst dosage showed higher degradation efficiency and started to decrease beyond the optimal dosage. In this study, the optimal dosage of catalyst was selected as 0.5 g/L instead of 0.75 g/L to minimise the cost of catalyst usage and catalyst separation. There was only slightly 0.1 % difference in degradation efficiency when using catalyst dosage of 0.5 g/L and 0.75 g/L.

### 4.2.3 Effect of solution pH

The effect of solution pH (pH 3, 5, 7, 9 and 11) was investigated on the photocatalytic degradation of Congo Red as illustrated in Figure 4.8. The pH was adjusted by using the 0.1 M HCl and 1 M NaOH. Figure 4.8 shows that increment of solution pH from pH 3 to 11 had decreased the degradation efficiency of Congo Red. It clearly showed that photocatalytic degradation of Congo Red performed well in solution pH range from 3 to 7.

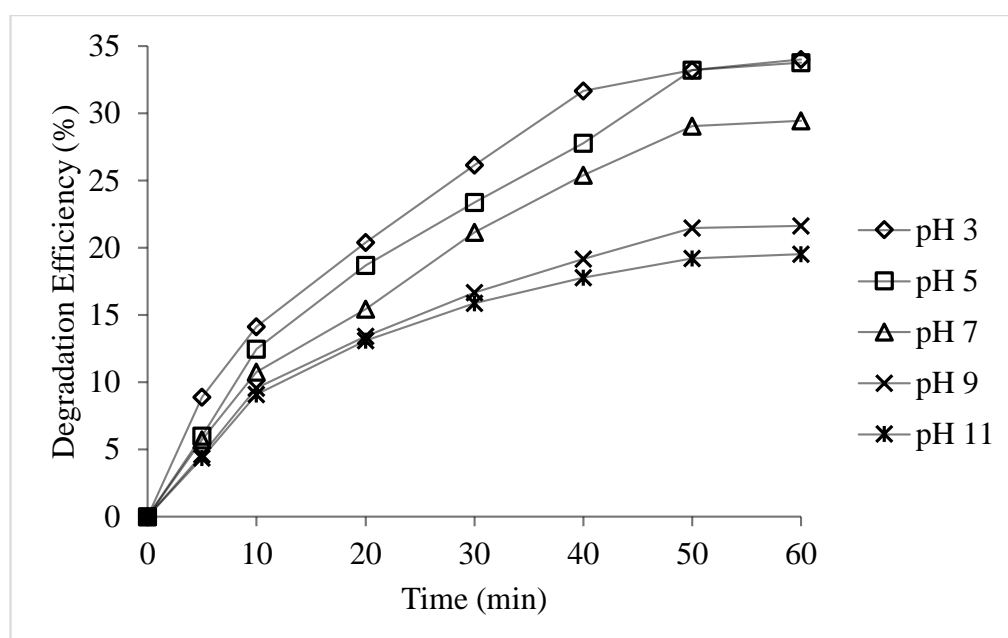


Figure 4.8: Effect of pH on the Photocatalytic Degradation of Congo Red in the Presence of Cellulose Biochar/ TiO<sub>2</sub>-700 (Catalyst Dosage = 0.5 g/L, Initial Dye Concentration = 10 mg/L, Solution Temperature = 30 °C, Reaction Time = 60 minutes).

The zero charge point is a condition which neutral or zero surface charge was found on the TiO<sub>2</sub>, this value might vary from 4.5 to 7.0 for different types of TiO<sub>2</sub> based particles (Chong, et al., 2010). In the acidic solution lower than pH 5, the surface of TiO<sub>2</sub> contained positive charge to the particles surface as the pH was lower than the zero charge point of Cellulose Biochar/ TiO<sub>2</sub>-700 which was pH 5.1 (Guettai and Amar, 2005). On the other hand, when Congo Red dissolved in water, it became anionic dye (Yu, et al., 2018). The positive charge on the surface of TiO<sub>2</sub> would cause a strong electrostatic force of

attraction between the anionic Congo Red molecule. Therefore, low solution pH increased the adsorption and degradation efficiency of Congo Red.

In the alkaline solution, the surface of TiO<sub>2</sub> contained the hydroxyl group that supplied negative charge to the catalyst surface. Both negative charge for the TiO<sub>2</sub> surface and Congo Red molecule caused repulsion force between them which reduced to diffusion rate of hydroxyl radical toward Congo Red (Jantawasu, Sreethawong and Chavadej, 2009). Hence, poor interaction and repulsion force between TiO<sub>2</sub> and anionic Congo Red molecule, which decreased the photocatalytic degradation. Zhang and Lu (2018) also reported similar solution pH trend in the photocatalytic degradation of anionic Reactive Brilliant Blue. The optimum pH of this research was pH 5 instead of pH 3 as the degradation efficiency were similar for pH 5 and pH 3 and it saved the treatment cost from the view of economic.

#### **4.2.4 Effect of PMS Dosage**

The effect of PMS dosages (0, 0.2, 0.3, 0.4 and 0.5 mM) was investigated on the photocatalytic degradation of Congo Red as illustrated in Figure 4.9. As noted in Figure 4.9, no significant photocatalytic degradation of Congo Red was observed without the addition of PMS as only 21.3 % degradation efficiency was achieved in 30 minutes. By adding the PMS dosage from 0.2 to 0.5 mM, the degradation efficiency of Congo Red increased from 73.4 to 100 % in 30 minutes.

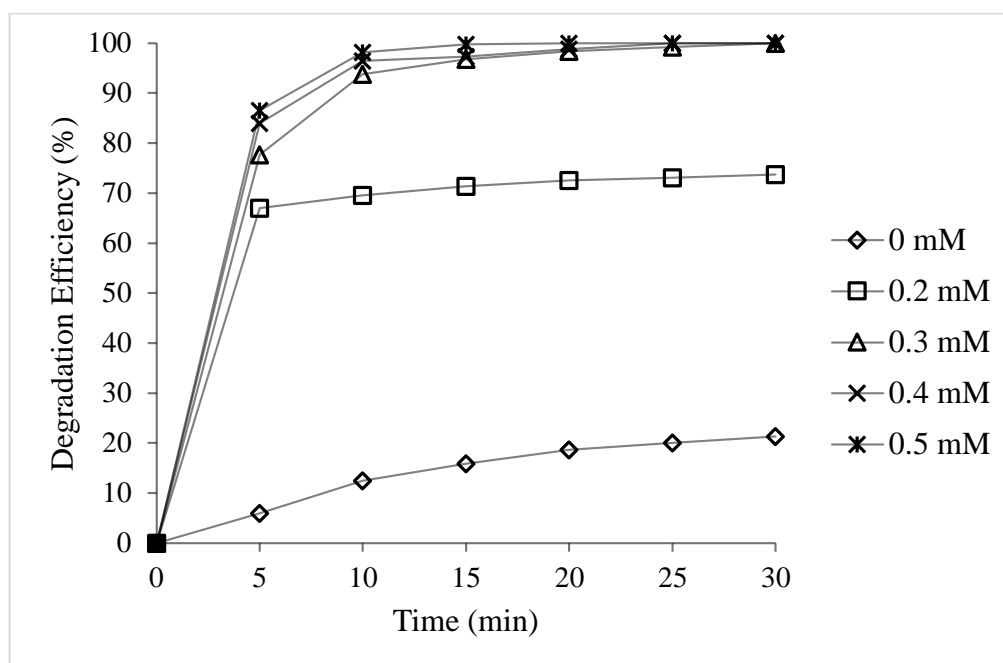


Figure 4.9: Effect of PMS Dosage on the Photocatalytic Degradation of Congo Red in the Presence of Cellulose Biochar/  $\text{TiO}_2$ -700 (Catalyst Dosage = 0.5 g/L, Dye Concentration = 10 mg/L, Solution Temperature = 30 °C, Reaction Time = 30 minutes, Initial pH = 5).

Without adding the PMS, the degradation efficiency of Congo Red was low as adsorption of dye molecule on the catalyst did not degrade dye molecule significantly. As addition of PMS, the degradation efficiency of Congo Red increased significantly. This was due to the capability of PMS to generate reactive oxygen species such as sulphate radical (Wang, et al., 2014). Sulphate radical is a more powerful oxidant than hydroxyl radical in term of decomposition of organic contaminants because sulphate radical showed higher oxidation potential and could be operated in a wider solution pH range for catalytic oxidation (Soltani, Tayyebi and Lee, 2018). Therefore, when increasing the PMS dosage, the quantity of sulphate radicals increased and the rate of degradation of Congo Red increased. Antoniou, et al. (2018) also reported similar result in the photocatalytic degradation of Microcystin-LR. The optimal PMS dosage was 0.3 mM as excessive PMS dosage would increase the cost of wastewater treatment.

#### 4.2.5 Effect of Initial Dye Concentration

The effect of initial dye concentration (10, 20, 30, 40 and 50 mg/L) was investigated on the photocatalytic degradation of Congo Red as depicted in Figure 4.10. It was observed that the degradation efficiency was decreased from 100 to 13.1 % when the concentration of Congo Red increased from 10 to 50 mg/L.

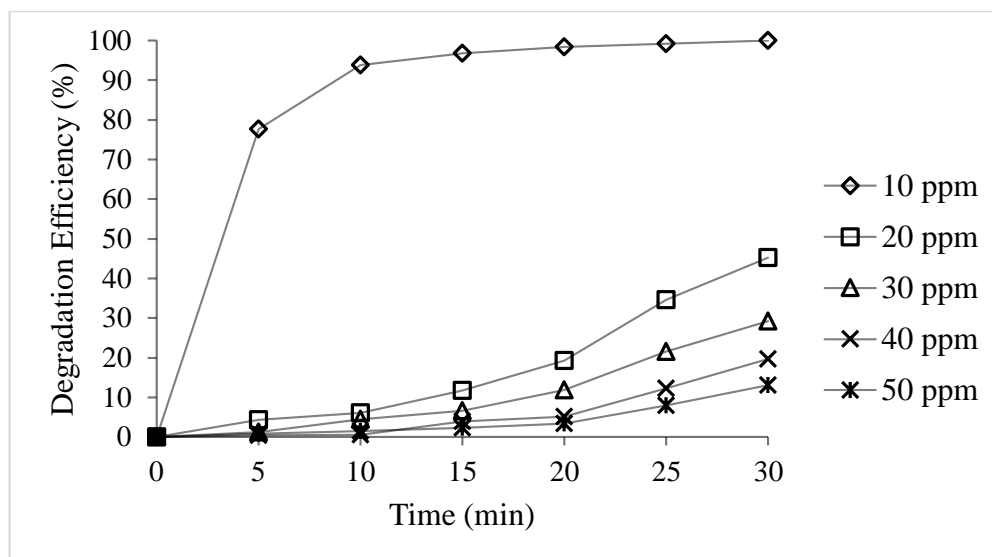


Figure 4.10: Effect of Initial Dye Concentration on the Photocatalytic Degradation of Congo Red in the Presence of Cellulose Biochar/ TiO<sub>2</sub>-700 (Catalyst Dosage = 0.5 g/L, PMS Dosage = 0.3 mM, Solution Temperature = 30 °C, Reaction Time = 30 minutes, Initial pH = 5).

There were a few reasons attributed to the decreased in degradation efficiency. At high dye concentration, the light penetration was reduced and most of the photon energy was absorbed by the dye molecule instead of the TiO<sub>2</sub> composite (Gupta, et al., 2011). Therefore, there would be a lower amount of hydroxyl groups generated for degradation of Congo Red. Besides, high dye concentration might cause all the catalyst active sites were covered and saturated by the dye molecules, which led to a decrement in hydroxyl groups generation on the catalyst surface (Gupta, et al., 2011).

As a result, the higher the initial concentration of Congo Red, the lower the degradation efficiency. Jantawas, Sreethawong and Chavadej (2009) reported similar initial dye concentration trend in the photocatalytic degradation

of Methyl Orange. The optimal initial dye concentration was 10 mg/L because it exhibited the highest degradation efficiency.

#### 4.2.6 Effect of Solution Temperature

The effect of solution temperature (30, 40, 50, 60 and 70 °C) was investigated on the photocatalytic degradation of Congo Red as depicted in Figure 4.11. It could be observed that the degradation efficiency was affected by raising the solution temperature. The degradation efficiency of Congo Red was increased from 77.6 to 96.1 % within 5 minutes as the solution temperature increased from 30 to 70 °C. However, insignificant difference in degradation efficiency for solution temperature from 50 to 70 °C. In 30 seconds, the degradation efficiency of Congo Red was increase from 32.4 to 71.6 % as increasing solution temperature from 30 to 70 °C.

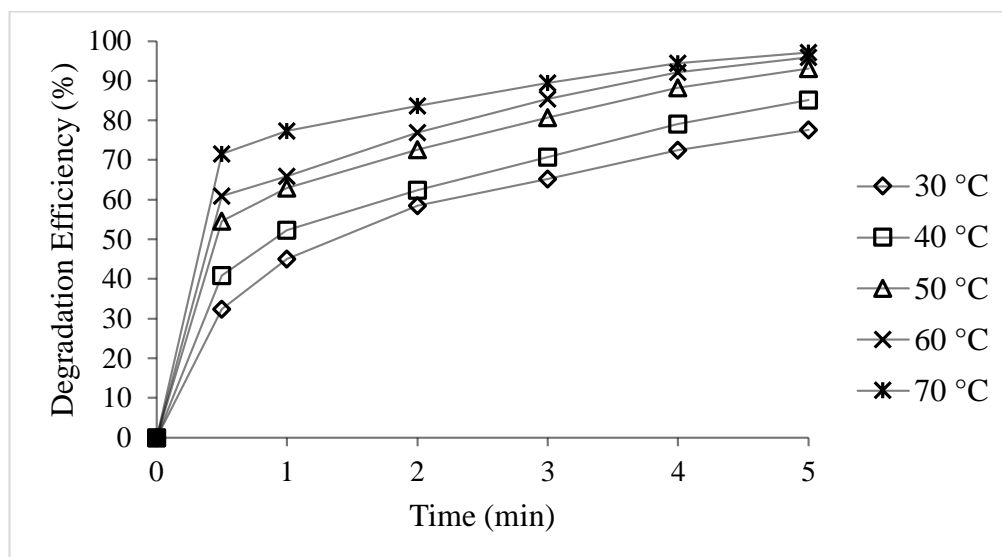


Figure 4.11: Effect of Solution Temperature on the Photocatalytic Degradation of Congo Red in the Presence of Cellulose Biochar/ TiO<sub>2</sub>-700 (Catalyst Dosage = 0.5 g/L, PMS Dosage = 0.3 mM, Dye Concentration = 10 mg/L, Reaction Time = 5 minutes, Initial pH = 5).

The increased in degradation efficiency of Congo Red was due to the increased of collision between adsorbent and adsorbate at high solution temperature which resulted in higher decolourisation activity (Gupta, et al., 2011). Moreover, the rate of recombination of electron-hole pair was reduced



so more hydroxyl radical involved in the degradation of Congo Red (Gaya and Abdullah, 2008).

As a result, the higher the solution temperature, the higher the degradation efficiency of Congo Red. Jain, et al. (2007) reported similar solution temperature trend in the photocatalytic degradation of Rhodamine B. The selected optimal solution temperature was 30 °C although the degradation efficiency was lower than higher temperature (40, 50, 60 and 70 °C). This was due to low solution temperature would lower the operating cost and also the degradation efficiency of Congo Red at 30 °C might be considered satisfactory.

#### 4.2.7 Effect of Types of Organic Dyes

The effect of types of organic dyes was investigated on the photocatalytic degradation. Five organic dyes used were Congo Red, Methyl Orange, Malachite Green, Methylene Blue and Rhodamine B. The results were depicted in Figure 4.12. It was observed that both Malachite Green and Congo Red showed 100 % degradation efficiency, then followed by Methyl Orange, Methylene Blue and lastly Rhodamine B.

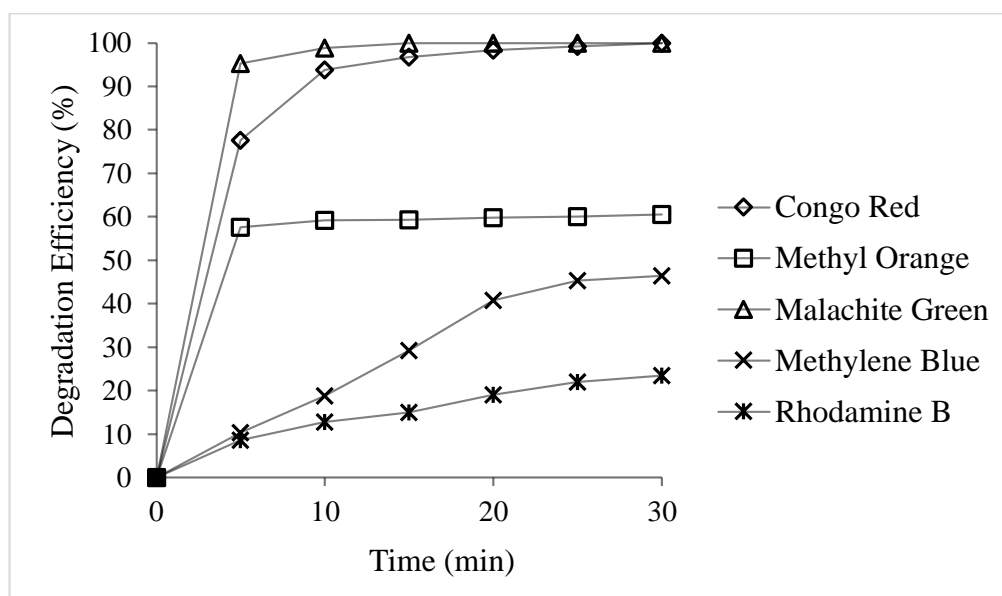


Figure 4.12: Photocatalytic Degradation of Type of Organic Dyes by Cellulose Biochar/ TiO<sub>2</sub>-700 (Catalyst Dosage = 0.5 g/L, PMS Dosage = 0.3 mM, Dye Concentration = 10 mg/L, Solution Temperature = 30 °C, Reaction Time = 30 minutes, Initial pH = 5).

The difference in degradation efficiency was due to difference molecular structures (Guerra, Santos and Araujo, 2012). Malachite Green had the highest rate of degradation compared to other organic dyes might be due to the cationic triphenylmethane structure which showed best degradation efficiency in the presence of hydroxyl radicals and oxidants (Rao and Venkatarangaiah, 2014). In other words, the molecular structure of Malachite Green was the simplest among all the organic dyes.

Congo Red and Methyl Orange were anionic azo dyes which consists of azo bond (-N=N-) with aromatic ring. As stated in previous section, anionic dye forms a strong electrostatic force of attraction when the catalyst surface become positive as these parameter studies carried out under acidic condition which promoted the degradation of dye. Congo Red showed higher degradation efficiency than Methyl Orange due the molecular structure of Congo Red was diazo instead of azo which had better rate of decomposition of dye (Pavithra, et al., 2019). On the other hand, Methylene Blue and Rhodamine B were cationic thiazine dye and cationic xanthene dye respectively which had resistance towards degradation due to the complex molecular structure and also repulsion force between dye and particles (Rao and Venkatarangaiah, 2014). The selected optimal type of organic dyes was Congo Red because it exhibited the highest degradation efficiency as well as the diazo molecular structure property.

### **4.3 Reusability Study**

The reusability study for photocatalytic degradation efficiency of Congo Red in the presence of cellulose biochar/ TiO<sub>2</sub>-700 composite was investigated. The used cellulose biochar/ TiO<sub>2</sub>-700 composite was collected followed by washing thoroughly using distilled water for three times before drying in the oven. According to Figure 4.13, the degradation efficiency of Congo Red in the presence of fresh cellulose biochar/ TiO<sub>2</sub>-700 and first reused cycle cellulose biochar/ TiO<sub>2</sub>-700 were 100 % and 91.2 % respectively after 30 minutes. It was observed that cellulose biochar/ TiO<sub>2</sub>-700 still maintained high photocatalytic degradation which indicated cellulose biochar/ TiO<sub>2</sub>-700 was reusable. Meanwhile, the degradation efficiency for second and third reused cycle cellulose biochar/ TiO<sub>2</sub>-700 were 72.9 % and 60.9 % respectively after 30

minutes. Therefore, it indicated that cellulose biochar/ TiO<sub>2</sub>-700 could be reused with minimal decrement in degradation efficiency.

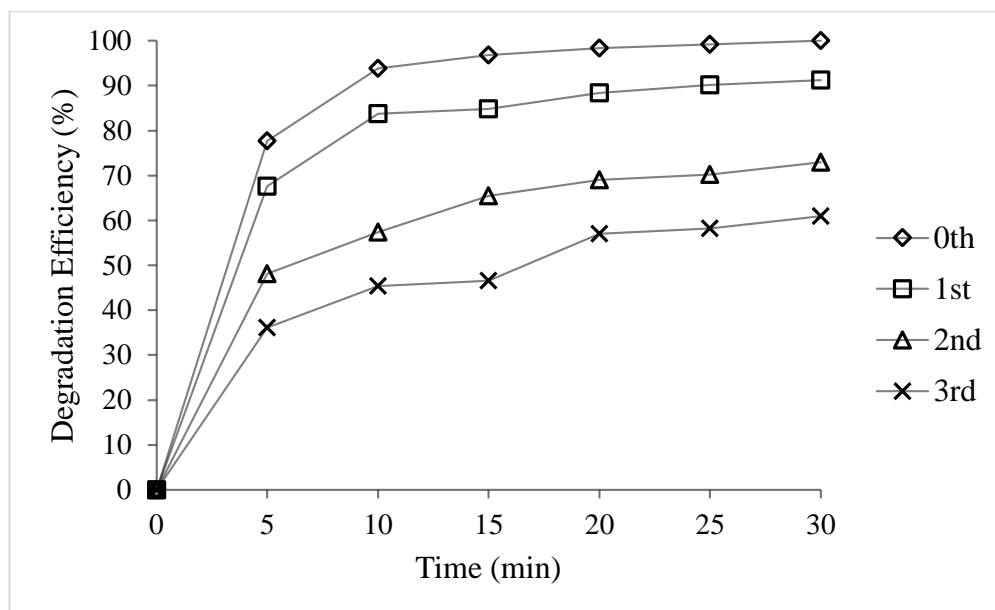


Figure 4.13: Photocatalytic Degradation of Congo Red by Fresh and Reuse Cellulose Biochar/ TiO<sub>2</sub>-700 (Catalyst Dosage = 0.5 g/L, PMS Dosage = 0.3 mM, Dye Concentration = 10 mg/L, Solution Temperature = 30 °C, Reaction Time = 30 minutes, Initial pH = 5).

There were a few similar decrement results had been reported recently. Lu, et al. (2019) reported that TiO<sub>2</sub>/ walnut shell biochar at the weight ratio of 0.2 to 1 showed a decrease in photocatalytic degradation efficiency of Methyl Orange from 100 % to 92.5 % after 5 cycles. Moreover, Zhang and Lu (2018) also reported TiO<sub>2</sub>/ biochar showed a decrement of degradation efficiency of Reactive Brilliant Blue from 80 % to 74 % after 5 cycles. As a result, cellulose biochar/ TiO<sub>2</sub>-700 composite could be reused for photocatalytic degradation of organic pollutants.

#### 4.4 Kinetic Study

Kinetic studies were carried out on the photocatalytic degradation of Congo Red to determine the reaction kinetic order of the process. The pseudo zero, first and second order were studied for the experimental data obtained using Congo Red at an initial concentration of 10 mg/L at different solution temperature.

Figure 4.14 shows a plot of  $\frac{1}{C_o} - \frac{1}{C_t}$  against time (t) for five different solution temperature. It could be observed that all the linear lines were regress to the data points. The photocatalytic degradation of Congo Red was pseudo second-order kinetic as it had relatively higher coefficient of determination ( $R^2$ ) value as compared to pseudo zero and first-order kinetic. It was consistent with the result reported by Zhang and Lu (2018) who studied the photocatalytic degradation of Reactive Brilliant Blue was followed pseudo second-order kinetic. The gradients of the linear lines were the second-order rate constant ( $k_{app}$ ). Table 4.2 shows the values of  $R^2$  and  $k_{app}$ . It was observed that the rate constant increased significantly from 0.1890 to 1.0534 ( $\frac{L}{mg\ min}$ ) as the solution temperature increased from 30 to 70 °C. This was due to higher temperature increased the collision between molecules as well as overcome the required reaction energy (Gupta, et al., 201)

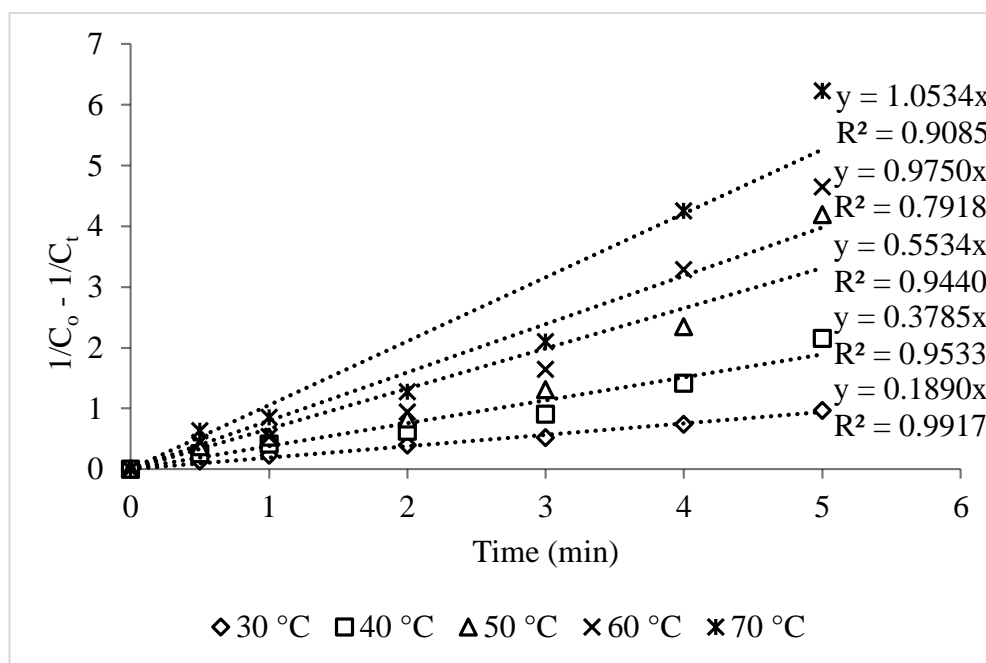


Figure 4.14: Pseudo Second-Order Reaction Kinetics Plot for Photocatalytic Degradation of Congo Red.

Table 4.2: Rate Coefficients for Degradation of Congo Red by Cellulose Biochar/ TiO<sub>2</sub>-700 under Different Temperature.

Temperature (°C)	Pseudo zero- order model		Pseudo first- order model		Pseudo second- order model	
	$R^2$	$k_{app}$ $\left(\frac{mg}{L\ min}\right)$	$R^2$	$k_{app}$ $\left(\frac{1}{min}\right)$	$R^2$	$k_{app}$ $\left(\frac{L}{mg\ min}\right)$
<b>30</b>	0.9440	0.5534	0.8793	0.3325	0.9917	0.1890
<b>40</b>	0.4443	0.5576	0.8962	0.4064	0.9533	0.3785
<b>50</b>	0.5458	0.6819	0.9440	0.5534	0.9440	0.5534
<b>60</b>	0.1061	0.8733	0.8789	0.6293	0.7918	0.9750
<b>70</b>	-0.236	1.0237	0.7690	0.7301	0.9085	1.0534

The correlation between  $k_{app}$  and solution temperature could be explained by using the Arrhenius equation as shown in Equation (4.1):

$$\ln k_{app} = \ln A_0 - \frac{E_a}{RT} \quad (4.1)$$

where  $k_{app}$  is the second-order rate constant,  $A_0$  is the pre-exponential factor  $\left(\frac{L}{mg\ min}\right)$ ,  $E_a$  is the activation energy  $\left(\frac{kJ}{mol}\right)$ ,  $R$  is the ideal gas constant  $\left(8.314 \frac{kJ}{mol\ K}\right)$  and  $T$  is the absolute temperature (K). Based on Figure 4.15, a good linear relationship between  $\ln k_{app}$  and  $1/T$  was obtained due to the high  $R^2$  value of 0.9627. The Arrhenius equation for the photocatalytic degradation of Congo Red is shown in Equation (4.2):

$$\ln k_{app} = 13.58 - 4584.5 \left(\frac{1}{T}\right) \quad (4.2)$$

The values of  $E_a$  and  $A_0$  could be determined from the slope  $\left(-\frac{E_a}{R}\right)$  and intercept  $(\ln A_0)$  respectively. The values of  $E_a$  and  $A_0$  for the photocatalytic degradation of Congo Red under different temperatures were  $38.16 \frac{kJ}{mol}$  and

$7.90 \times 10^5 \frac{L}{mg \cdot min}$  respectively. Yetim and Tekin (2017) reported that the textile dyes consist mixture of Disperse Red 92, Acid Red 27 and Acid Orange 10 had a  $E_a$  of  $65.4 \frac{kJ}{mol}$ . Therefore, photocatalytic degradation of Congo Red was easier than the textile dyes mixture.

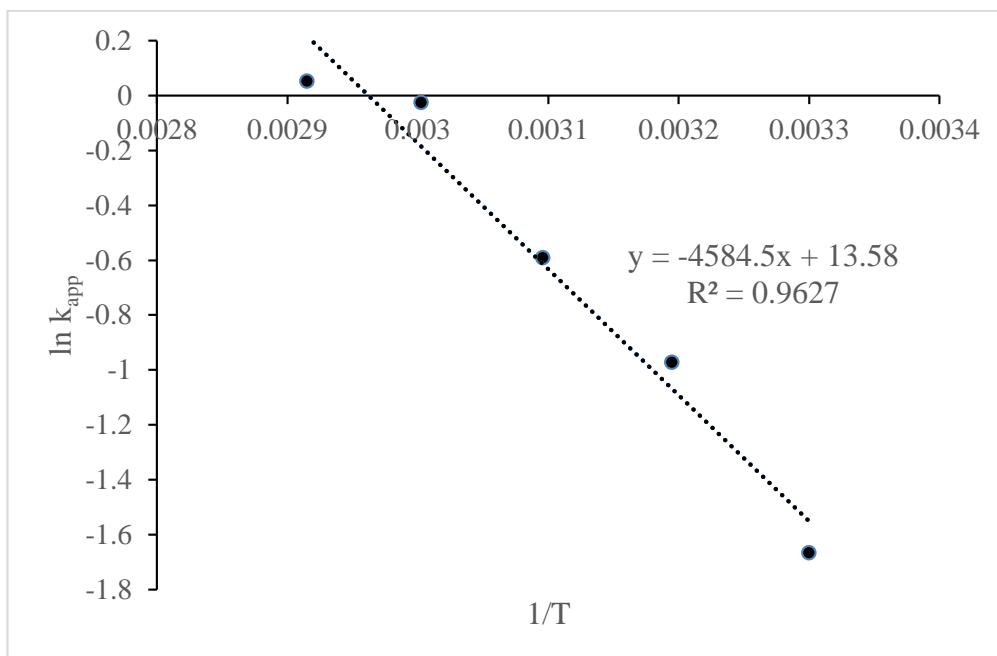


Figure 4.15: Arrhenius Plot of  $k_{app}$  against  $1/T$ .

#### 4.5 COD Analysis

The COD removal efficiency of Congo Red in the presence of photocatalyst and PMS (catalyst dosage = 0.5 g/L, PMS dosage = 0.3 mM, dye concentration = 10 mg/L, solution temperature = 30 °C, reaction time = 120 minutes, initial pH = 5), photocatalyst (catalyst dosage = 0.5 g/L, dye concentration = 10 mg/L, solution temperature = 30 °C, reaction time = 120 minutes, initial pH = 5) and photolysis (dye concentration = 10 mg/L, solution temperature = 30 °C, reaction time = 120 minutes, initial pH = 5) were investigated. The COD values before and after reaction had been determined by the Colorimetric Determination Method 8000. Figure 4.16 shows the COD removal efficiency under different conditions.

It could be observed that the COD removal rate for photolysis in the absence of catalyst was 0 % during pre-adsorption stage. COD removal rates

were 84.5 %, 29.2 % and 1.1 % for photocatalytic degradation and photolysis, respectively. Similar observation had been reported by other researchers. Lu, et al. (2019) reported that 83.2 % COD removal efficiency using biochar/ TiO<sub>2</sub> for the photocatalytic degradation of Methyl Orange after 150 minutes. Jain, et al. (2007) stated that 85.6 % COD removal efficiency for the photocatalytic degradation of Rhodamine B after 60 minutes.

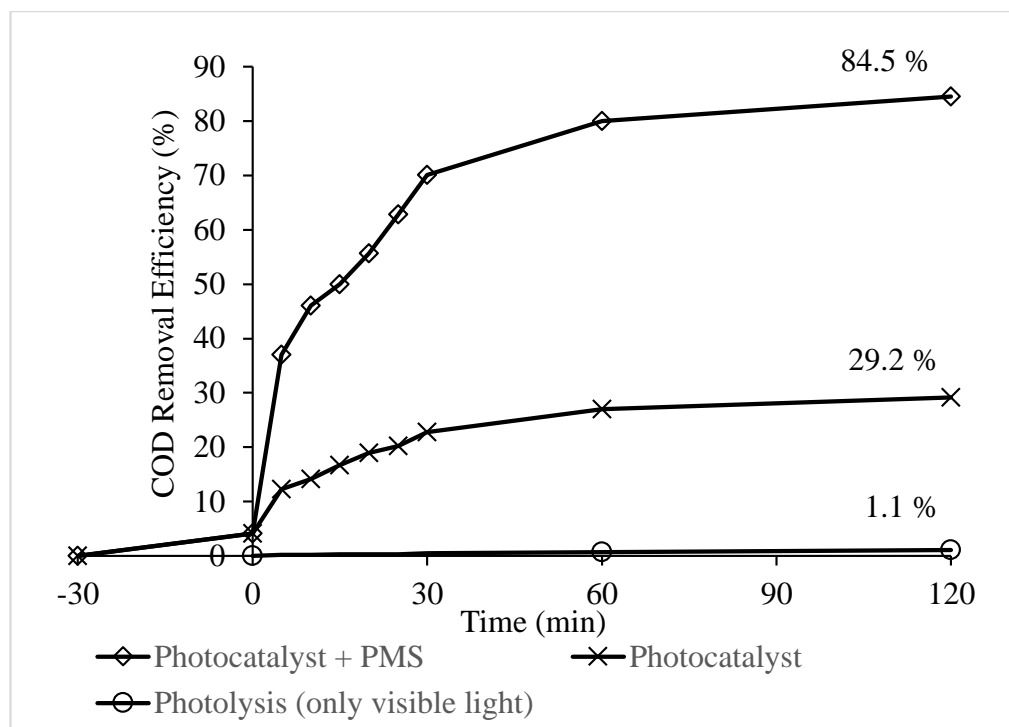


Figure 4.16: The COD Removal Efficiency of Congo Red by the Cellulose Biochar/ TiO<sub>2</sub>-700 and PMS, Cellulose Biochar/ TiO<sub>2</sub>-700 and Photolysis (only visible light).

#### 4.6 Summary

Sol-gel method was used to synthesised cellulose biochar/ TiO<sub>2</sub> composites and calcined at different temperature for photocatalytic degradation of Congo Red. The characteristics of cellulose biochar/ TiO<sub>2</sub> composites were studied using the XRD, SEM-EDX, FTIR, TGA analyses and zeta potential analyses. The effect of various parameters such as type of catalysts, catalyst dosage, solution pH, PMS dosage, initial dye concentration, solution temperature and type of organic dyes were studied on the photocatalytic degradation of Congo Red to determine the optimum conditions. The optimum conditions for the photocatalytic

degradation were 0.5 g/L of cellulose biochar/ TiO<sub>2</sub>-700 with 0.3 Mm of PMS used on an initial dye concentration of 10 mg/L under 30 °C and pH 5. Under these conditions, the degradation efficiency of Congo Red was 100 % in 30 minutes whereas the COD removal efficiency was 84.5 % in 120 minutes. Besides, the reusability of cellulose biochar/ TiO<sub>2</sub>-700 in the photocatalytic degradation of Congo Red was also studied. Last but not least, the photocatalytic degradation of Congo Red was followed pseudo second-order kinetic order.



## CHAPTER 5

### CONCLUSION AND RECOMMENDATIONS

#### 5.1 Conclusion

In this research, cellulose biochar/ TiO<sub>2</sub> composites were synthesised using sol-gel method and being calcined at different temperature for photocatalytic degradation of Congo Red. The characteristics of cellulose biochar/ TiO<sub>2</sub> composites were studied using the XRD, SEM-EDX, FTIR, TGA and zeta potential analyses. The XRD patterns showed that anatase and rutile phase TiO<sub>2</sub> had been distributed on the cellulose biochar surface of the composite materials. The SEM results suggested that TiO<sub>2</sub> particles had been embedded on the cellulose biochar surface and prevent agglomeration of particles in the cellulose biochar/ TiO<sub>2</sub> composite materials. The EDX analysis indicated that cellulose biochar/ TiO<sub>2</sub> composites were composed mainly of carbon, oxygen and titanium atoms. FTIR spectroscopy showed that O-H stretching, C-H stretching and Ti-O stretching were presence in the cellulose biochar/ TiO<sub>2</sub> composite materials. Zeta potential analysis indicated that the zero charge point of cellulose biochar/ TiO<sub>2</sub>-700 was pH 5.1.

The effect of various operating parameters such as type of catalysts, catalyst dosage, solution pH, PMS dosage, initial dye concentration, solution temperature and type of organic dyes were studied on the photocatalytic degradation of Congo Red to determine the optimum conditions. It was found that increasing the calcination temperature of cellulose biochar/ TiO<sub>2</sub> composites increased the photocatalytic degradation efficiency of Congo Red before it reached the optimum point and decreased beyond the calcination temperature. The optimum conditions for the photocatalytic degradation of Congo Red were 0.5 g/L of cellulose biochar/ TiO<sub>2</sub>-700 with 0.3 mM of PMS used to treat an initial dye concentration of 10 mg/L under 30 °C and solution pH 5. Under these conditions, the degradation efficiency of Congo Red was 100 % in 30 minutes whereas the COD removal efficiency was 84.5 % in 120 minutes.

Moreover, the reusability of cellulose biochar/ TiO<sub>2</sub>-700 in the photocatalytic degradation of Congo Red was also studied. The degradation

efficiency decreased to 91.2 %, 72.9 % and 60.9 % for first, second and third reused cycle respectively. Besides, the photocatalytic degradation of Congo Red was followed pseudo second-order reaction kinetic with  $E_a$  and  $A_0$  values of  $38.16 \frac{kJ}{mol}$  and  $7.90 \times 10^5 \frac{L}{mg \cdot min}$  respectively.

## 5.2 Recommendations for future work

The pure  $TiO_2$  and the cellulose biochar/  $TiO_2$  composites should be characterised by Brunauer-Emmett-Teller (BET) surface analysis in order to study the effect of calcination temperature on the specific surface area and the porosity. Specific surface area was significant property of catalyst as it determined the photocatalytic degradation efficiency. This was due to the large specific surface area might allow  $TiO_2$  to be distributed on the cellulose biochar surface or pore which prevent agglomeration of  $TiO_2$ . Besides, more electron can be protonated from the VB which resulted in more hydroxyl radicals for the degradation of organic dyes. Therefore, it was important to study specific surface area and porosity of cellulose biochar/  $TiO_2$  composites.

Inductively Coupled Plasma-Optical Emission Spectroscopy (ICP-OES) can also be carried out, to characterise the cellulose biochar/  $TiO_2$  composites. This was due to the analytical grade of the ICP-OES can determined the trace amount of Ti component. Therefore, ICP-OES can identified the impurities presence in cellulose biochar/  $TiO_2$  composites which can be traced from the original source and eliminated impurities in future works.

## REFERENCES

- Abdelsamad, A. M. A., Gad-Allah, T. A., Mahmoud, F. A. and Badawy, M. I., 2018. Enhanced photocatalytic degradation of textile wastewater using Ag/ZnO. *Journal of Water Process Engineering*, 25, pp. 88-95.
- Abdullah, M. A., Nazir, M. S., Raza, M. R., Wahjoedi, B. A. and Yussof, A. W., 2016. Autoclave and ultra-sonication treatments of oil palm empty fruit bunch fibers for cellulose extraction and its polypropylene composite properties. *Journal of Cleaner Production*, 126, pp. 686-697.
- Alhaji, M. H., Sanaullah, K., Khan, A., Hamza, A., Muhammad, A., Ishola, M. S., Rigit, A. R. H. and Bhawani, S. A., 2017. Recent developments in immobilizing titanium dioxide on supports for degradation of organic pollutants in wastewater - a review. *International Journal of Environmental Science and Technology*, 14, pp. 2039-2052.
- Al-Hamdi, A. M., Rinner, U. and Sillanpaa, M., 2017. Tin dioxide as a photocatalyst for water treatment: a review. *Process Safety and Environmental Protection*, 107, pp. 190-205.
- Allen, N. S., Mahdjoub, N., Vishnyakov, V., Kelly, P. J. and Kriek, R. J., 2018. The effect of crystalline phase (anatase, brookite and rutile) and size on the photocatalytic activity of calcined polymorphic titanium dioxide (TiO<sub>2</sub>). *Polymer Degradation and Stability*, 150, pp. 31-36.
- Ani, I. J., Akpan, U. G., Olutoye, M. A. and Hameed, B. H., 2018. Photocatalytic degradation of pollutants in petroleum refinery wastewater by TiO<sub>2</sub> and ZnO based photocatalysts: Recent development. *Journal of Cleaner Production*, 205, pp. 930-954.
- Antoniou, M. G., Boraie, I., Solakidou, M., Deligiannakis, Y., Abhishek, M., Lawton, L. A. and Edwards, C., 2018. Enhancing photocatalytic degradation of the cyanotoxin microcystin-LR with the addition of sulfate-radical generating oxidants. *Journal of Hazardous Materials*, 360, pp. 461-470.
- Asgari, G., Faradmal, J., Nasab, H. Z. and Ehsani, H., 2019. Catalytic ozonation of industrial textile wastewater using modified C-doped MgO eggshell membrane powder. *Advanced Powder Technology*, 30, pp. 1297-1311.

Asghar, A., Raman, A. A. A. and Daud, W. M. A. W., 2014. Advanced oxidation processes for in-situ production of hydrogen peroxide/ hydroxyl radical for textile wastewater treatment: a review. *Journal of Cleaner Production*, 87, pp. 826-838.

Asim, N., Syuhami, M. F., Badiei, M. and Yarmo, M. A., 2014. WO<sub>3</sub> modification by synthesis of nanocomposites. *APCBEE Procedia*, pp. 175-180.

Bello, M. M., Rahman, A. A. A. and Asghar, A., 2019. A review on approaches for addressing the limitations of fenton oxidation for recalcitrant wastewater treatment. *Process Safety and Environmental Protection*, 126, pp. 119-140.

Bilinska, L., Blus, K., Gmurek, M. and Ledakowicz, S., 2019. Coupling of electrocoagulation and ozone treatment for textile wastewater reuse. *Chemical Engineering Journal*, 358, pp. 992-1001.

Brito, G. F. D. S., Oliveria, R., Grisolia, C. K., Guirra, L. S., Weber, I. T. and Almeida, F. V. D., 2019. Evaluation of advanced oxidative processes in biodiesel wastewater treatment. *Journal of Photochemistry and Photobiology A: Chemistry*, 375, pp. 85-90.

Cai, X. X., Li, J., Liu, Y. G., Yan, Z. L., Tan, X. F., Liu, S. B., Zheng, G. M., Gu, Y. L., Hu, X. J. and Jiang, L. H., 2017. Titanium dioxide coated biochar composites as adsorptive and photocatalytic degradation materials for the removal of aqueous organic pollutants. *Journal of Chemical Technology and Biotechnology*, 93, pp. 783-791.

Carmen, Z. and Daniela, S., 2012. Textile organic dyes – characteristics, polluting effects and separation/elimination procedures from industrial effluents – a critical overview. *Organic pollutants ten years after the stockholm convention - environmental and analytical update*, [e-journal] Available through: <http://www.intechopen.com/books/organic-pollutants-ten-years-after-the-stockholm-convention-environmental-and-analytical-update/textile-organic-dyes-characteristicspolluting-effects-and-separation-elimination-procedures-from-in> [Accessed 6 June 2019].

Carp, O., Huisman, C. L. and Reller, A., 2004. Photoinduced reactivity of titanium dioxide. *Progress in Solid State Chemistry*, 32, pp. 33-177.

Cetinkaya, S. G., Morcali, M. H., Akarsu, S., Ziba, C. A. and Dolaz, M., 2018. Comparison of classic fenton with ultrasound fenton processes on industrial textile wastewater. *Sustainable Environment Research*, 28, pp. 165-170.

Chanwala, J., Kaushik, G., Dar, M. A., Upadhyay, S. and Agrawal, A., 2018. Process optimization and enhanced decolorization of textile effluent by *Planococcus* sp. isolated from textile sludge. *Environmental Technology and Innovation*, 13, pp. 122-129.

Chen, D., Wang, X. N., Zhang, X. Q., Yang, Y., Xu, Y. and Qian, G. R., 2019. Facile fabrication of mesoporous biochar/ZnFe<sub>2</sub>O<sub>4</sub> composite with enhanced visible-light photocatalytic hydrogen evolution. *International Journal of Hydrogen Energy*, [e-journal] Available through: Universiti Tunku Abdul Rahman Library website <<https://library.utar.edu.my/>> [Accessed 29 June 2019].

Chen, H., Liu, Y., Xu, X., Sun, M., Jiang, M., Xue, G., Li, X. and Liu, Z., 2018. How does iron facilitate the aerated biofilter for tertiary simultaneous nutrient and refractory organics removal from real dyeing wastewater?. *Water Research*, 148, pp. 344-358.

Chen, Y. Q., Zhang, X., Chen, W., Yang, H. P. and Chen, H. P., 2017. The structure evolution of biochar from biomass pyrolysis and its correlation with gas pollutant adsorption performance. *Bioresource Technology*, 246, pp. 101-109.

Cheng, C. K., Deraman, M. R., Ng, K. H. and Khan, M. R., 2015. Preparation of titania doped argentine photocatalyst and its photoactivity towards palm oil mill effluent degradation. *Journal of Cleaner Production*, 112, pp. 1128-1135.

Cheng, T. S., Lan, D. N. U., Phillips, S. and Tran, L. Q. N., 2018. Characteristics of oil palm empty fruit bunch fiber and mechanical properties of its unidirectional composites. *Polymer Composites*, 40, pp. 1158-1164.

Chiban, M., Soudani, A., Sinan, F. and Persin, M., 2011. Wastewater treatment by batch adsorption method onto micro-particles of dried *withania frutescens* plant as a new adsorbent. *Journal of Environmental Management*, 95, pp. 61-65.

Chong, M. N., Jin, B., Chow, C. W. K. and Saint, C., 2010. Recent developments in photocatalytic water treatment technology: a review. *Water Research*, 44, pp. 2997-3027.

Christie, R. M., 2015. *Colour chemistry*. 2nd edition. Cambridge: The Royal Society of Chemistry.

Cinperi, N. C., Ozturk, E., Yigit, N. O. and Kitis, M., 2019. Treatment of woolen textile wastewater using membrane bioreactor, nanofiltration and reverse osmosis for reuse in production processes. *Journal of Cleaner Production*, 223, pp. 837-848.

Collivignarelli, M. C., Abba, A., Miino, M. C. and Damiani, S., 2019. Treatments for color removal from wastewater: state of the art. *Journal of Environmental Management*, 236, pp. 727-745.

Colmenares, J. C., Varma, R. S. and Lisowski, P., 2016. Sustainable hybrid photocatalysts: titania immobilized on carbon materials derived from renewable and biodegradable resources. *Green Chemistry*, 18(21), pp. 5736-5750.

Dai, Y. J., Zhang, N. X., Xing, C. M., Cui, Q. X. and Sun, Q. Y., 2019. The adsorption, regeneration and engineering applications of biochar for removal organic pollutants: a review. *Chemosphere*, 223, pp. 12-27.

Danks, A. E., Hall, S. R. and Schnepf, Z., 2016. The evolution of “sol-gel” chemistry as a technique for materials synthesis. *Materials Horizons*, 3, pp. 91-112.

Daud, W. M. A. W. and Ali, W. S. W., 2004. Comparison on pore development of activated carbon produced from palm shell and coconut shell. *Bioresource Technology*, 93, pp. 63-69.

Delannoy, M., Yehya, S., Techer, D., Razafitianamaharavo, A., Richard, A., Caria, G., Baroudi, M., Montarges-Pelletier, E., Rychen, G. and Feidt, C., 2018. Amendment of soil by biochars and activated carbons to reduce chlordecone bioavailability in piglets. *Chemosphere*, 210, pp. 486-494.

Dong, H., Zeng, G. M., Tang, L., Fan, C. Z., Zhang, C., He, X. X. and He., 2015. An overview on limitations of TiO<sub>2</sub>-based particles for photocatalytic degradation of organic pollutants and the corresponding countermeasures. *Water research*, 79, pp. 128-146.

Elizalde-Gonzalez, M. P. and Hernandez-Montoya, V., 2007. Characterization of mango pit as raw material in the preparation of activated carbon for wastewater treatment. *Biochemical Engineering Journal*, 36, pp. 230-238.

Elkhalifa, S., Al-Ansari, T., Mackey, H. R. and McKay, G., 2019. Food waste to biochars through pyrolysis: a review. *Resources, Conservation and Recycling*, 144, pp. 310-320.

El-Sheikh, A. H., Newman, A. P., Al-Daffae, A., Phull, S., Cresswell, N. and York, S., 2004. Deposition of anatase on the surface of activated carbon. *Surface and Coatings Technology*, 187, pp. 284-292.

Fagan, R., McCormack, D., Hinder, S. and Pillai, S., 2016. Photocatalytic properties of g-C<sub>3</sub>N<sub>4</sub>-TiO<sub>2</sub> heterojunctions under UV and visible light conditions. *Materials*, 9, pp. 286-301.

Fischer, K., Gawel, A., Rosen, D., Krause, M., Latif, A. A., Griebel, J., Prager, A. and Schulze, A., 2017. Low temperature synthesis of anatase/ rutile/ brookite TiO<sub>2</sub> nanoparticles on a polymer membrane for photocatalysis. *Catalyst*, 7, pp. 209-223.

Fu, P., Hu, S., Xiang, J., Sun, L. S., Li, P. S., Zhang, J. Y. and Zheng, C. G., 2009. Pyrolysis of maize stalk on the characterization of chars formed under different devolatilization conditions. *Energy Fuels*, 23, pp. 4605-4611.

Fujishima, A., Zhang, X. T. and Tryk, D. A., 2008. TiO<sub>2</sub> photocatalysis and related surface phenomena. *Surface Science Reports*, 63, pp. 515-582.

Gaya, U. I. and Abdullah, A. H., 2008. Heterogeneous photocatalytic degradation of organic contaminants over titanium dioxide: a review of fundamentals, progress and problems. *Journal of Photochemistry and Photobiology C: Photochemistry Reviews*, 9, pp. 1-12.

Gomis-Berenguer, A., Velasco, L. F., Velo-Gala, I. and Ania, C. O., 2016. Photochemistry of nanoporous carbons: perspectives in energy conversion and environmental remediation. *Journal of Colloid and Interface Science*, 490, pp. 879-901.

Gopi, S., Balakrishnan, P., Chandrahara, D., Poovathankandy, D. and Thomas, S., 2019. General scenarios of cellulose and its use in the biomedical field. *Materials Today Chemistry*, 13, pp. 59-78.

Guerra, E., Gosetti, F., Marengo, E., Llompert, M. and Garcia-Jares, C., 2019. Study of photostability of three synthetic dyes commonly used in mouthwashes. *Microchemical Journal*, 146, pp. 776-781.

Guerra, W. N. A., Santos, J. M. T. and Araujo, L. R. R. D., 2012. Decolorization and mineralization of reactive dyes by a photocatalytic process using ZnO and UV radiation. *Water Science and Technology*, 66, pp. 158-164.

Guettai, N. and Amar, H. A., 2005. Photocatalytic oxidation of methyl orange in presence of titanium dioxide in aqueous suspension. Part I: parametric study. *Desalination*, 185, pp. 427-437.

Gupta, V. K., Jain, R., Mittal, A., Saleh, T. A., Nayak, A., Agarwal, S. and Sikarwar, S., 2011. Photo-catalytic degradation of toxic dye amaranth on TiO<sub>2</sub>/UV in aqueous suspensions. *Materials Science and Engineering: C*, 32, pp. 12-17.

Gupta, V. K., Jain, R., Nayak, A., Agarwal, S. and Shrivastava, M., 2011. Removal of the hazardous dye—tartrazine by photodegradation on titanium dioxide surface. *Materials Science and Engineering: C*, 31, pp. 1062-1067.

Hameed, S., Sharma, A., Pareek, V., Wu, H. and Yu, Y., 2019. A review on biomass pyrolysis models: kinetic, network and mechanistic models. *Biomass and Bioenergy*, 123, pp. 104-122.

Hao, Z., Wang, C., Yan, Z., Jiang, H. and Xu, Huacheng., 2018. Magnetic particles modification of coconut shell-derived activated carbon and biochar for effective removal of phenol from water. *Chemosphere*, 211, pp. 962-969.



Hassan, M. M. and Carr, C. M., 2018. A critical review on recent advancements of the removal of reactive dyes from dye house effluent by ion-exchange adsorbents. *Chemosphere*, 209, pp. 201-219.

Holkar, C. R., Jadhav, A. J., Pinjari, D. V., Mahamuni, N. M. and Pandit, A. B., 2016. A critical review on textile wastewater treatments: possible approaches. *Journal of Environmental Management*, 182, pp. 351-366.

Hossain, L., Sarker, S. K. and Khan, M. S., 2018. Evaluation of present and future wastewater impacts of textile dyeing industries in Bangladesh. *Environmental Development*, 26, pp. 23-33.

Hu, C., Wang, Y. Z. and Tang, H. X., 2000. Preparation and characterization of surface bond-conjugated  $\text{TiO}_2/\text{SiO}_2$  and photocatalysis for azo dyes. *Applied Catalysis B: Environmental*, 30, pp. 277-285.

Hussain, S. N., Ahmad, A., Ali, A., Sattar, H. and Asghar, H. M. A., 2015. Wastewater treatment of textile industry via adsorption and electrochemical regeneration. *International Conference on Advances in Environment Research*, 87, pp. 13-19.

IHS, 2018. *Dyes-chemical economics handbook*. [online]. Available at: <<https://ihsmarkit.com/products/dyes-chemical-economics-handbook.html>> [Accessed 6 June 2019].

Isik, Z., Arıkan, E. B., Bouras, H. D. and Dizge, N., 2019. Bioactive ultrafiltration membrane manufactured from *Aspergillus carbonarius* M333 filamentous fungi for treatment of real textile wastewater. *Bioresource Technology Reports*, 5, pp. 212-219.

Ito, T., Adachi, Y., Yamanashi, Y. and Shimada, Y., 2016. Long-term natural remediation process in textile dye-polluted river sediment driven by bacterial community changes. *Water Research*, 100, pp. 458-465.

Jadhav, A. J. and Srivastava, V. C., 2013. Adsorbed solution theory based modeling of binary adsorption of nitrobenzene, aniline and phenol onto granulated activated carbon. *Chemical Engineering Journal*, 229, pp. 450-459.

Jain, R., Mathur, M., Sikarwar, S. and Mittal, A., 2007. Removal of the hazardous dye rhodamine B through photocatalytic and adsorption treatments. *Journal of Environmental Management*, 85, pp. 956-964.

Jantawas, P., Sreethawong, T. and Chavadej, S., 2009. Photocatalytic activity of nanocrystalline mesoporous-assembled TiO<sub>2</sub> photocatalyst for degradation of methyl orange monoazo dye in aqueous wastewater. *Chemical Engineering Journal*, 155, pp. 223-233.

Judd, S. and Jefferson, B., 2003. *Membranes for industrial wastewater recovery and re-use*. Langford Lane: Elsevier Advanced Technology.

Katheresan, V., Kansedo, J. and Lau, S. Y., 2018. Efficiency of various recent wastewater dye removal methods: a review. *Journal of Environmental Chemical Engineering*, 6, pp. 4676-4697.

Kaur, K. and Jindal, R., 2018. Synergistic effect of organic-inorganic hybrid nanocomposite ion exchanger on photocatalytic degradation of rhodamine-B dye and heavy metal ion removal from industrial effluents. *Journal of Environmental Chemical Engineering*, 6, pp. 7091-7101.

Khaki, M. R. D., Shafeeyan, M. S., Rahman, A. A. A. and Daud, W. M. A. W., 2017. Application of doped photocatalysts for organic pollutant degradation- a review. *Journal of Environmental Management*, 198, pp. 78-94.

Khataee, A. R. and Kasiri, M. B., 2010. Photocatalytic degradation of organic dyes in the presence of nanostructured titanium dioxide: influence of the chemical structure of dyes. *Journal of Molecular Catalysis A: Chemical*, 328, pp. 8-26.

Khataee, A. R., Pons, M. N. and Zahraa, O., 2009. Photocatalytic degradation of three azo dyes using immobilized TiO<sub>2</sub> nanoparticles on glass plates activated by UV light irradiation: influence of dye molecular structure. *Journal of Hazardous Materials*, 168, pp. 451-457.

Khataee, A., Kayan, B., Gholami, P., Kalderis, D. and Akay, S., 2017. Sonocatalytic degradation of an anthraquinone dye using TiO<sub>2</sub>-biochar nanocomposite. *Ultrasonics Sonochemistry*, 39, pp. 120-128.

Kim, J. R. and Kan, E., 2016. Heterogeneous photocatalytic degradation of sulfamethoxazole in water using a biochar supported TiO<sub>2</sub> photocatalyst. *Journal of Environmental Management*, 180, pp. 94-101.

King Saud University, 2015. Metal oxides as photocatalysts. *Journal of Saudi Chemical Society*, 19, pp. 462-464.

Klemm, D., 1998. *Comprehensive cellulose chemistry*. New York: Wiley-VCH, Weinheim.

Kong, S. H., Loh, S. K., Bachmann, R. T., Rahim, S. A. and Salimon, J., 2014. Biochar from oil palm biomass: a review of its potential and challenges. *Renewable and Sustainable Energy Reviews*, 39, pp. 729-739.

Konstantinou, I. K. and Albanis, T. A., 2003. TiO<sub>2</sub>-assisted photocatalytic degradation of azo dyes in aqueous solution: kinetic and mechanistic investigations a review. *Applied Catalysis B: Environmental*, 49, pp. 1-14.

Laqbaqbi, M., Garcia-Payo, M. C., Khayet, M., El Kharraz, J. and Chaouch, M., 2019. Application of direct contact membrane distillation for textile wastewater treatment and fouling study. *Separation and Purification Technology*, 209, pp. 815-825.

Lee, J. H. and Yang, Y. S., 2005. Effect of hydrolysis conditions on morphology and phase content in the crystalline TiO<sub>2</sub> nanoparticles synthesized from aqueous TiCl<sub>4</sub> solution by precipitation. *Materials Chemistry and Physics*, 93, pp. 237-242.

Lee, S. L., Ho, L. N., Ong, S. A., Wong, Y. S., Voon, C. H., Khalik, W. F., Yusoff, N. A. and Nordin, N., 2018. Exploring the relationship between molecular structure of dyes and light sources for photodegradation and electricity generation in photocatalytic fuel cell. *Chemosphere*, 209, pp. 935-943.

Lee, Y. Y., Jung, H. S. and Kang, Y. T., 2017. A review: effect of nanostructures on photocatalytic CO<sub>2</sub> conversion over metal oxides and compound semiconductors. *Journal of CO<sub>2</sub> Utilization*, 20, pp. 163-177.

Li, J. F., Li, Y. M., Wu, Y. L. and Zheng, M. Y., 2014. A comparison of biochars from lignin, cellulose and wood as the sorbent to an aromatic pollutant. *Journal of Hazardous Materials*, 280, pp. 450-457.

Liang, J., Ning, X. A., Sun, J., Song, J., Hong, Y. and Cai, H., 2018. An integrated permanganate and ozone process for the treatment of textile dyeing wastewater: efficiency and mechanism. *Journal of Cleaner Production*, 204, pp. 12-19.

Liang, S., Xiao, K., Mo, Y. H. and Huang, X., 2011. A novel ZnO nanoparticle blended polyvinylidene fluoride membrane for anti-irreversible fouling. *Journal of Membrane Science*, 394, pp. 184-192.

Lisowski, P., Colmenares, J. C., Masek, O., Lisowski, W., Lisovytskiy, D., Kaminska, A. and Lomot, D., 2017. Dual functionality of TiO<sub>2</sub>/biochar hybrid materials: photocatalytic phenol degradation in the liquid phase and selective oxidation of methanol in the gas phase. *ACS Sustainable Chemistry and Engineering*, 5, pp. 6274-6287.

Lobos, M. L. N., Sieben, J. M., Comignani, V., Duarte, M., Volpe, M. A. and Moyano, E. L., 2016. Biochar from pyrolysis of cellulose: An alternative catalyst support for the electro-oxidation of methanol. *International Journal of Hydrogen Energy*, 41(25), pp. 10695-10706.

Lu, L., Shan, R., Shi, Y. Y., Wang, S. X. and Yuan, H. R., 2019. A novel TiO<sub>2</sub>/biochar composite catalysts for photocatalytic degradation of methyl orange. *Chemosphere*, 222, pp. 391-398.

Lv, G. and Wu, S., 2012. Analytical pyrolysis studies of corn stalk and its three main components by TG-MS and Py-GC/MS. *Journal of Analytical and Applied Pyrolysis*, 97, pp. 11-18.

Mahamallik, P. and Pal, A., 2017. Degradation of textile wastewater by modified photo-fenton process: application of Co(II) adsorbed surfactant-modified alumina as heterogeneous catalyst. *Journal of Environmental Chemical Engineering*, 5, pp. 2886-2893.

Mahmoodi, N. M., Abdi, J., Oveisi, M., Asli, M. A. and Vossoughi, M., 2018. Metal-organic framework (MIL-100 (Fe)): synthesis, detailed photocatalytic dye degradation ability in colored textile wastewater and recycling. *Materials Research Bulletin*, 100, 357-366.

Makrigianni, V., Giannakas, A., Daikopoulos, C., Deligiannakis, Y. and Konstantinou, I., 2015. Preparation, characterization and photocatalytic performance of pyrolytic-tire-char/TiO<sub>2</sub> composites, toward phenol oxidation in aqueous solutions. *Applied Catalysis B: Environmental*, 174, pp. 244-252.

Marschall, R. and Wang, L., 2014. Non-metal doping of transition metal oxides for visible-light photocatalysis. *Catalysis Today*, 225, pp. 111-135.

Martins, A. C., Cazetta, A. L., Pezoti, O., Souza, J. R. B., Zhang, T., Pilau, E. J., Asefa, T. and Almeida, V. C., 2017. Sol-gel synthesis of new TiO<sub>2</sub> /activated carbon photocatalyst and its application for degradation of tetracycline. *Ceramics International*, 43, pp. 4411-4418.

Masters, G. M., 2013. *Introduction to environmental and engineering and science*. 3<sup>rd</sup> ed. Prentice Hall.

Mayakaduwa, S. S., Kumarathilaka, P., Herath, I., Ahmad, M., Al-Wabel, M., Ok, Y. S., Usman, A., Abduljabbar, A. and Vithanage, M., 2015. Equilibrium and kinetic mechanisms of woody biochar on aqueous glyphosate removal. *Chemosphere*, 80, pp. 1-6.

Mehrpooya, M., Khalili, M. and Sharifzadeh, M. M. M., 2018. Model development and energy and exergy analysis of the biomass gasification process (based on the various biomass sources). *Renewable and Sustainable Energy Reviews*, 91, pp. 869-887.

Mishra, A., Mehta, A. and Basu, S., 2018. Clay supported TiO<sub>2</sub> nanoparticles for photocatalytic degradation of environmental pollutants: a review. *Journal of Environmental Chemical Engineering*, 6, pp. 6088-6107.

Mohamad, M., Abustan, I., Samuding, K., Mohamad, N. and Mohamad, A., 2018. Potentiality of pressmud-EFB and soil mixtures as an adsorption material. *Materials Today: Proceedings*, 5, pp. 21652-21660.

Mohamed, M. M., Othman, I. and Mohamed, R. M., 2007. Synthesis and characterization of  $\text{MnO}_x/\text{TiO}_2$  nanoparticles for photocatalytic oxidation of indigo carmine dye. *Journal of Photochemistry and Photobiology A: Chemistry*, 191, pp. 153-161.

Mozaia, S., Tomaszewska, M. and Morawski, A. W., 2005. Photocatalytic degradation of azo-dye acid red 18. *Desalination*, 185, pp. 449-456.

Mui, E. L. K., Cheung, W. H., Valix, M. and McKay, G., 2010. Dye adsorption onto char from bamboo. *Journal of Hazardous Materials*, 177, pp. 1001-1005.

Muniandy, L., Adam, F., Mohamed, A. R., Ng, E. P. and Rahman, N. R. A., 2016. Carbon modified anatase  $\text{TiO}_2$  for the rapid photo degradation of methylene blue: A comparative study. *Surfaces and Interfaces*, 5, pp. 19-29.

Natarajan, S., Bajaj, H. C. and Tayade, R. J., 2017. Recent advances based on the synergetic effect of adsorption for removal of dyes from waste water using photocatalytic process. *Journal of Environmental Sciences*, 65, pp. 201-222.

Nguyen, C. H., Fu, C. C. and Juang, R. S., 2018. Degradation of methylene blue and methyl orange by palladium-doped  $\text{TiO}_2$  photocatalysis for water reuse: efficiency and degradation pathways. *Journal of Cleaner Production*, 202, pp. 413-427.

O'Regan, B. and Gratzel, M., 1991. A low-cost, high-efficiency solar cell based on dye-sensitized colloidal  $\text{TiO}_2$  films. *Nature*, 353, pp. 737-740.

Okahsia, Y., Furukawa, Y., Ishimoto, K., Narita, C., Intharapichai, K. and Ohara, H., 2018. Comparison of cellulose nanofiber properties produced from different parts of the oil palm tree. *Carbohydrate Polymers*, 198, pp. 313-319.

Ong, C. B., Ng, L. Y. and Mohammad, A. W., 2018. A review of ZnO nanoparticles as solar photocatalysts: synthesis, mechanisms and applications. *Renewable and Sustainable Energy Reviews*, 81, pp. 536-551.

Pavithra, K. G., Kumar, P. S., Jaikumar, V. and Rajan, P. S., 2019. Removal of colorants from wastewater: a review on sources and treatment strategies. *Journal of Industrial and Engineering Chemistry*, 75, pp. 1-19.

Pazdzior, K., Wrebiak, J., Klepacz-Smoika, A., Gmurek, M., Bilinska, L., Kos, L., Sojka-Ledakowicz, J. and Ledakowicz, S., 2016. Influence of ozonation and biodegradation on toxicity of industrial textile wastewater. *Journal of Environmental Management*, 195, pp. 166-173.

Pekakis, P. A., Xekoukoulotakis, N. P. and Mantzavinos, D., 2006. Treatment of textile dyehouse wastewater by TiO<sub>2</sub> photocatalysis. *Water Research*, 40, pp. 1276-1286.

Peng, X. M., Wang, M., Hu, F. P., Qiu, F. X., Dai, H. L. and Cao, Z., 2018. Facile fabrication of hollow biochar carbon-doped TiO<sub>2</sub>/CuO composites for the photocatalytic degradation of ammonia nitrogen from aqueous solution. *Journal of Alloys and Compounds*, 770, pp. 1055-1063.

Polini, A. and Yang, F., 2017. *Physicochemical characterization of nanofiber composites*. Cambridge: Matthew Deans.

Proskuryakova, L., Saritas, O. and Sivaev, S., 2017. Global water trends and future scenarios for sustainable development: the case of Russia. *Journal of Cleaner Production*, 170, pp. 867-879.

Ragupathy, S., Raghu, K. and Prabu, P., 2014. Synthesis and characterization of TiO<sub>2</sub> loaded cashew nut shell activated carbon and photocatalytic activity on BG and MB dyes under sunlight radiation. *Spectrochimica Acta Part A: Molecular and Biomolecular Spectroscopy*, 138, pp. 314-320.

Rao, A. S. and Venkatarangaiah, V. T., 2014. The effect of cathode materials on indirect electrochemical oxidation of methyl orange, malachite green and methylene blue. *Portugaliae Electrochimica Acta 2014*, 32(3), pp. 213-231.

Saini, R. D., 2017. Textile organic dyes: polluting effects and elimination methods from textile waste water. *International Journal of Chemical Engineering Research*, 9, pp. 121-136.

Shan, A. Y., Ghazi, T. I. M. and Rashid, S. A., 2010. Immobilisation of titanium dioxide onto supporting materials in heterogeneous photocatalysis: a review. *Applied Catalysis A: General*, 389, pp. 1-8.

Shanmugarajah, B., Chew, I. M., Mubarak, N. M., Choong, T. S., Yoo, C. and Tan, K., 2018. Valorization of palm oil agro-waste into cellulose biosorbents for highly effective textile effluent remediation. *Journal of Cleaner Production*, 210, pp. 697-709.

Shende, T. P., Bhanvase, B. A., Rathod, A. P., Pinjari, D. V. and Sonawane, S. H., 2017. Sonochemical synthesis of graphene-Ce-TiO<sub>2</sub> and graphene-Fe-TiO<sub>2</sub> ternary hybrid photocatalyst nanocomposite and its application in degradation of crystal violet dye. *Ultrasonics Sonochemistry*, 41, pp. 582-589.

Silva-Castroa, V., Durán-Alvarezb, J. C., Mateos-Santiagoa, J., Flores-Caballeroa, A. A., Lartundo-Rojasc, L. and Manzo-Robledo, A., 2017. Photo-electrochemical and interfacial-process analysis of WO<sub>3</sub> nanostructures supported on TiO<sub>2</sub>: an approach to BPA oxidation. *Materials Science in Semiconductor Processing*, 72, pp. 115-121.

Silvestri, S., Stefanello, N., Sulkovski, A. A. and Foletto, E. L., 2019. Preparation of TiO<sub>2</sub> supported on MDF biochar for simultaneous removal of methylene blue by adsorption and photocatalysis. *Journal of Chemical Technology and Biotechnology*.

Soltani, T., Tayyebi, A. and Lee, B. K., 2018. Quick and enhanced degradation of bisphenol A by activation of potassium peroxydisulfate to SO<sub>4</sub> with Mn-doped BiFeO<sub>3</sub> nanoparticles as a heterogeneous Fenton-like catalyst. *Applied Surface Science*, 441, pp. 853-861.

Sreeja, P. H. and Sosamony, K. J., 2015. A comparative study of homogeneous and heterogeneous photo-fenton process for textile wastewater treatment. *Procedia Technology*, 24, pp. 217-223.

Suhas, Gupta, V. K., Carrott, P. J. M., Singh, R., Chaudhary, M. and Kushwaha, S., 2016. Cellulose: a review as natural, modified and activated carbon adsorbent. *Bioresource Technology*, 216, pp. 1066-1076.

Szilagyi, I. M., Forizs, B., Rosseler, O., Szegedi, A., Németh, P., Kiraly, P., Tarkanyi, G., Vajna, B., Varga-Josepovits, K., Laszlo, K., Toth, A. L., Baranyai, P. and Leskela, M., 2012. WO<sub>3</sub> photocatalysts: Influence of structure and composition. *Journal of Catalysis*, 294, pp. 119-127.

Tara, N., Arslan, M., Hussain, Z., Iqbal, M., Khan, Q. M., and Afzal, M., 2019. On-site performance of floating treatment wetland macrocosms augmented with



dye-degrading bacteria for the remediation of textile industry wastewater. *Journal of Cleaner Production*, 217, pp. 541-548.

Trache, D., Hussin, M. H., Chuin, C. T. H., Sabar, S., Fazita, M. R. N., Taiwo, O. F. A., Hassan, T. M. and Haafiz, M. K. M., 2016. Microcrystalline cellulose: isolation, characterization and bio-composites application: a review. *International Journal of Biological Macromolecules*, 93, pp. 789-804.

Tran, H., Scott, J., Chiang, K. and Amal, R., 2006. Clarifying the role of silver deposits on titania for the photocatalytic mineralisation of organic compounds. *Journal of Photochemistry and Photobiology A: Chemistry*, 183, pp. 41-52.

Verma, A. K., Dash, R. R. and Bhunia, P., 2011. A review on chemical coagulation/ flocculation technologies for removal of colour from textile wastewaters. *Journal of Environmental Management*, 93, pp. 154-168.

Wang, Y., Sun, H., Ang, H. M., Tade, M. O. and Wang, S., 2014. Synthesis of magnetic core/ shell carbon nanosphere supported manganese catalysts for oxidation of organics in water by peroxymonosulfate. *Journal of Colloid and Interface Science*, 433, pp. 68-75.

Wong, C. L., Tan, Y. N. and Mohamed, A. R., 2011. A review on the formation of titania nanotube photocatalysts by hydrothermal treatment. *Journal of Environmental Management*, 92, pp. 1669-1680.

Worch, E., 2012. Adsorption technology in water treatment – fundamentals, processing and modelling. Berlin: Walter de Gruyter GmbH and Co. KG.

Wu, S. S., Cao, H. Q., Yin, S. F., Liu, X. W. and Zhang, X. R., 2009. Amino acid-assisted hydrothermal synthesis and photocatalysis of SnO<sub>2</sub> nanocrystals. *The Journal of Physical Chemistry C*, 113, pp. 17893-17898.

Wu, Z., Cheng, Z. and Ma, W., 2011. Adsorption of Pb(II) from glucose solution on thiol-functionalized cellulosic biomass. *Bioresource Technology*, 104, pp. 807-809.

Xiang, L. Y., Mohammed, M. A. P. and Baharuddin, A. S., 2016. Characterisation of microcrystalline cellulose from oil palm fibres for food applications. *Carbohydrate Polymers*, 148, pp. 11-20.

Xu, A. W., Gao, Y. and Liu, H. Q., 2002. The preparation, characterization, and their photocatalytic activities of rare earth doped TiO<sub>2</sub> nanoparticles. *Journal of Catalysis*, 207(2), pp. 151-157.

Xu, Z. L., Tabata, I., Hirogaki, K., Hisada, K., Wang, T., Wang, S., and Hori, T., 2011. Preparation of platinum-loaded cubic tungsten oxide: a highly efficient visible light-driven photocatalyst. *Materials Letters*, 65(9), pp. 1252-1256.

Yang, X. J., Wang, S., Sun, H. M., Wang, X. B. and Lian, J. S., 2014. Preparation and photocatalytic performance of Cu-doped TiO<sub>2</sub> nanoparticles. *Trans. Nonferrous Met. Soc. China*, 25, pp. 504-509.

Yetim, T. and Tekin, T., 2017. A kinetic study on photocatalytic and sonophotocatalytic degradation of textile dyes. *Periodica Polytechnica Chemical Engineering*, 61(2), pp. 102-108.

Yu, P., Hu, T., Chen, H. H., Wu, F. F. and Liu, H., 2018. Effective removal of congo red by triarrhena biochar loading with TiO<sub>2</sub> nanoparticles. *Scanning*, pp. 1-7.

Zanganeh, H., Zinatizadeh, A. A. L., Habibi, M., Akia, M. and Isa, M. H., 2014. Photocatalytic oxidation of organic dyes and pollutants in wastewater using different modified titanium dioxides: a comparative review. *Journal of Industrial and Engineering Chemistry*, 26, pp. 1-36.

Zhang, H. Y., Wang, Z. W., Li, R. N., Guo, J. L., Li, Y., Zhu, J. M. and Xie, X. Y., 2017. TiO<sub>2</sub> supported on reed straw biochar as an adsorptive and photocatalytic composite for the efficient degradation of sulfamethoxazole in aqueous matrices. *Chemosphere*, 185, pp. 351-360.

Zhang, S. and Lu, X. J., 2018. Treatment of wastewater containing reactive brilliant blue KN-R using TiO<sub>2</sub>/BC composite as heterogeneous photocatalyst and adsorbent. *Chemosphere*, 206, pp. 777-783.

Zhang, X., Ye, C., Pi, K., Huang, J., Xia, M. and Gerson, A.R., 2019. Sustainable treatment of desulfurization wastewater by ion exchange and bipolar membrane electrodialysis hybrid technology. *Separation and Purification Technology*, 211, pp. 330-339.

Zhao, D. and Wu, X., 2017. Nanoparticles assembled SnO<sub>2</sub> nanosheet photocatalysts for wastewater purification. *Materials Letters*, 210, pp. 354-357.

Zhao, J., Chen, C. and Ma, W., 2005. Photocatalytic Degradation of Organic Pollutants Under Visible Light Irradiation. *Topics in Catalysis*, 35, pp. 269-278.

Zhou, X., Zhou, Y., Liu, J., Song, S., Sun, J., Zhu, G., Gong, H., Wang, L., Wu, C. and Li, M., 2019. Study on the pollution characteristics and emission factors of PCDD/Fs from disperse dye production in China. *Chemosphere*, 228, pp. 328-334.

## APPENDICES

## APPENDIX A: EDX Analysis

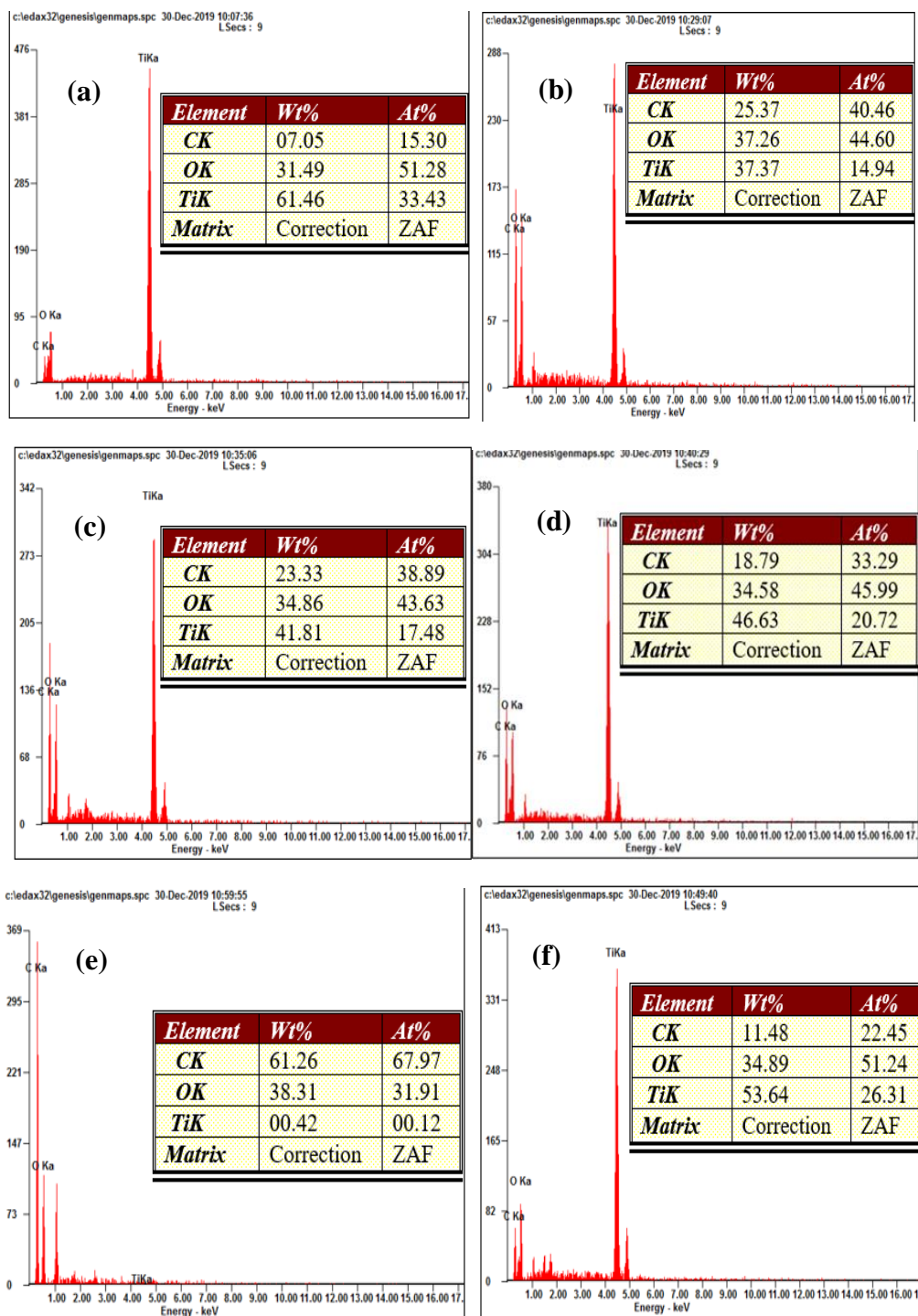


Figure A.1: EDX Analysis for (a) Pure TiO<sub>2</sub>, Cellulose Biochar/ TiO<sub>2</sub> Composite at Various Calcination Temperature (b) 300 °C, (c) 500 °C, (d) 700 °C, (e) 900 °C and (f) Cellulose Biochar.

## APPENDIX B: Preparation of Various Concentrations of Organic Dyes

To determine the concentration of organic dye which required for the research from a stock solution. Therefore, dilution process was needed. When the concentration of stock solution was knowing, the desired concentration and volume of organic dye can be obtained by calculating the required volume of stock solution by using the following equation:

$$C_1V_1 = C_2V_2$$

where

$C_1$  = Stock solution's concentration, g/L

$V_1$  = Stock solution's volume, L

$C_2$  = Diluted solution's final concentration, g/L

$V_2$  = Diluted solution's final volume, L

After the value of  $V_1$  was computed, stock solution of  $V_1$  was measured and then poured into volumetric flask which distilled water was added until the volume reached the marked line. To prepare a stock solution of 40 % Congo Red with the concentration of 500 mg/L in 0.5 L, the mass of Congo Red required was calculated as following:

$$\begin{aligned} \text{Mass of Congo Red} &= \frac{1}{0.40} \times 500 \frac{\text{mg}}{\text{L}} \times 0.5 \text{ L} \\ &= 625 \text{ mg} \\ &= 0.625 \text{ g} \end{aligned}$$

Therefore, 0.625 g of Congo Red was dissolved in 0.5 L of distilled water to obtain the stock solution with concentration of 500 mg/L in 0.5 L. The volume of 40 % Congo Red stock solution of 500 mg/L required to prepare different concentration of organic dyes in 100 mL solution is shown in Table B.1. The volume of 40 % Congo Red with 500 mg/L required to prepare 100 mL of 10 mg/L Congo Red was calculated as following:

$$\left(500 \frac{mg}{L}\right) (V_1) = \left(10 \frac{mg}{L}\right) (100mL)$$

$$V_1 = 2 mL$$

Therefore, 2 mL of Congo Red stock solution was required to prepare 100 mL of 10 mg/L Congo Red.

Table B.1: Volume of 40 % Congo Red Stock Solution of 500 mg/L Required to Prepare Different Concentration of Organic Dyes in 100 mL Solution.

<b>Concentration of Congo Red (mg/L)</b>	<b>Volume of 40 % Congo Red Stock Solution of 500 mg/L Required (mL)</b>
<b>10</b>	2
<b>20</b>	4
<b>30</b>	6
<b>40</b>	8
<b>50</b>	10

## APPENDIX C: Calibration Curve of Congo Red

The calibration curve of Congo Red is depicted in Figure C.1.

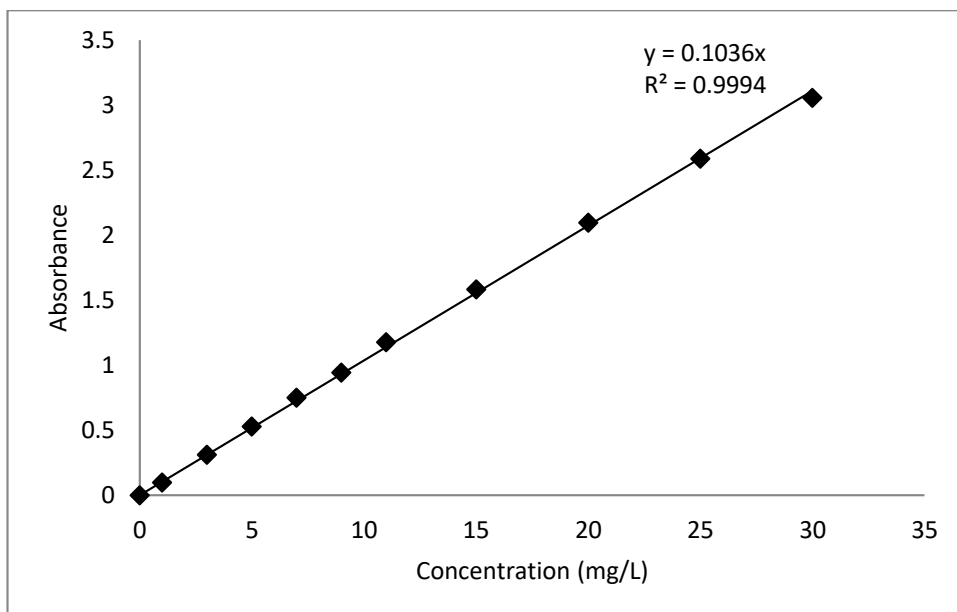


Figure C.1: Calibration Curve of Congo Red.

## APPENDIX D: Reaction Kinetics Plot

A plot of pseudo zero-order of  $C_o - C_t$  against time (min) for five different solution temperature is shown in Figure D.1 whereas a plot of pseudo first-order of  $\ln\left(\frac{C_o}{C_t}\right)$  against time (min) for five different solution temperature is shown in Figure D.2.

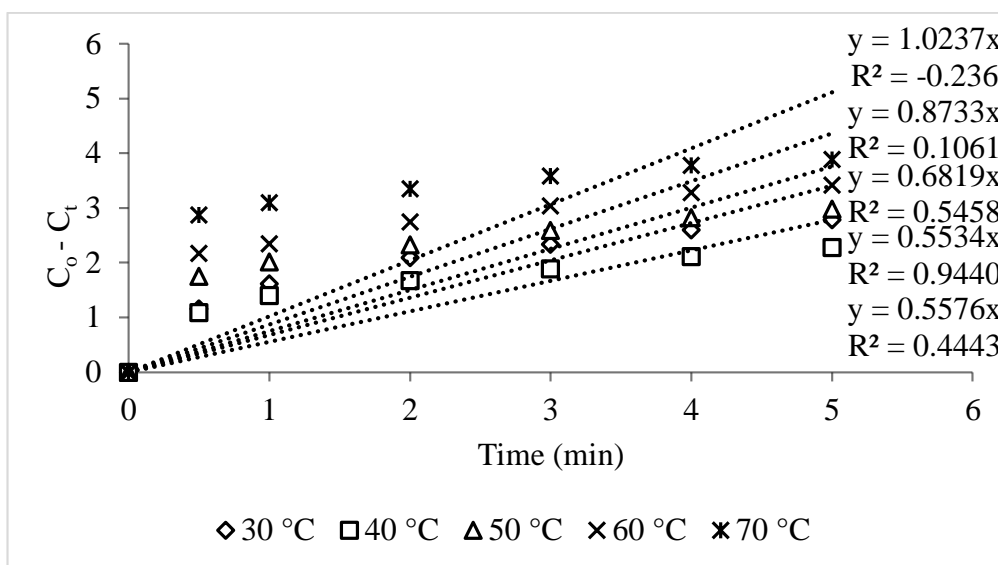


Figure D.1: Pseudo Zero-Order Reaction Kinetics Plot for Photocatalytic Degradation of Congo Red.

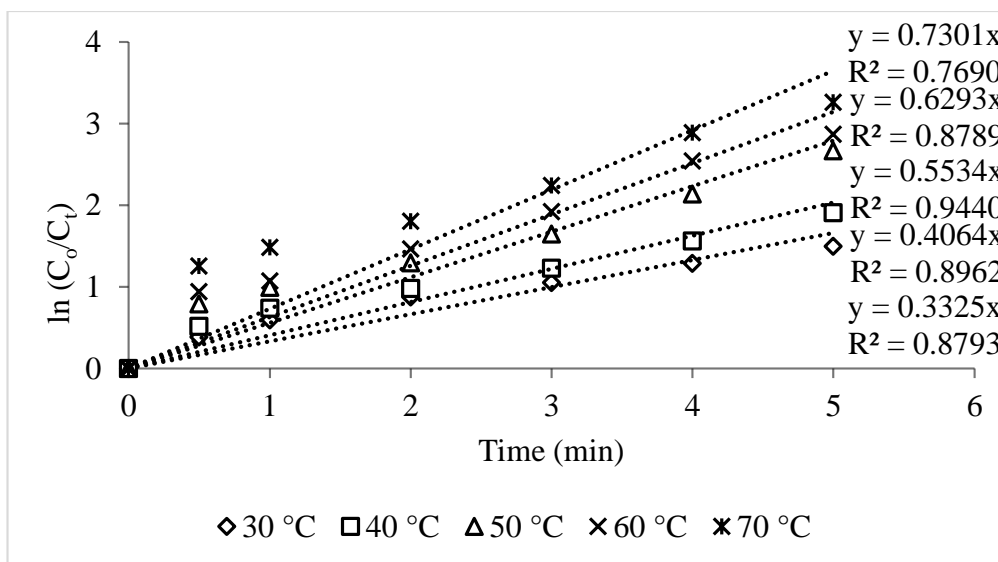


Figure D.2: Pseudo First-Order Reaction Kinetics Plot for Photocatalytic Degradation of Congo Red.